[redacted]

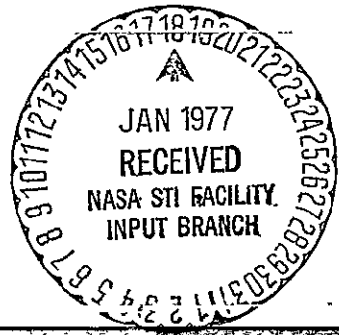

[redacted]

Lockheed

HUNTSVILLE RESEARCH & ENGINEERING CENTER

LOCKHEED MISSILES & SPACE COMPANY, INC.

A SUBSIDIARY OF LOCKHEED AIRCRAFT CORPORATION

HUNTSVILLE, ALABAMA

Lockheed

Missiles & Space Company, Inc.

HUNTSVILLE RESEARCH & ENGINEERING CENTER

Cummings Research Park
4800 Bradford Drive,
Huntsville, Alabama

STUDY LEADING TO THE REFINEMENT OF THE SRB STRUCTURAL ANALYSIS PROGRAM

FINAL REPORT

November 1976

Contract NAS8-31750

Prepared for National Aeronautics and Space Administration
Marshall Space Flight Center, Alabama 35812

by

William E. Jones
Robert L. Eidson

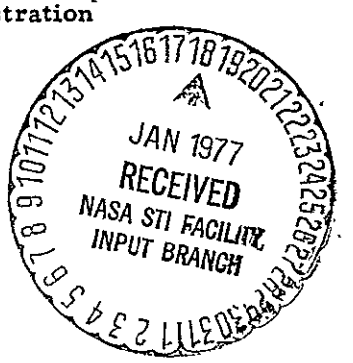

APPROVED: B. Hobson Shirley

B. Hobson Shirley, Supervisor
Engineering Sciences Section

J. S. Farrior

J. S. Farrior
Resident Director

FOREWORD

This document presents the results of work performed by Lockheed-Huntsville Research & Engineering Center under Contract NAS8-31750 for the National Aeronautics and Space Administration, George C. Marshall Space Flight Center.

The NASA-MSFC technical monitor for this study is John E. Key, EP42, Structures and Propulsion Laboratory. The performance period for this study was from 1 December 1975 through 30 November 1976.

Lockheed-Palo Alto Research Laboratory contributors to this effort were B.O. Almroth and F.A. Brogan.

SUMMARY

This report contains the results of a study to develop modeling techniques to refine the STAGS SRB mathematical models. The objective was to increase the computational efficiency while obtaining adequate accuracy in the STAGS results. The parameter studies reported in Section 2 led to the formulation of an SRB mathematical model that is highly accurate and yet results in a significant savings in computer run time compared to previously used models. With the use of proper modeling techniques, the STAGS computer program is a valuable and efficient tool for the SRB structural analysis.

The constructed SRB math model was used for the analysis of the 85/32/5 (VV/VH/θ) cavity collapse load condition for the aft end of the SRB structure. Linear, nonlinear collapse and bifurcation buckling analyses were performed. The linear and bifurcation buckling analyses showed that structural integrity and positive margins of safety will be maintained for the applied maximum load case using a design factor of 1.25. The nonlinear collapse analysis predicts stresses in the skirt above the yield for a load factor of 1.0. Applying the 1.25 design factor gives a negative margin of safety against the material ultimate. The predicted collapse occurs at a load factor higher than 1.25.

CONTENTS

1. INTRODUCTION

Structural analysis of the solid rocket booster (SRB) is one of the prime responsibilities of NASA-MSFC's Engineering Analysis Division of the Structures and Propulsion Laboratory. Many different finite element and finite difference computer programs are used by MSFC in carrying out their responsibilities. Some of these computer programs were developed by Lockheed Missiles & Space Company. In particular Lockheed programs STAGS A, STAGS B, BOSOR, and SPAR are used extensively by MSFC, partly because MSFC participated in the development and helped sponsor these programs and are quite familiar with them.

In the course of their detailed work, MSFC encountered some limitations in the output of the subject programs. Since much expensive SRB hardware is involved it is imperative that the structural analyses produce accurate results. The purpose of this effort was to ensure that the subject programs produced accurate results for all required analysis conditions and applications. The latest version of the STAGS finite difference program, STAGS C, was installed, checked out and an SRB model formulated for the accurate analysis of the cavity collapse load conditions. Some discrepancies in the STAGS analyses performed by NASA support personnel have occurred in the past. These problem areas were investigated and the causes determined and solutions obtained.

STAGS is a computer program developed at Lockheed-Palo Alto and is intended for analysis of a shell type structure. The structure to be considered may consist of up to 30 different shell branches that are treated by use of finite difference discretization. A shell branch is any part of the structure that is thin. In addition to the shell branches, the structure may include some

finite elements: elastic bars, shear panels, beams and nonlinear triangular plate elements.

The code can be used for:

- Linear stress analysis
- Geometrically nonlinear elastic stress analysis
- Inelastic stress analysis, geometrically linear or nonlinear
- Bifurcation buckling analysis with linear or geometrically nonlinear prestress (elastic), and
- Small vibration analysis with prestress based on linear or geometrically nonlinear analysis (elastic)
- Transient response analysis, linear or geometrically nonlinear, elastic or inelastic.

Any combination of point forces, line loads and distributed surface tractions can be applied. Loading by specification of displacements or thermal gradients (through the shell wall and over the shell surface) is also permitted. Any configuration of boundary conditions or other displacement constraints can be included in the analysis. Reference 2 contains the instructions for the use of the STAGS code.

This report contains five technical sections; four of which describe the tasks performed and the final section lists several conclusions and recommendations of areas requiring further study efforts.

2. STAGS MODEL PARAMETER STUDY

2.1 EFFECTS OF GRID SPACING ON LINEAR ANALYSIS

Problems in connection with the use of the STAGS finite difference computer program have been experienced during the analysis of the SRB structure by NASA support personnel. Some of these problems were the result of improper grid configurations being used in the models. Parameter studies were made to determine the proper grid layout for accurate results in the linear, nonlinear, and bifurcation buckling analyses. Results concerning the proper grid spacing for the bifurcation buckling analysis are presented in Section 2.2 and for a nonlinear analysis in Section 2.3.

The aft portion of the SRB cylindrical body and the attached conical skirt, loaded by the cavity-collapse phenomena during water entry, are the structural components under investigation. The body is a ring stiffened cylinder of constant wall thickness reinforced with tee-stiffeners and clevis joints between body segments. The aft end of the cylinder has a spherical closure which supports the rocket nozzle. The motor case structure and components are fabricated from D6AC steel. A reinforcing tee-ring is located at the cylinder-skirt intersection.

The conical skirt is a ring-stringer stiffened shell with skin thickness varying both lengthwise and circumferentially. Additional components, such as holddown posts and nozzle actuator support brackets, are integrated into the skirt structure. The skirt structure is fabricated from aluminum. A simplified view of this portion of the SRB configuration is shown in Fig. 2-1 (without the nozzle). In all analyses, $\phi = 0$ is the keel side and $\phi = 180$ is the lee side for the water cavity collapse load cases.

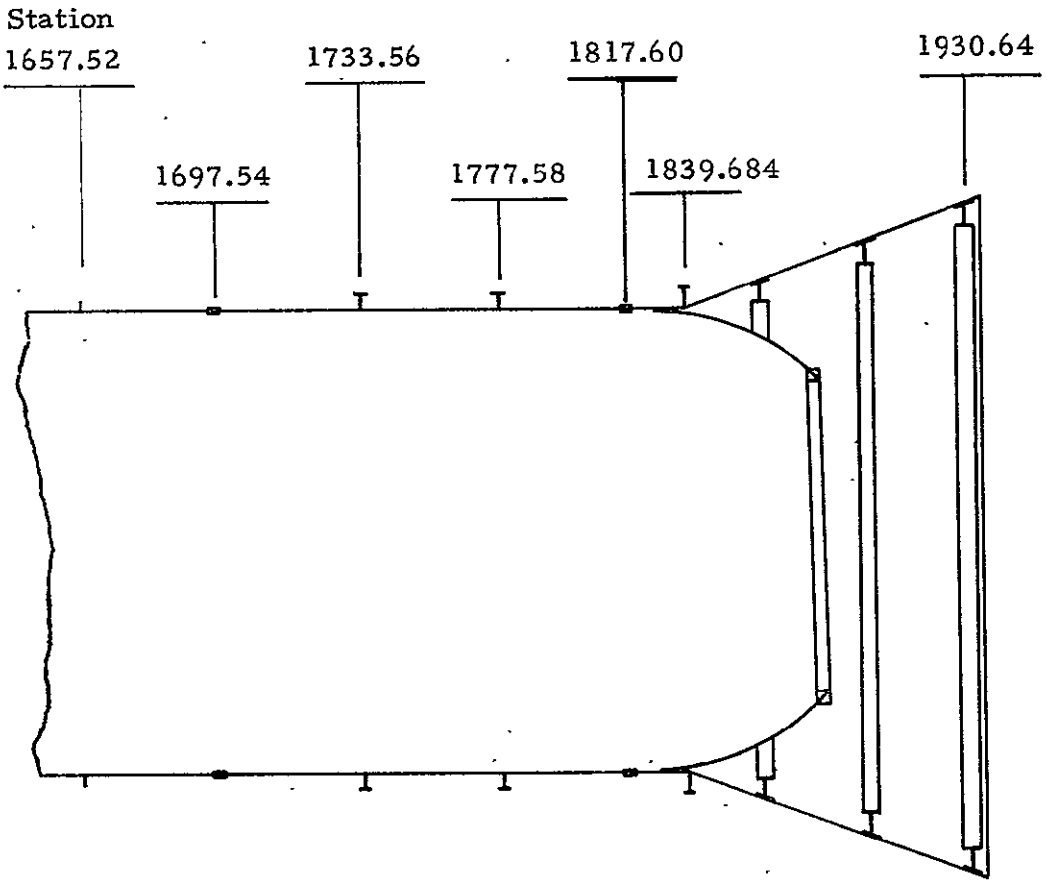

Fig. 2-1 - Aft SRB Configuration

The major discrepancy in the previous analyses is in the cone-cylinder intersection area. Brown personnel experienced discrepancies in stress values and deformations between two seemingly identical models; i.e., different results were obtained when the reinforcing tee-ring was modeled on the cylinder portion as compared to results obtained when it was modeled on the cone portion of the structure, all other parameters held constant. Presented in this section are data on the effect of variable grid size on the accuracy of the analysis in this region.

The simplified cone-cylinder model shown in Fig. 2-2 was used for the "grid study." The same length, radius, cone angle, etc., were maintained for the simplified SRB model, but a constant skin thickness was used. In addition, all components were assumed to be made of the same material. No stiffeners were added to the structure except for the reinforcing ring at the cone-cylinder intersection. Initially a 90 degree segment of the structure, with symmetry planes at the side boundaries, was used; this was later reduced to a much smaller segment after it was determined that the number of grid divisions in the circumference had no effect on the results for the internal pressure loading used in this study. The structure is modeled as two "branches"; one is the cylinder and the other is the cone. In STAGS each general shell component is modeled as a separate branch and the geometry, material properties and loading are specified for that branch. The boundary conditions at the junction of these branches is specified by the user for compatibility in the structure.

The model was first checked for symmetry and to determine if the correct cylinder wall stresses were accurately computed by the program.

Computer runs were then executed for the sample problem using a range of longitudinal and circumferential grid spacings. The accuracy increased with a finer grid spacing in the longitudinal direction, i.e., more grid divisions per length. For each grid configuration the analysis was executed twice, once with the reinforcing ring on the cylinder and again with the ring on the cone branch. The aspect ratio, ratio of length to width,

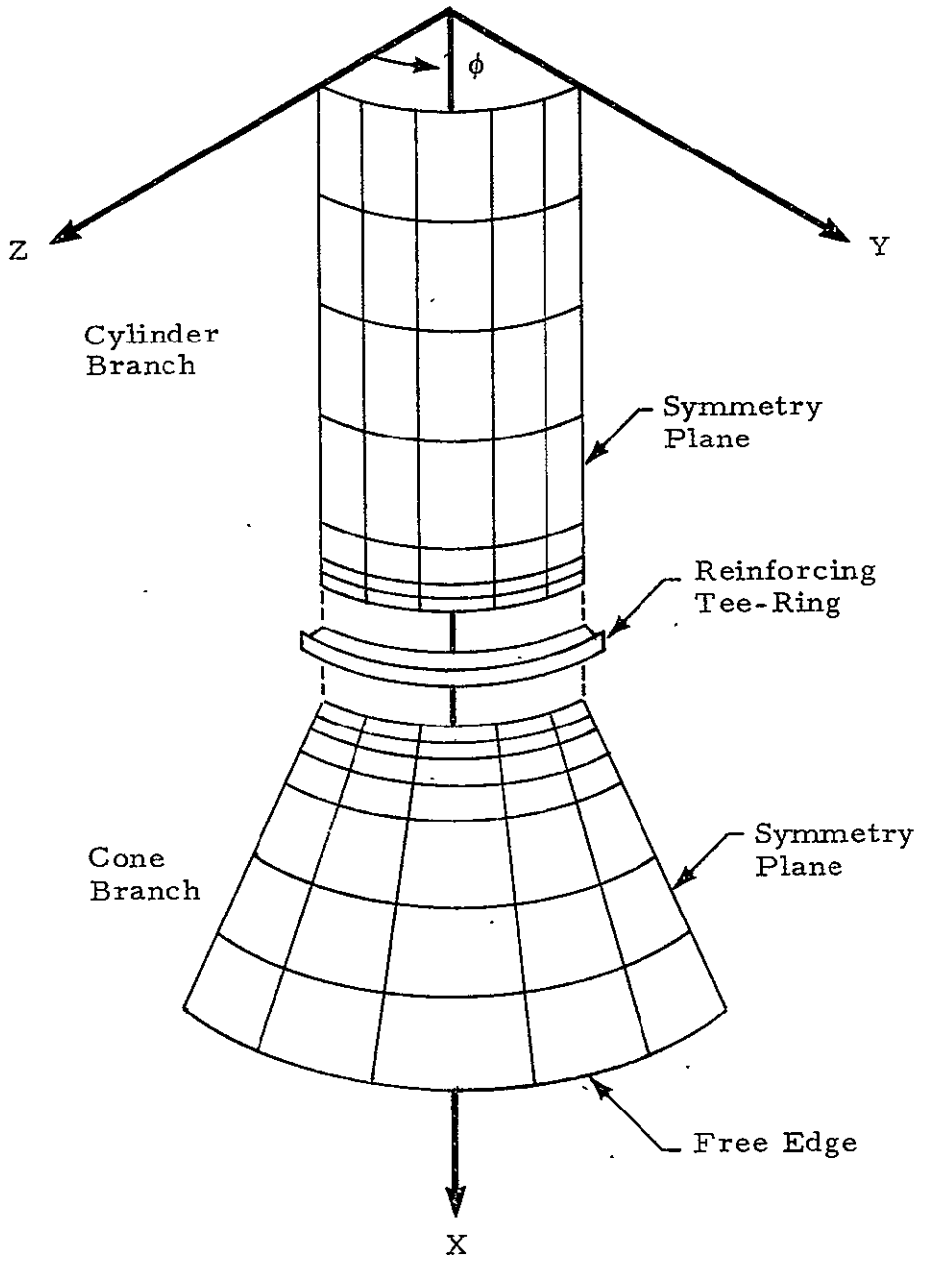

Fig. 2-2 - Simplified SRB Model

of the grid was seen to have no effect on the results. Several grid sizes were investigated using both uniform and nonuniform grid point spacing.

It was found that a variable grid spacing produced comparable results with the uniform grid spacing while significantly reducing computer run costs. This was achieved by allowing large grid spacings in areas of small stress gradients, and small grid spacings in areas of large stress gradients. This method of grid layout is the most efficient arrangement for minimizing computer run time for a desired level of accuracy.

Table 2-1 shows the effect of longitudinal grid size on the results. The longitudinal grid spacing adjacent to the intersection is given in inches. The grid spacing was the same in the two branches, cone and cylinder. This spacing was held constant for at least two grid spacings each side of the intersection. CYL denotes the analysis with the reinforcing ring attached to the cylinder branch and CONE denotes the analysis with the ring on the conical skirt. The tee-ring was modeled as a rigid stiffener. As the longitudinal grid size is reduced the radial displacement, W, and rotation, β, become more comparable for the two analyses. Note the results for the 2.0 and 0.5 inch grids.

To understand why "β" (Table 2-1) changes sign between the "CYL and CONE" analyses, for any shell structure there exists a "boundary layer" at the shell edges of the same order of size as the $(\text{radius} \times \text{thickness})^{1/2}$ within which the shell theory does not give an accurate representation of the stress field. However, if the shell approximations are applicable in the major part of the structure, shell theory will give good estimates of these stresses and displacements outside this boundary layer. The edges at the intersection of the cone and cylinder branches are in this boundary layer and approximations and interpolation must be used to obtain compatibility and continuity with the rest of the structure. The finite difference integration scheme used in STAGS also must be modified at the boundary. A "whole station" method of grid points and integration points is used to produce the greatest accuracy for the shell analysis. This scheme is shown

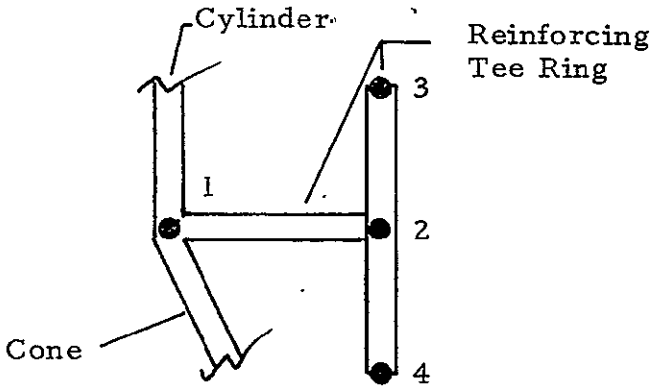

Table 2-1

GRID STUDY

Item	Grid Size (in.)		10.0	5.0	2.0	0.5	Branch ≠ Ring
1	$\sigma_1 = \sigma_2$*	CYL	6840	-274	-586	-468	-467
		CONE	6979	148	-462	-442	
2	σ_3**	CYL	4168	5494	1994	30	-232
		CONE	10600	5765	2108	434	
3	σ_4**	CYL	9512	-6042	-3166	-966	-618
		CONE	3358	-5467	-3032	-1319	
4	W***	CYL	0.305	-0.00069	-0.00148	-0.00118	
5		CONE	0.0176	-0.00038	-0.00116	-0.00118	
6	β	CYL	0.00153	0.00447	0.00524	0.00236	
7		CONE	0.00084	-0.00333	-0.00447	-0.00165	
8	M_x	CYL	-60.6	-625	-1043	-1310	
9		CONE	-59.9	-563	-954	-1225	

At Intersection

*σ_1, σ_2 are hoop stresses, psi.

**σ_3, σ_4 are axial bending stresses, psi

***W ≡ radial deflection, positive outward (in.)

$\beta \equiv \frac{\partial W}{\partial x}$ change in slope in the axial direction.

$M_x \equiv$ axial local bending moment (in-lb)

≠ reinforcing tee-ring results with tee ring modeled as a separate branch.

in Fig. 2-3. Only one set of grid points is used but two sets of integration points, one for the bending strain energy (integration area A) and one for the membrane strain energy (integration area B). This method has been shown to produce better results than the half-station integration scheme that was used in STAGS A. Modifications have to be made to the integration scheme for accurate analyses at these boundary grid points. A plot of the rotations on either side of the intersection for the 0.5 inch grid spacing analysis in Table 2-1 is shown in Fig. 2-4. The solid curves gives the rotations for the analysis with the reinforcing ring on the conical branch. The dashed curve represents the analysis with the ring on the cylinder branch. The difference in the rotations calculated at the intersection is seen to be less than a fourth of a degree for modeling the ring on the cone or the cylinder branch. The calculated inflection point is within 0.20 inch of the intersection line by either analysis. Thus, one can see why β (Table 2-1) has an apparent but insignificant discrepancy.

The stresses at four points on the ring are also given in Table 2-1. The stresses at points 1 and 2 are the hoop tension values and 3 and 4 are the axial bending stresses. Runs were also made with the ring web modeled as a separate branch with the flange as a stiffener. This allows bending of the web and less rotation of the flange than when the ring was modeled as a rigid member. The ring web deformation is plotted in Fig. 2-5 and compared with the rigid ring rotation. The reduction in bending is noted in the stress values for points 3 and 4 in the last column of Table 2-1. The ring web axial stress value is the same as that shown in the column for the 0.5 inch spacing where the ring was a rigid member.

The discrepancies between the CONE and CYL runs are also partially due to the interpolation using several consecutive node properties either side of a node to determine the displacements at that node. Where a large discontinuity exists in the model, geometrical and/or stiffness, too coarse a grid size will not allow an accurate solution in this particular area. At the cone-cylinder intersection with the stiff reinforcing ring, the large grid size

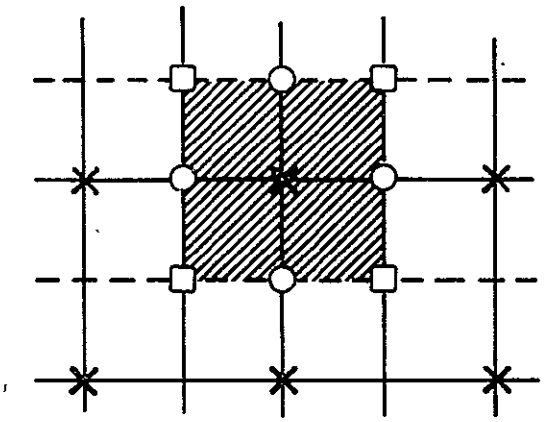

× Grid points for w and integration points

□ Grid points for u, v

Half-Station Scheme in STAGS A

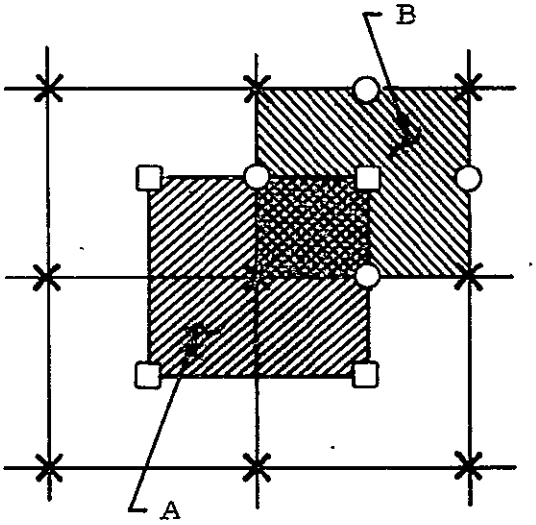

× Grid points (u, v, w) and integration points for bending energy

□ Integration points for membrane energy

Whole-Station Scheme in STAGS B and C

Fig. 2-3 - Some Schemes for Two-Dimensional Finite Difference

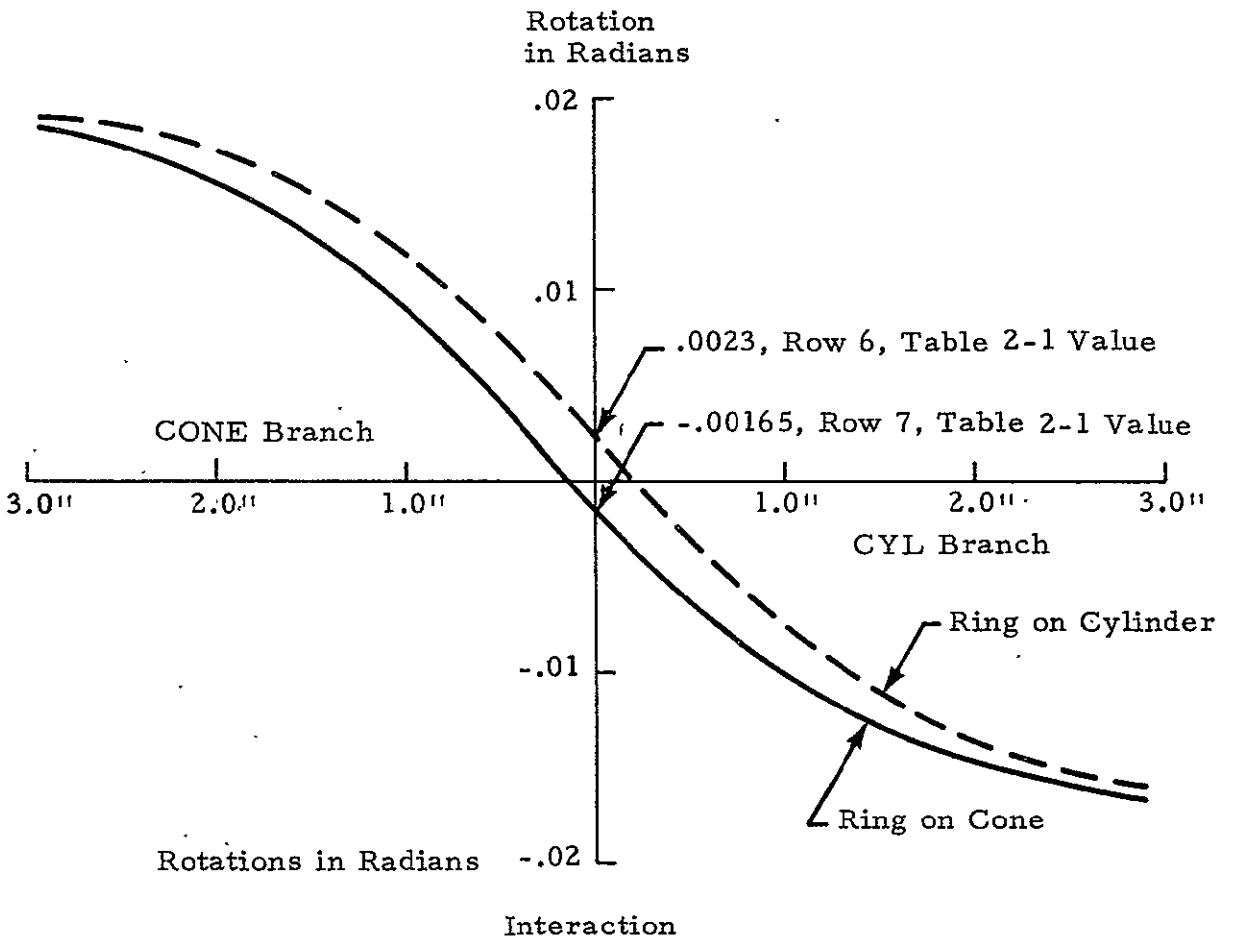

Fig. 2-4 - Branch Rotations at the Intersection

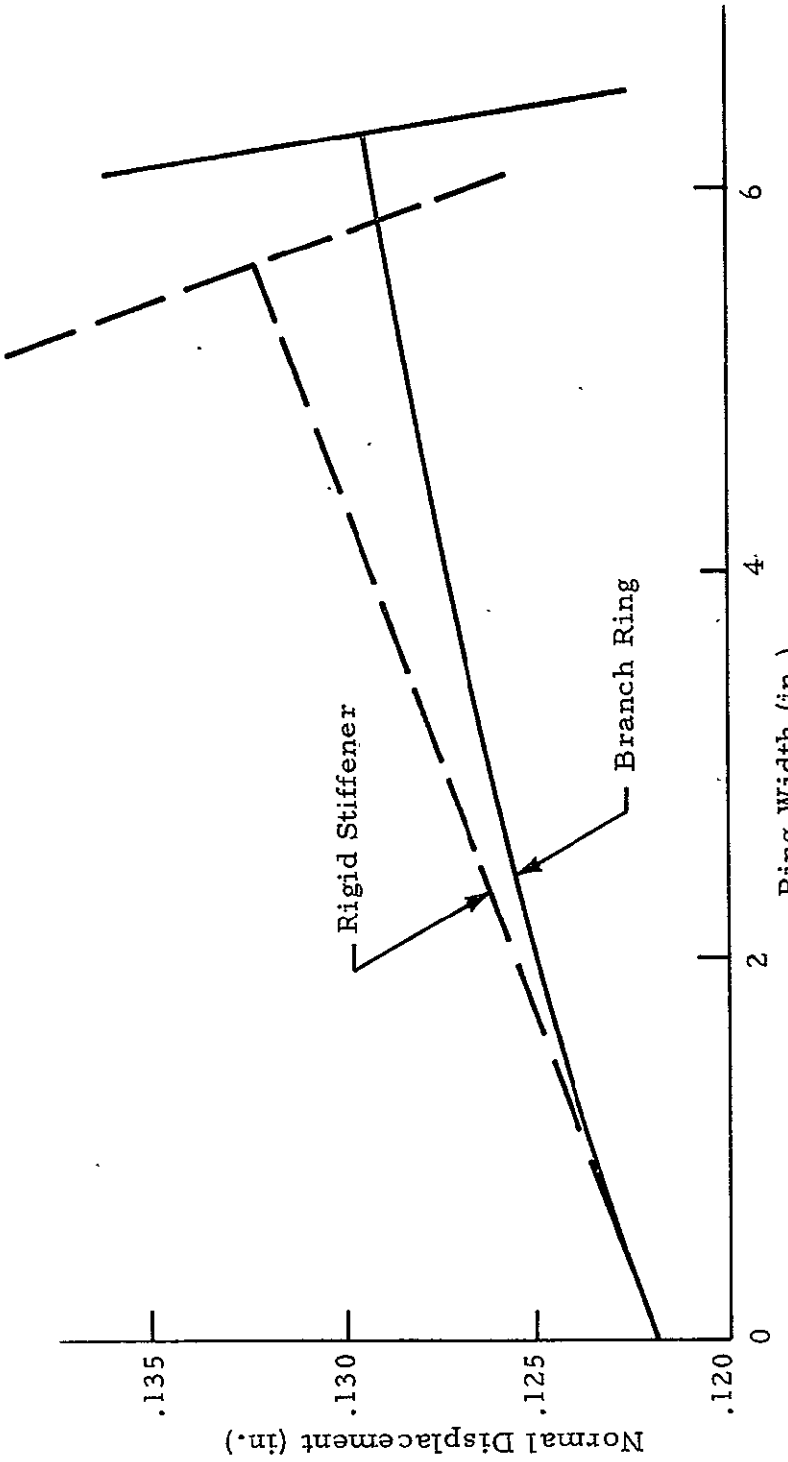

Fig. 2-5 - Ring Branch Deformation

inhibits the true radial displacement at that point. The effect of grid size on the radial displacement at the intersection is shown in Fig. 2-6. Two curves are shown; the solid graph shows the results with the same grid spacing on both sides on the intersection. The dashed curve shows the effect of maintaining a course grid in a branch on one side of the intersection while having a fine grid on the other branch. A fine grid spacing must be maintained in the immediate area of discontinuity for accurate results. A coarse grid can then be established in the rest of the model with no appreciable effect on the results and considerable savings in run time.

2.2 EFFECTS OF GRID SPACING ON BIFURCATION BUCKLING ANALYSIS

In a stiffened thin skin structure, buckling (local as well as general) can be the predominant factor governing design. Therefore, a thorough bifurcation buckling/nonlinear collapse analysis is needed for the aft portion of the SRB under cavity collapse loads. The nonlinear collapse analysis will be discussed in Section 2.3.

To determine the effect of grid size on the magnitude of in-plane bifurcation buckling loads the simplified cone-cylinder model described in Section 2.1 without stiffeners was investigated. Loading was due to a uniform axial ring load applied along the tangent to the cone at the aft end of the skirt. The branch lengths of the cone and cylinder were each divided into 11, 21 and 41 rows on separate runs with the same number of rows in each branch. Table 2.2 and Fig. 2-.7 show the computed eigenvalues* for each run. Note that the eigenvalue is converging as the grid spacing is decreased. STAGS B was used in this analysis. The numerical procedure used in STAGS B allows for convergence of eigenvalues from above with decreasing grid spacing. Too coarse a grid spacing in the longitudinal direction

*The eigenvalue is the value by which the applied base loads must be multiplied in order to give the bifurcation buckling load. In this report, eigenvalue, bifurcation buckling load factor, and critical load factor will be used interchangeably.

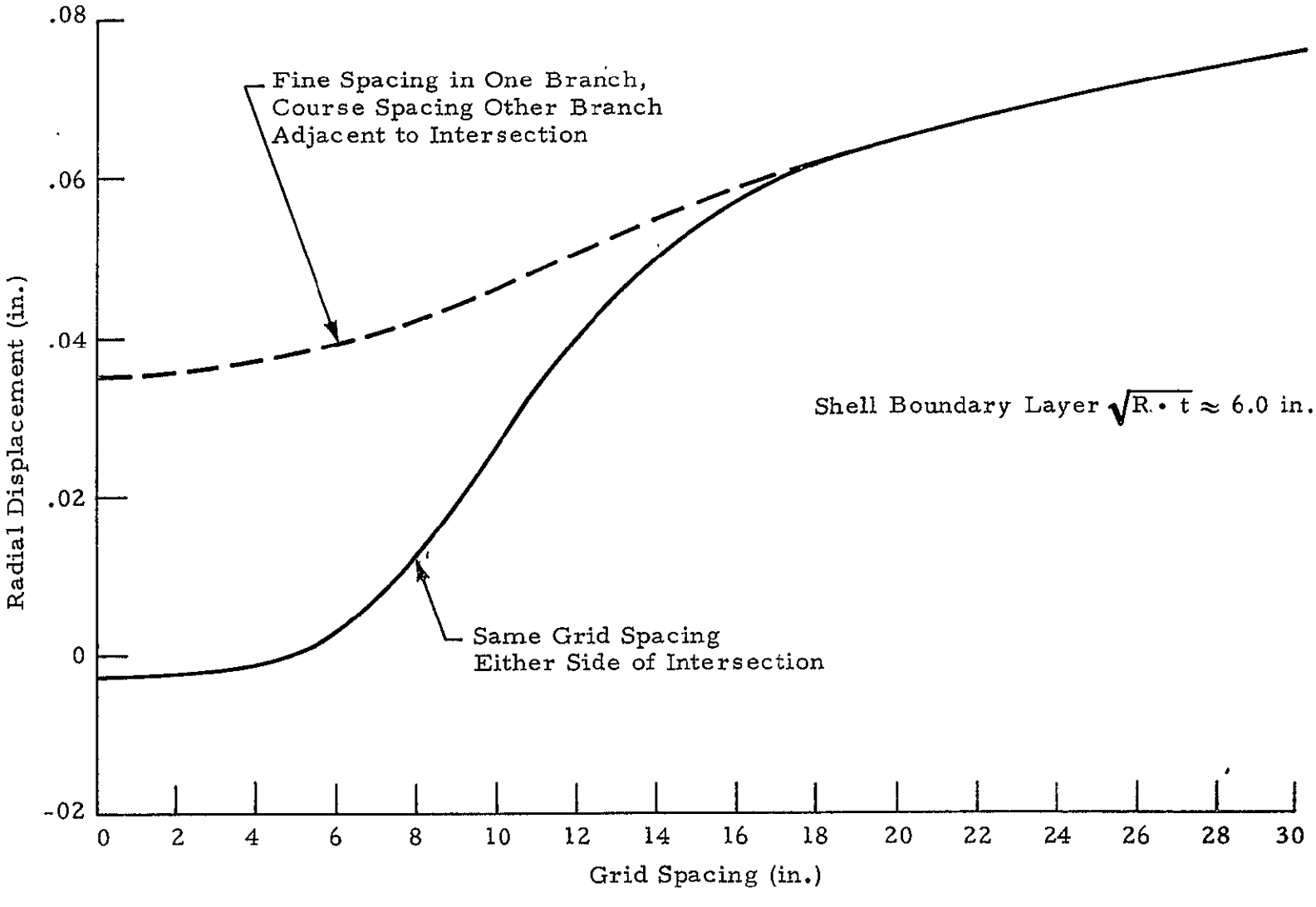

Fig. 2-6 - Grid Spacing Effect on Deformation

Table 2-2
BIFURCATION BUCKLING EIGENVALUES

No. of Divisions In Each Branch	Eigenvalue
11	9.44
21	5.60
41	4.83

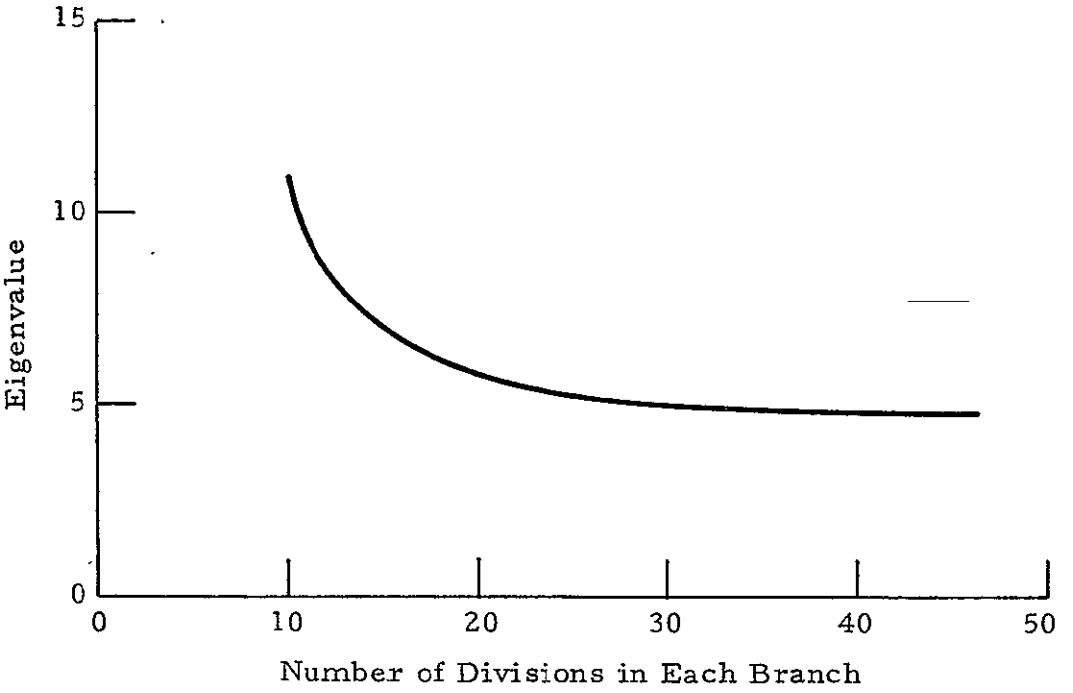

Fig. 2-7 - Bifurcation Buckling vs Grid Spacing Simplified Cone-Cylinder Model Using STAGS B

results in very high values for the critical load factor. It was determined that in order to achieve accurate bifurcation buckling load factors, the initial grid should be sized so that the half wavelength of the bifurcation buckling mode (that portion of the mode between inflection points) contains at least three intermediate grid points. In STAGS C the convergence of bifurcation buckling load factors is from below with decreasing grid spacing. However, the conclusions concerning intermediate grid points are still applicable.

Several STAGS C bifurcation buckling analyses were performed to obtain results for the 85/32/5 cavity collapse pressure distribution described in detail in Section 4 of this report. The 180 deg thin skin shell model described in Section 2.3 was used in the analysis. Effectiveness of discrete stiffeners was determined by successively adding more stiffeners in analyses with the same grid. Finally, different grid patterns were set up to determine the effect of grid layout.

With an unstiffened structure, the critical load factor was found to be 0.08. With the two stiffeners included on the dome-nozzle interface and motor case-skirt intersection, the critical load factor increased to 0.11. For both the critical load factors mentioned above, buckling was predicted at the aft end of the skirt. However, in these analyses, none of the circumferential or meridional stiffeners in the skirt were included. To account for the meridional stiffeners an equivalent thickness of the skirt was calculated. The equivalent thickness was determined so that the bending stiffness of the skin of equivalent thickness is the same as the stiffness of the skin with meridional stiffeners included.

Modifying the previous structure with the three circumferential stiffeners along the skirt, along with the equivalent thickness, the critical load factor was found to be $\lambda = 0.32$, with buckling predicted in the cylindrical motor case just forward of the dome-motor case intersection approximately at Station 1800.

Finally, the model was modified to include the equivalent thickness in the skirt as well as ten discrete stiffeners: a stub, two tee rings, and two clevis joints along the motor case; the stiffener at the aft end of the dome; the main attach ring at the motor case-skirt intersection; and three stiffeners equally spaced along the skirt. This model includes all discrete stiffeners on this portion of the SRB except the integral longitudinal stiffeners which were included in the orthotropic skin. Bifurcation buckling results for this model with different grid layouts are presented in Table 2-3. Note that grid spacings have a significant effect on the critical load factors and therefore on the predicted buckling locations.

As pointed out earlier, in STAGS C the convergence of the bifurcation buckling load is from below with decreasing grid spacing. Convergence from below makes possible the occurrence of spurious solutions. Since the bifurcation buckling load for the detailed model under the same loading was at a load factor of 2.5 (see Section 4) the results from the simplified model are suspect. Therefore, the detailed model described in Section 3 was chosen for all succeeding analyses.

Table 2-3
BIFURCATION BUCKLING LOAD FACTORS

Grid in Motor Case	Critical Load Factor	Branch	Station	Angle (deg)
17 x 13 EC, UL*	0.94	Motor Case	1660	75
17 x 19 EC, UL	1.20	Motor Case	1762	180
17 x 25 EC, UL	1.03	Skirt	1880	180
17 x 19 UC, UL	0.98	Motor Case	1663	75
14 x 13 EC, EL	0.46	Motor Case	1630	180

*EC-Equal spacing in circumferential direction, UL-Unequal spacing in longitudinal direction, etc.

2.3 NONLINEAR ANALYSIS

A more reliable method to determine impending collapse is to perform a nonlinear collapse analysis. In the nonlinear collapse analysis the desired range of loading is divided into intervals or increments. Each succeeding load increment includes the geometric nonlinearities (nonlinearities resulting due to large deformation theory) resulting from all preceding load increments. The loading from each increment is summed to achieve the desired level of loading. Incremental loadings can be mechanical or thermal in nature.

Since the Univac 1108 C version of STAGS is relatively new, its nonlinear analysis results were checked by use of the finite element program NEPSAP and the finite difference programs STAGS B and BOSOR4. NEPSAP is a Lockheed-developed three-dimensional finite element computer program for the nonlinear thermo-elastic-plastic and creep analysis of arbitrary structures undergoing large deformations. BOSOR4 is a comprehensive computer program for the analysis of stress, stability, and vibration modes of segmented, ring-stiffened, branched shells of revolution and prismatic shells and panels. It performs large deflection axisymmetric stress analysis, small deflection non-axisymmetric stress analysis, modal vibration analysis with axisymmetric nonlinear prestress included, and buckling analysis with axisymmetric or non-symmetric prestress.

A 1 deg meridional slice of a simplied SRB cone-cylinder model was used to check out the nonlinear analysis. The model was composed of one-half inch thick aluminum. The cylindrical section of the model was fixed at the forward end. For the analysis the reference surface of the shell was placed at the midplane of the thickness. Loading on the structure was due to a uniform meridional line load applied at the aft end of the conical section. A schematic showing the model, boundary conditions, and the point of application of the line load is given in Fig. 2-8. Also given in Fig. 2-8 are load

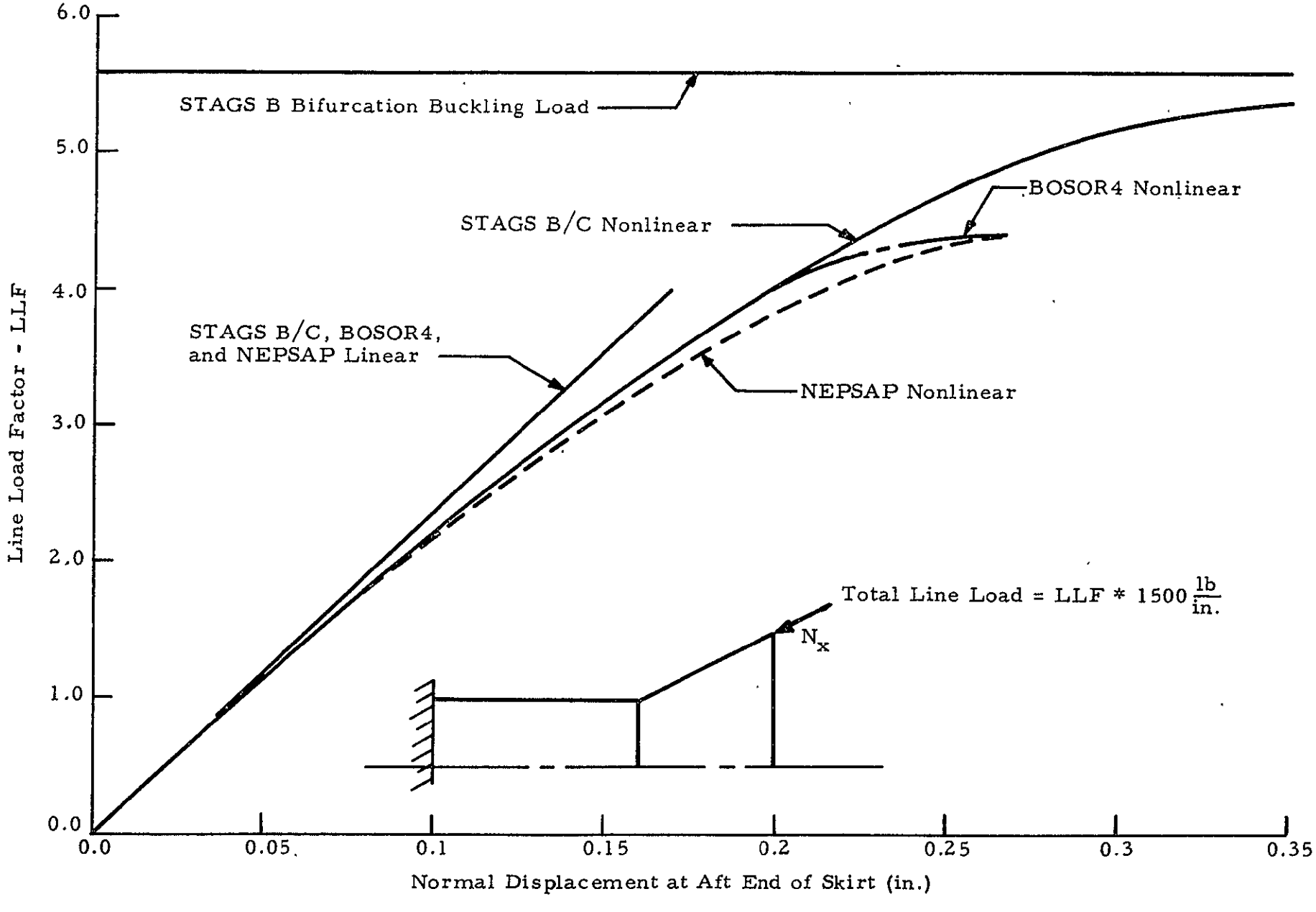

Fig. 2-8 - Load-Deflection Curves for Nonlinear Analysis

displacement curves derived from the computer codes NEPSAP, BOSOR, STAGS B and STAGS C. For the purpose of the discussion here no distinction between STAGS B and STAGS C will be made since identifical results were obtained from these programs. In Fig. 2-8 the magnitude of applied loading is indicated by the line load factor LLF which is merely a multiplier of the applied base load of 1500 lb/in. (for instance LLF = 2.0 implies a line load of 3000 lb/in.).

For the linear analysis indicated in the figure a small line load (LLF = 0.4) was applied to the structure. This small magnitude of load was chosen to minimize the nonlinear effects in the corresponding nonlinear runs used for comparison. NEPSAP, BOSOR, and STAGS all produced identical results at this load level. The curve in Fig. 2-8 labeled linear analysis has been extended to a value of LLF = 4.0 to indicate the magnitude of nonlinearities that exist in the other runs.

Collapse loads indicated by STAGS were at a line load factor of approximately LLF = 5.4 whereas BOSOR and NEPSAP indicate collapse in the range of LLF = 4.4 to LLF = 4.8. Several things affect the load level at which collapse occurs. The type of terms included in the energy expressions and the numerical method of solving the resultant equations can affect the level at which collapse is indicated. However, probably the most significant reason for differences in the collapse level is the method by which STAGS automatically reduces the size of the load increment when convergence within a load increment is difficult. For both BOSOR and NEPSAP a constant load increment of LLF = 0.4 was used. For impending collapse, when the load increment is too large, numerical instabilities can occur, causing erroneous results for this last load increment. Difficulty in convergence occurred for BOSOR and NEPSAP at LLF = 4.0, LLF = 4.4, and LLF = 4.8. For BOSOR the displacement pattern at LLF = 4.8 was completely different from previous solutions, probably representing a solution in the postbuckling range. A BOSOR bifurcation buckling analysis was not performed to determine the corresponding eigenvalue (LLF) and buckling location. For NEPSAP, the displacement

pattern was consistent for LLF = 4.8; however, the incremental displacement in going from LLF = 4.4 to LLF = 4.8 was approximately ten times the total displacement that had occurred at the end of the preceding step, indicating the onset of collapse. For the STAGS nonlinear analysis, when convergence was difficult, the size of the load increment was automatically cut in half and then halved again when necessary to achieve convergence. Within the whole analysis using STAGS, the size of the load increment decreased from a value of LLF = 0.5 in the early stages to a value of LLF = 0.031 in the latter stages of the analysis. By using this procedure STAGS was able to achieve convergence up to a value of LLF = 5.406 at which maximum allowable execution time for the analysis was reached and analysis was then terminated. Due to the relatively small load increment needed in STAGS to achieve convergence it is evident that collapse is impending. Indicated in Fig. 2-8 is a STAGS bifurcation buckling load of LLF = 5.6. The STAGS nonlinear analysis is asymptotic to this buckling load, thereby showing compatibility between collapse and buckling analysis.

It should be mentioned here that at no time did there exist any discrepancies between the nonlinear STAGS results and the linear STAGS results as NASA support personnel experienced. For their analysis, there were significant differences in the slopes of the load displacement curves between the linear analysis and the initial load increments of the nonlinear analysis. In order to determine the reason for discrepancies NASA support personnel experienced, exact models and load conditions used by them would have to be studied. The end results of the nonlinear analysis parameter study was to derive a simplified model with computer run times significantly less than those for the detailed model described in Section 3. To this end a simplified model was constructed.

The 180 deg simplified model includes all stiffeners in the detailed model with the exception of the hold-down posts. Ten discrete stiffeners in all have been included; a stub, two tee-rings, and two clevis joints along the motor case; the stiffener at the aft end of the dome; the main attach

ring at the motor case-skirt intersection; and three stiffeners equally spaced along the skirt. The following thickness and materials were used for each branch:

Motor Case — Steel, Thickness = 0.5 in.
Dome — Steel, Thickness = 0.362 in.
Skirt — Aluminum, Thickness = 0.5 in.

In addition, orthotropic material properties were used in the skirt to account for the longitudinal stiffeners.

The 90/45/10 cavity collapse pressure distribution described in the initial NASA loads document was used in the analysis. The same pressure distributions exist for the 85/32/5 load case described in Section 3 but at a reduced magnitude. Undeformed plots of the simplified model are given in Figs. 2-9 and 2-10. These plots were obtained from the NEPSAP program.

A nonlinear collapse analysis was performed using the aforementioned simplified model. The results at Station 1800 for ϕ = 180 deg (this is the point in the structure with greatest nonlinearity in load path) are shown in Fig. 2-11. Also shown in the figure are the results from the detailed model described in Section 3. The initial slopes of the load-displacement curves for the two models differ for two reasons: (1) the hold-down posts and thickened skin portion of the skirt have not been included in the simplified model, and (2) a thickness of 0.5 was used in the simplified model whereas a thickness of 0.52 was used in the detailed model. Due to the simplifications for the parameter study, the simplified model is slightly more flexible than the detailed model. This is evident on inspection of Fig. 2-11. Still, displacements differ by less than 15% for the two models. Convergence in the detailed model at a load factor greater than 1.5 was not obtained, indicating the onset of collapse. However, in the simplified model, convergence did not become a problem until a load factor of 1.7 was reached.

ORTHOGRAPHIC VIEW Y-Z PLANE

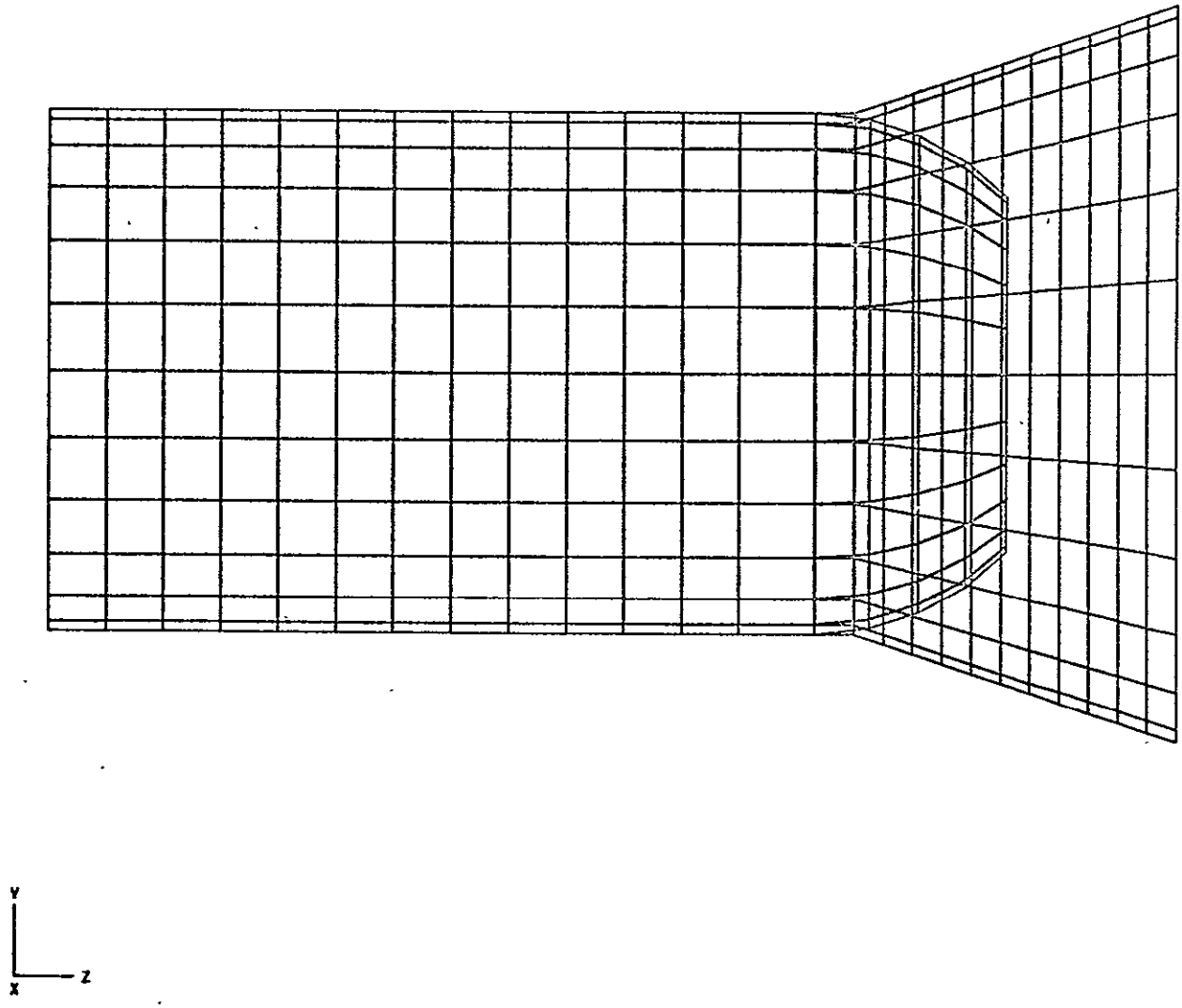

Fig. 2-9 - Orthographic View of Simplified SRB Thin Shell Model

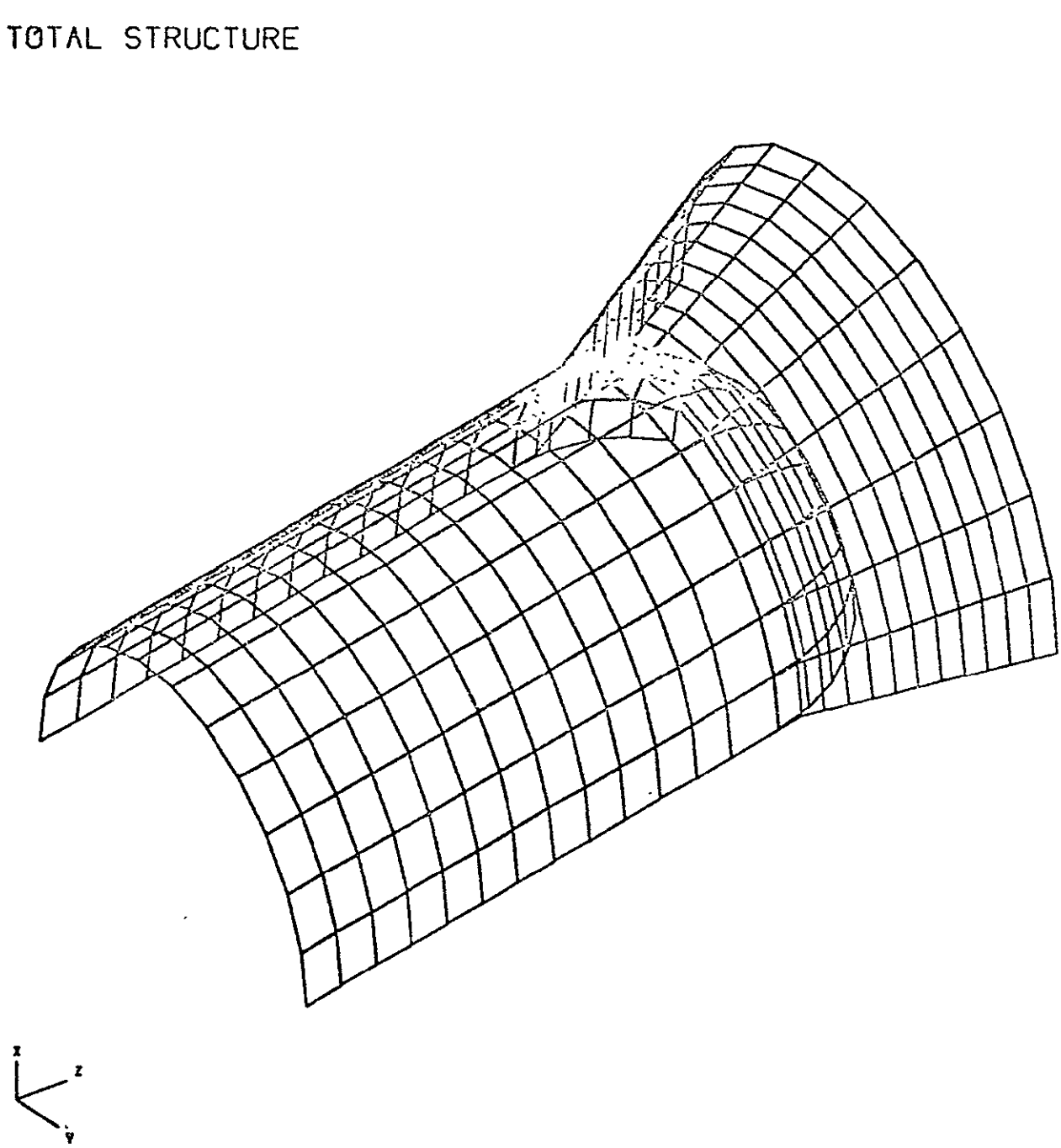

Fig. 2-10 - Isometric View of Simplified SRB Thin Shell Model

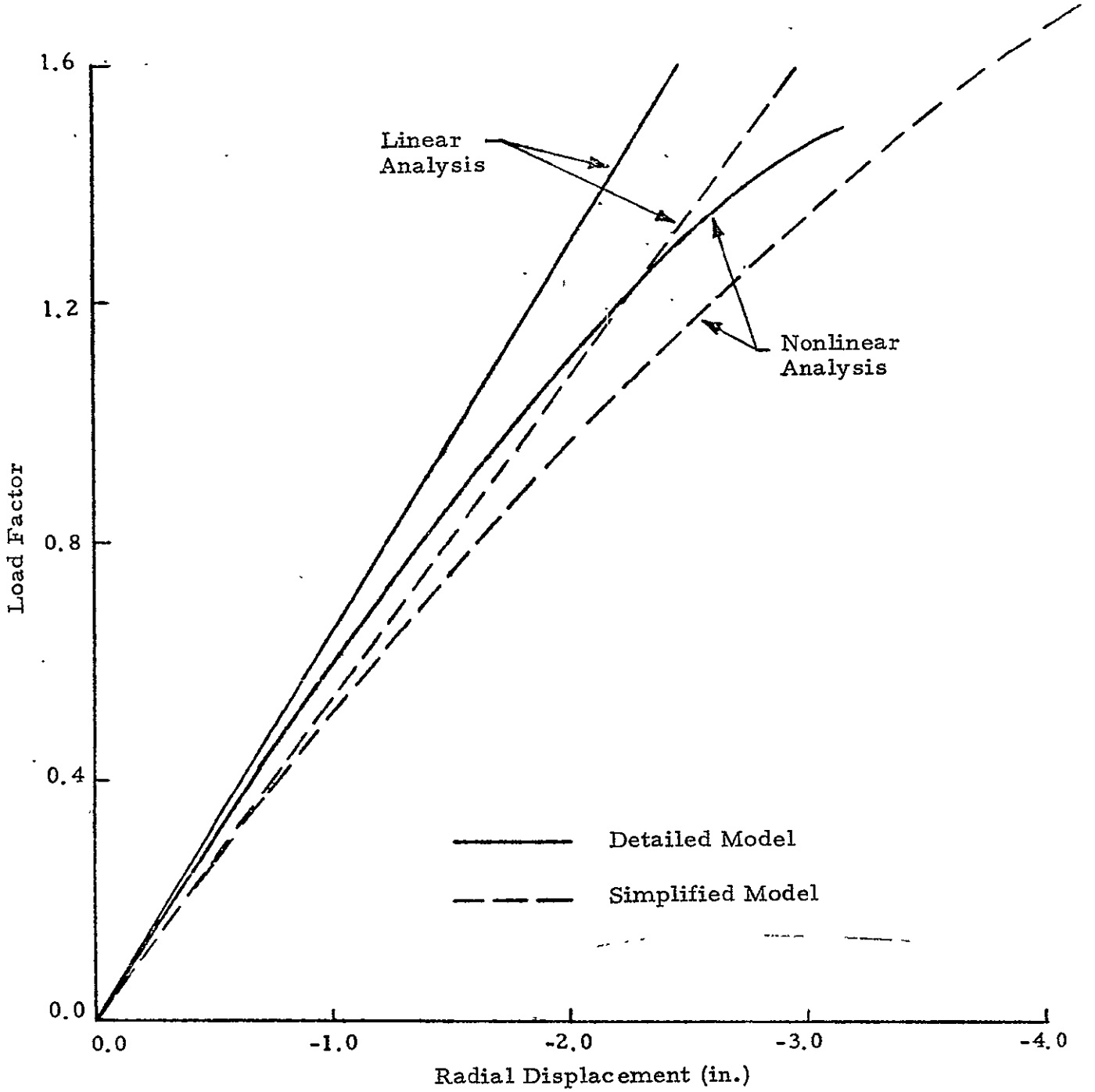

Fig. 2-11 - SRB Motor Case, Station 1800, ϕ = 180 deg, 90/45/10, Cavity Collapse Loads

The simplified model described above offered reasonably good overall load-displacement characteristics. However, to determine the structural integrity of the SRB these overall results are not enough. Very detailed stresses within the skin are needed and these could not be determined using the simplified model. For this reason, the detailed model described in Section 3 was used for all succeeding analyses.

2.4 REFERENCE SURFACE LOCATION

In the STAGS program, both versions B and C, a thin shell is located by defining a reference surface and the offset from the reference surface to the midplane of the shell. NASA support personnel have determined discrepancies dependent upon the way in which the midplane of the shell is defined. A series of STAGS C computer runs was made to determine the effect of reference surface location on results.

The simplified unstiffened cone-cylinder model described in Section 2.3 was used in this study. Linear responses of the structure were determined. The reference surface was located at the midplane of the shell and also at the outer surface of the shell (skin centerline offset at a distance of one-half the thickness from the reference surface).

Under internal pressure loads identical results were obtained, regardless of the location of the reference surface. For the reference surface located at the midplane of the shell wall and line loads applied at the aft end of the skirt, the calculated stress resultants along the aft end of the skirt were identical to the applied line loads. However, under the same loadings, with the reference surface located at the outer skin surface, significant variations in the stress resultants from the applied line loads occurred at the point of load application. It was determined that line loads in STAGS B and STAGS C are applied at the reference surface, not at the skin centerline. Therefore when the reference surface is not at the skin midplane, the meridional line load plus a moment to compensate for the eccentricity must be

applied. When applying this equivalent load system with the reference surface at the outer surface of the shell, the results achieved were identical to those with the reference surface at the midplane of the shell.

It should also be pointed out that the discrepancies occurring due to reference surface location were quite localized and completely damped out within the "boundary layer" region defined by the meridional distance $(\text{thickness} \times \text{radius})^{1/2}$.

2.5 IMPERFECTION SENSITIVITY

Imperfections from manufacturing tolerances could possibly affect the load carrying capability of the aft portion of the SRB. A tolerance of ± 0.5 inch on the overall diameter of the motor case is specified on the part drawings. It is apparent that slight variations in initial geometry would have little effect on the response of the structure for nonsymmetric loading patterns. However, for the symmetric pressure distributions that exist for vertical entry of the SRB on water impact there is a possibility that imperfections could significantly affect the collapse loads of the structure.

The STAGS C computer program handles imperfections by a user written subroutine, WIMP. Basically, this subroutine defines variations in normal displacements from the original reference surface due to imperfections. The prescribed structure (original structure with imperfections) is assumed to be in a stress free state, and a nonlinear analysis is performed on this stress free structure.

In order to study the effect of imperfections in the motor case the following variations in normal displacements along the circumference were assumed:

$$W_1(\theta) = -\frac{T}{2}\cos 2\theta \qquad 0 \leq \theta \leq 180 \text{ deg}$$

where T is the specified tolerance on the diameter. In the motor case T = 0.5 inch. Variations along the axis of the motor case were of the form

$$W_2(x) = \frac{1}{2}\left[1 - \cos\left(\frac{x - x_i}{x_j - x_i}\ 2\pi\right)\right] \qquad x_i \leq x \leq x_j$$

where x_i and x_j are axial coordinates at the beginning and end of the axial imperfection. The total variation in normal displacements was then

$$W(\theta, x) = W_1(\theta)\, W_2(x)$$

Note that at the end points for the imperfections ($x = x_i$, $x = x_j$, $\theta = 0$ deg, $\theta = 180$ deg) the slopes are zero so that no discontinuities exist in the skin.

Using the STAGS C program, the imperfections as defined above were applied to the detailed SRB model described in Section 3 of this report. The end points for the longitudinal variation in imperfections were chosen to be at the tee rings on the motor case. This corresponds approximately to the point of maximum pressure for the 90/0/0 load case described in Revision B to the SRB loads document (Ref. 1). Pressure distributions for the 90/0/0 load case were applied to the structure.

Results of the linear and nonlinear analysis with and without imperfections are shown in Fig. 2-12. The lee side ($\theta = 180$ deg) radial displacement midway between the tee rings is plotted against the load factor. The load factor is the multiplier for the 90/0/0 pressure distribution defined in the loads document (i.e., a load factor of 1.0 defines the 90/0/0 loading condition and a load factor of 2.0 doubles this). Comparison of the results for the model with and without imperfections indicate that the magnitudes of imperfections in the motor case due to manufacturing tolerances do not significantly affect the response of the structure. In fact, at a load factor of 2.6 the displacements were within 1% of each other.

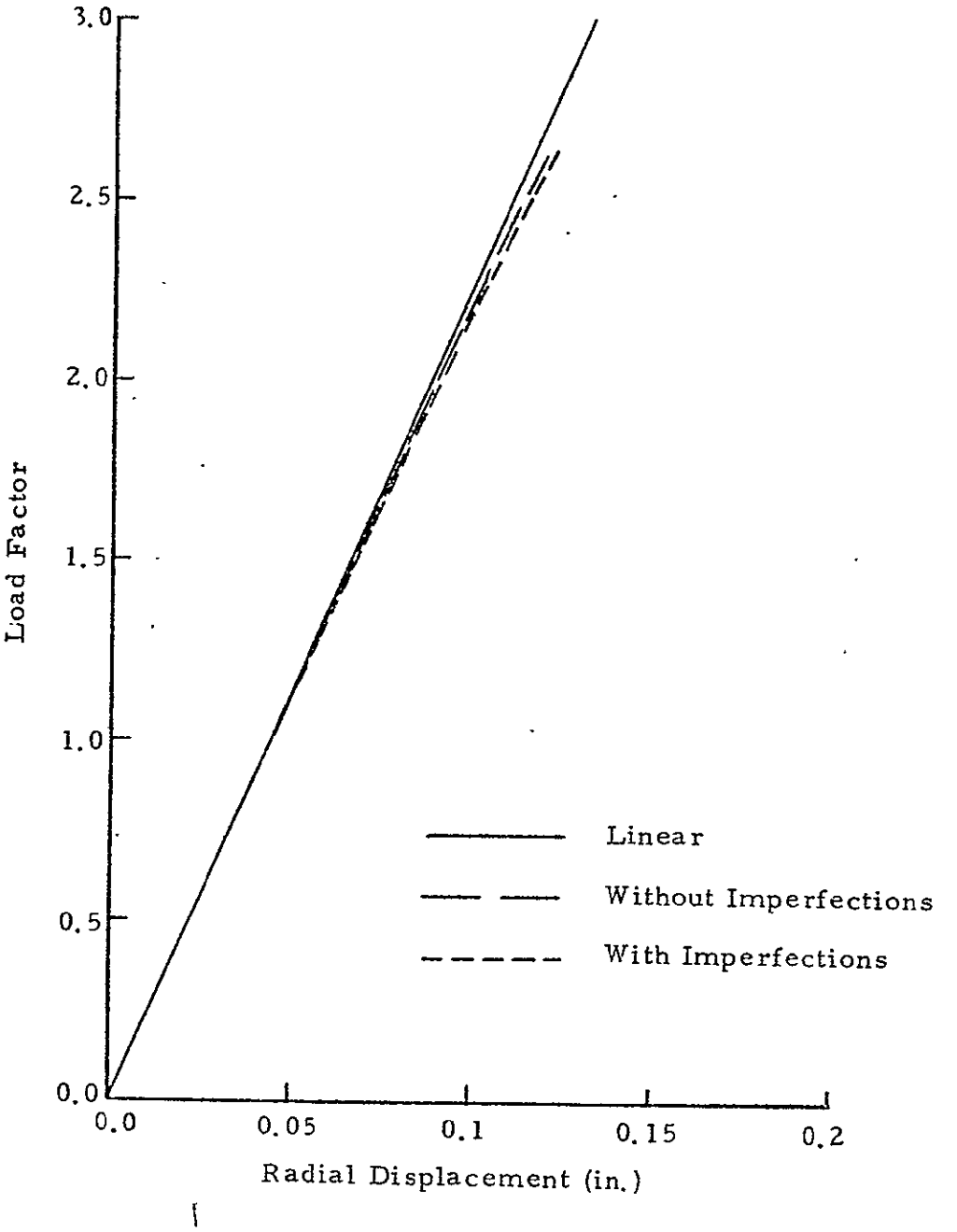

Fig. 2-12 - Motor Case Radial Displacement on Lee Side, Midway Between Tee Rings for 90/0/0 Load Case

The manufacturing tolerances on the SRB skirt are of the same order of magnitude as those in the motor case. Also, the pressure loads on the skirt for the 90/0/0 load case are smaller than those on the motor case. Since imperfection sensitivity was not detected in the motor case, it is anticipated that the skirt will exhibit the same characteristics.

The load factor value at which nonlinear collapse occurs might be significantly affected by imperfections, but a load factor of a least 3.0 would be reached before collapse. Load factors beyond 3.0 are of little interest in the determination of the structural integrity of the SRB (see Section 4).

3. STAGS C SRB MATHEMATICAL MODEL

3.1 STRUCTURE DESCRIPTION

The aft portion of the SRB cylindrical body and the attached conical skirt, loaded by the cavity-collapse phenomena during water entry, are the structural components to be modeled. The body is a ring stiffened cylinder of constant wall thickness reinforced with rectangular stiffeners, tee-stiffeners and clevis joints between body segments. The aft end of the cylinder has a hemispherical closure which supports the rocket nozzle. The motor case structure and components are fabricated from D6AC steel. A reinforcing tee-ring is located at the cylinder-skirt intersection.

The conical skirt is a ring-stringer stiffened shell with skin thickness varying both lengthwise and circumferentially. Additional components, such as holddown posts and nozzle actuator support brackets, are integrated into the skirt structure. The skirt structure is fabricated from 2219-T87 aluminum. A simplified view of this portion of the SRB configuration showing the major geometry dimensions is shown in Fig. 3-1 (without the nozzle).

The data have been compiled from the SRB drawings and coded into the STAGS C format. The skirt data were taken from NASA-MSFC 14A00305 (12 January 1976) drawing and the SRM data from Thiokol IU50185 and IU50129.

3.2 SRB MATHEMATICAL MODEL

The math model is a 180 degree symmetrical structure composed of four branches: Branch 1 is the motor case cylinder from the reinforcing ring at Station 1613.50 to the aft dome tangent point at Station 1828.85; Branch 2 is the aft dome; Branch 3 is the remaining portion of the cylinder between the aft dome tangent point and the cone-cylinder intersection; Branch 4 is the

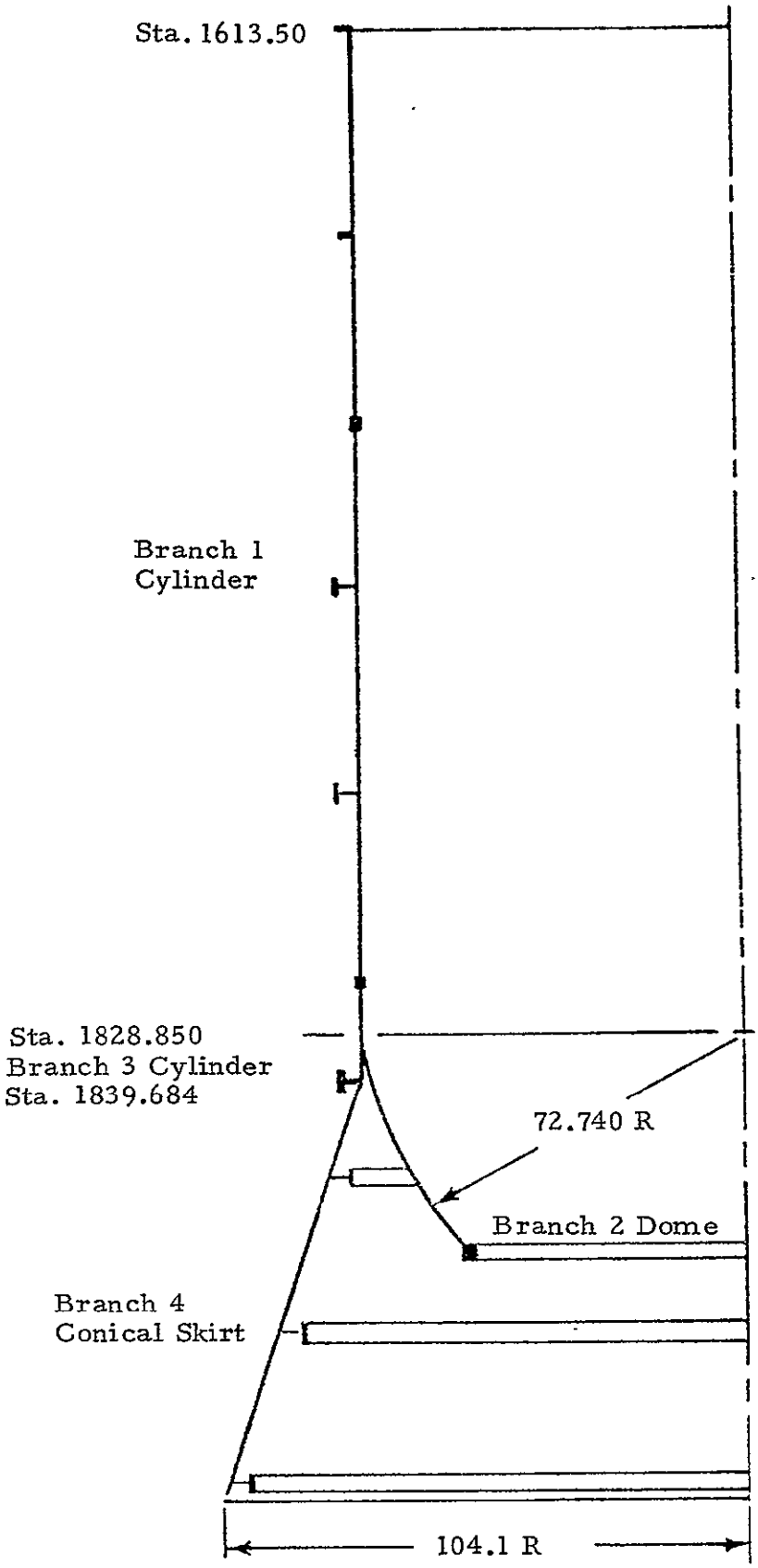

Fig. 3-1 - STAGS SRB Model Configuration, Basic Geometry

conical skirt. The tee-rings and clevis joints are included on Branch 1 and the heavy nozzle attach ring on Branch 2. The large reinforcing tee-ring at the cone-cylinder intersection is included on Branch 3. The three internal rings and the longitudinal stiffeners are included on the skirt as well as the holddown posts and actuator support brackets. The heavier primary stiffeners that tie into the rings at the aft end of the stiffeners are modeled as discrete stiffeners and the lighter intermediate stiffeners are smeared into the skin. The skin then becomes orthotropic with increased stiffness in the longitudinal direction. This maintains the structural stiffness in the model but reduces the number of grid points required in the circumferential direction. This model has 3944 nodes and 6587 equations.

The variation in wall thickness in Branches 2 and 4 are input using Subroutine WALL. The subroutine for inputting stiffeners off the gridlines has not been completed and checked out for STAGS C, so the holddown post diagonal members had to be input point-by-point on the gridlines. The stiffness properties were prorated between the affected nodes.

Two SRB math models are used for the cavity collapse analyses. They are designated as the "original" and the "rotated" model. The "original" SRB math model used for the analyses is oriented such that the $\pm Y_B$ plane is taken as the model plane of symmetry (Ref. MSFC 14A00305). The (+) Y_B is considered 0 deg, the keel side, and (-) Y_B as the 180 deg reference, the lee side for the pressure loading. In this orientation the skirt holddown posts are located at 60 and 120 deg, see Fig. 3-2. Another SRB model has been constructed in which the plane of symmetry has been rotated 90 deg so that the $\pm Z_B$ plane is taken as the plane of symmetry. This model is designated as the "rotated model." In this configuration the holddown posts are located at 30 and 150 deg. The 0 deg reference in this model is also considered the keel side. This configuration is shown in Fig. 3-3. The total number of rows and columns has been held constant for both models with the only changes being made in the nodal column locations.

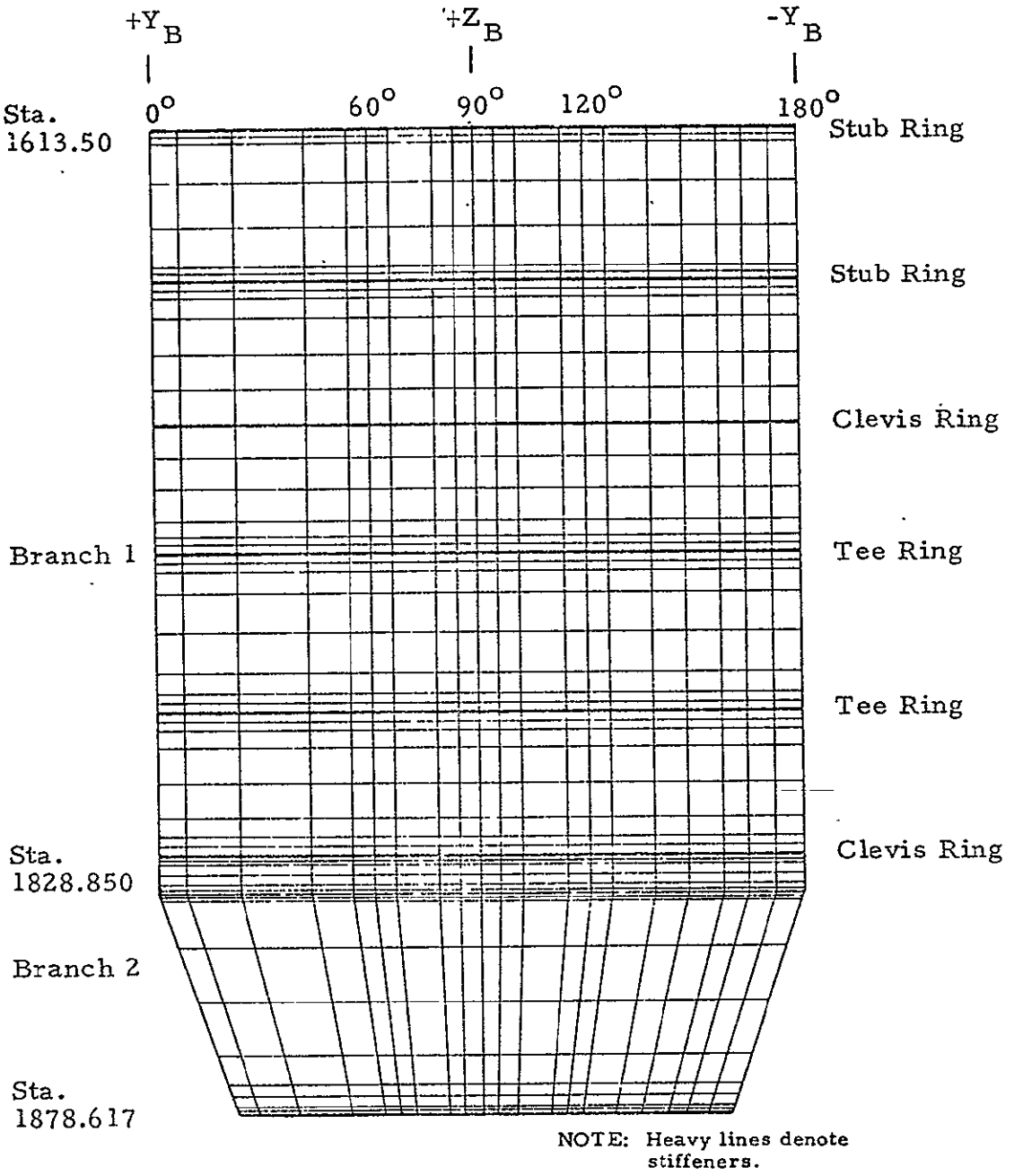

Fig. 3-2a - Original Model Branches 1 and 2: Grid Layout

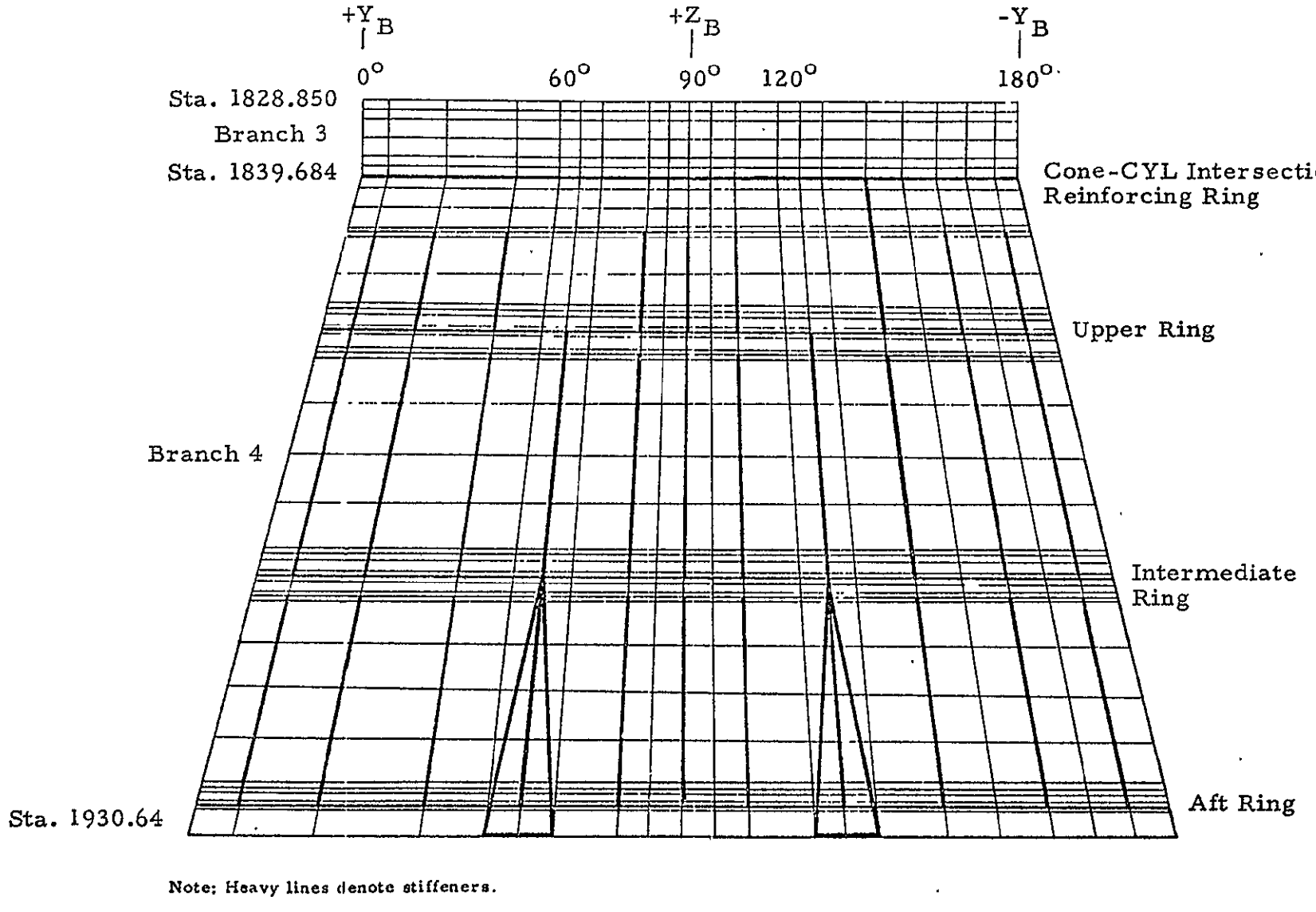

Fig. 3-2b – Original Model Branches 3 and 4: Grid Layout

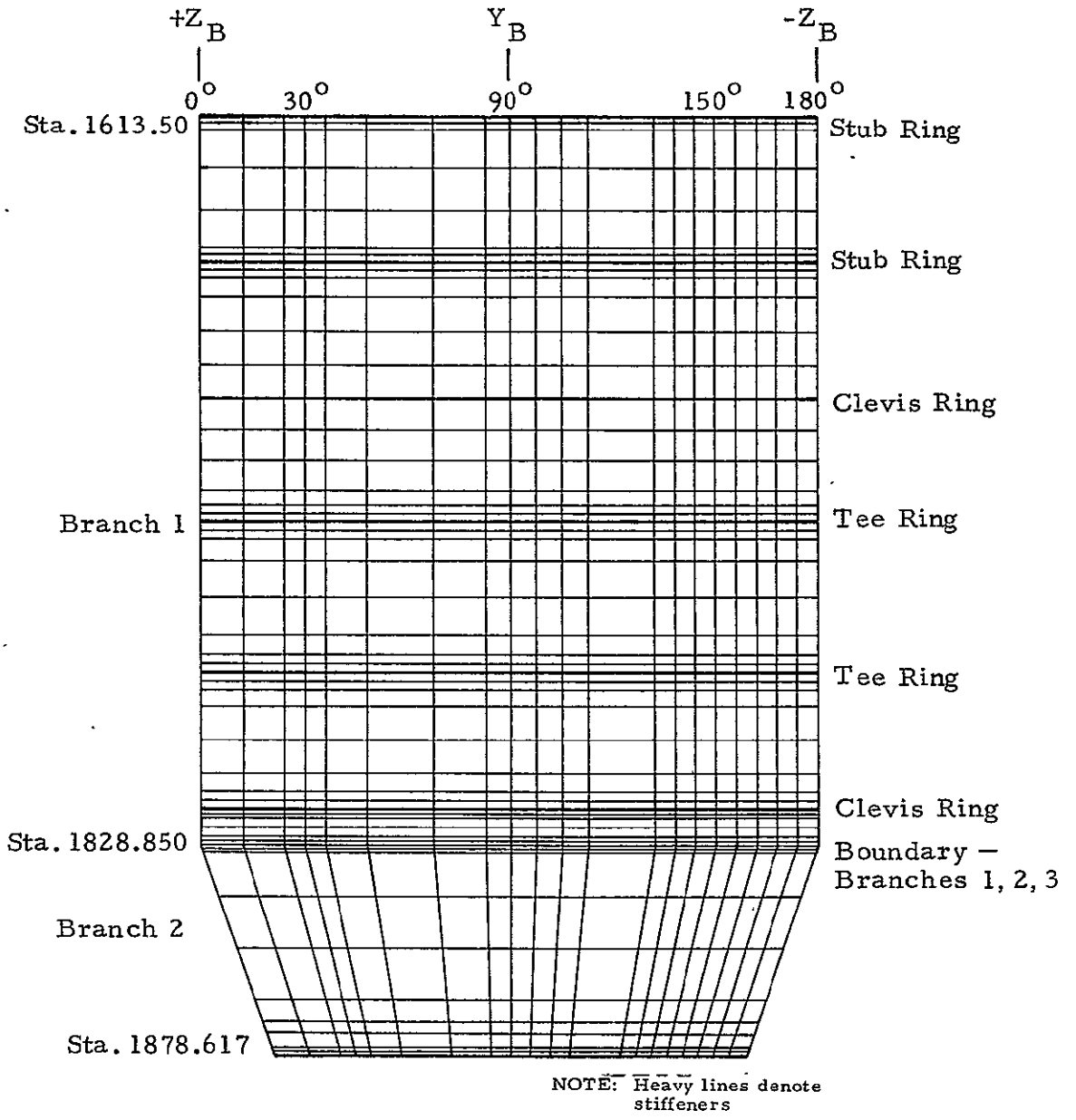

Fig. 3-3a - Rotated Model Branches 1 and 2: Grid Layout

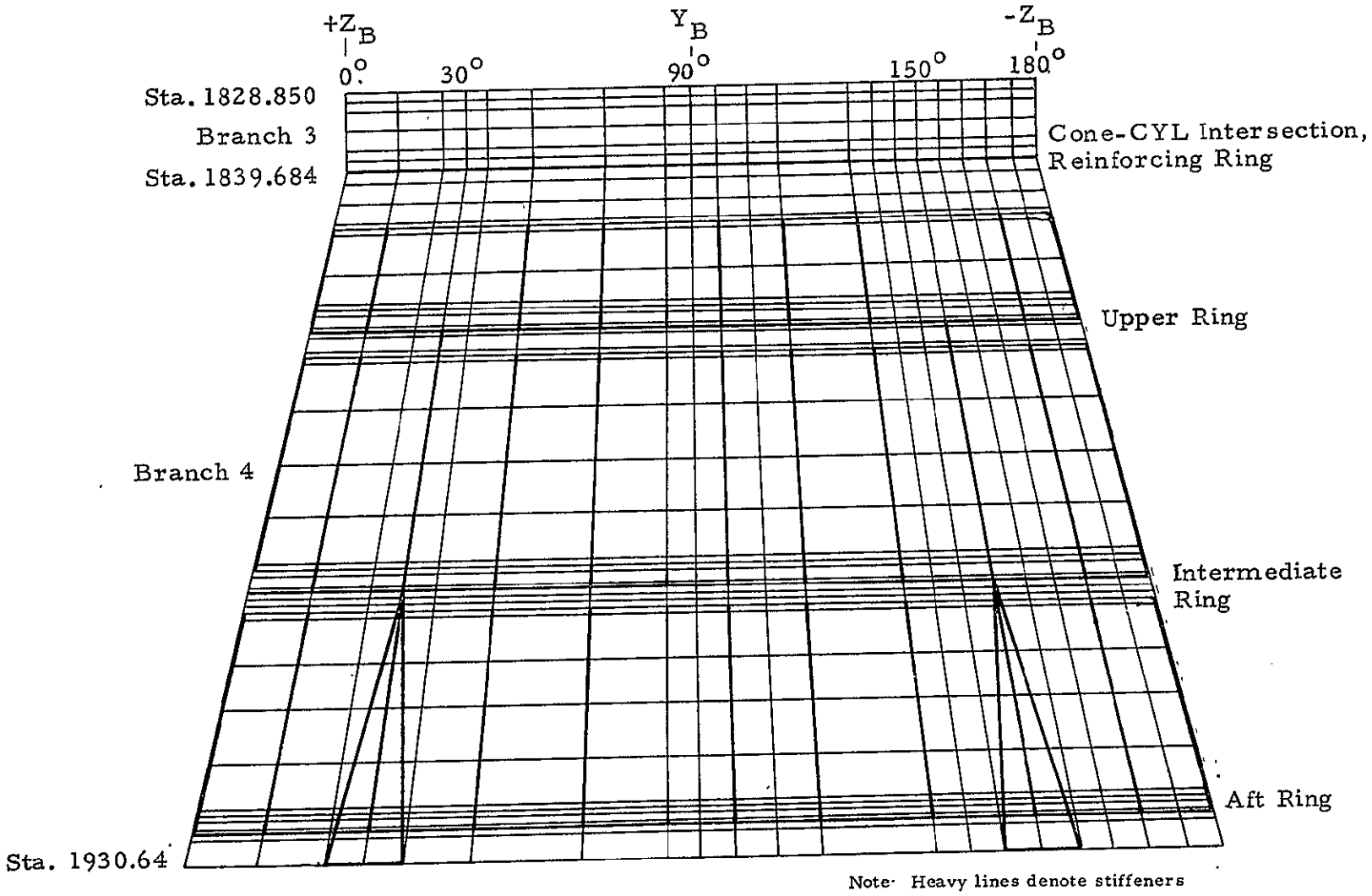

Fig. 3-3b - Rotated Model, Branches 3 and 4: Grid Layout

The reference surface for each branch in the model was assumed to be the outside skin surface. This was chosen to simplify the data input in the skirt branch and reduce the possibility of having input data errors. The outside skin surface of the conical skirt is a constant radius at any given longitudinal station; while the inside surface is stepped for the changing thickness in both the longitudinal and circumferential directions.

Tables 3-1 and 3-2 are listings of the WALL subroutine for the original and rotated models, respectively. The variation of wall thickness versus X and Y coordinates for Branches 2 and 4 and the smeared stiffener data for Branch 4 are given. Tables 3-3 and 3-4 are the corresponding additional STAGS C input data listings for a linear analysis for both models, respectively. Refer to the STAGS C user's manual for interpretation of the data listings. Note the ordered sequence of the branches and the interconnection of the node numbering sequences from one branch to another. This is the most efficient sequence for model accuracy and computer run time. The results of the parameter and grid spacing studies reported in Section 2 were used in determining the nodal locations for the model.

3.3 MODEL RUN TIMES

Typical run times on the NASA-MSFC Univac 1108 system for a linear analysis using this model was 20 minutes CPU and 13 minutes I/O for a total time charge of 33 minutes. A bifurcation buckling analysis to determine the first eigenvalue and mode shape took 38 minutes CPU and 40 minutes I/O.

3.4 MATERIAL PROPERTIES

The material properties used in the model and the allowable stress values for checking the results are given in Table 3-5 for both the D6AC steel motor case material (Branches 1, 2 and 3) and the 2219 aluminum skirt structure (Branch 4).

Table 3-1

WALL SUBROUTINE LISTING, ORIGINAL MODEL ($\pm Y_B$)

```
@FOR,UAS WALL,WALL
HSA -E3 -10/16/76-00:57:58 (0,1)
-47
C   -- SEE JP SECTIONAL PROPERTIES IN DATA STATEMENTS
C      COL = COLUMN LOCATIONS ALONG CIRCUMFERENCE
C      ROW = ROW-SECTION LOCATIONS ALONG LENGTH (NOT NECESSARILY ROW NO.)
C      THICK = THICKNESS FOR SECTIONS ACCORDING TO (ROW,COL)
C      ISTF = NO. OF STIFFENERS IN COLUMN SECTION
C      XSTF = BEGINNING AND ENDING ROWS FOR SMEARED STIFFENERS
C
C
      DIMENSION ISTF(8),XSTF(6)
      DIMENSION COL(17),ROW(14)
      DIMENSION THICK(16,14)
      DATA COL/0.0,7.5,22.5,42.0,54.0,60.0,66.0,78.0,90.0,102.0,114.0,
     1         120.0,126.0,138.0,157.5,172.5,180.0/
      DATA ROW/0.0,7.723,8.25,18.006,18.5,24.006,24.5,51.481,52.0,57.481
     1        ,59.0,83.39,83.9,90.956/
      DATA THICK/16*1.375,2*0.9,2*0.9875,2*1.375,4*0.9875,2*1.375,.9875
     2,0.9875,2*0.90,
     32*0.425,2*0.6,2*1.375,4*0.6,2*1.375,.60,0.6,2*0.425,
     42*0.4625,2*0.55,2*1.375,4*0.55,2*1.375,.55,.55,2*0.4625,
     54*0.5,2*1.375,4*0.5,2*1.375,4*.50,
     62*0.4625,0.4685,0.5,2*1.375,0.5,2*0.4625,.5,2*1.375,.50,.4685,2*
     60.4625,
     72*0.425,0.437,0.5,2*1.375,0.5,2*0.425,0.5,2*1.375,.5,.437,2*.425,
     92*0.4625,0.4685,0.5,2*1.375,0.5,2*0.4625,0.5,2*1.375,0.5,0.4685,
     $2*0.4525,
     94*0.5,2*1.375,4*0.5,2*1.375,4*0.5,
     13*0.4525,0.5,2*1.375,0.5,2*0.4625,0.5,2*1.375,0.5,3*0.4525,
     13*0.425,0.5,2*1.375,0.5,2*0.425,0.5,2*1.375,0.5,3*0.425,
     23*0.4525,0.5,2*1.375,0.5,2*0.4625,0.5,2*1.375,0.5,3*0.4525,
     34*0.5,2*1.375,4*0.5,2*1.375,4*0.5,
     44*0.5,2*1.375,4*0.5,2*1.375,4*0.5/
      DATA ISTF/1,2,3,2,0,0,2,2/
      DATA XSTF/7.723,18.006,24.006,51.481,57.481,83.390./
      DIMENSION DROW(11),DTHICK(11)
      DATA DROW/90.0,91.086,92.174,101.872,113.478,125.185,
     1128.0,130.0,131.0,132.0,133.171/
      DATA DTHICK/6*0.362,0.42,0.6,0.9,1.75,3.0/
C
C        CHANGE THIS CARD FOR EXECUTION OF STAGS  FOR 4 BRANCHES
C
      IF(IBRNCH.EQ.4) GO TO 75
      IF(IBRNCH.EQ.2) GO TO 76
      RETURN
   76 CONTINUE
      ICFB=3
      DO 71 I=1,11
      TL(I)=DTHICK(I)
      IF((X-DROW(I)).LT.0.001) GO TO 72
   71 CONTINUE
   72 Z=TL(I)/2.0
      EX3(I)=0.3E8
      EY3(I)=0.3E8
```

Table 3-1 (Continued)

```
      U21(1)=0.33
      S3(1)=0.11E8
      ZET3(1)=0.0
      RHO3(1)=0.3
      LAYS=1
      LSTRS=0
      ISTFF=0
      IPRM=0
      RHOA=0.0
      RETURN
   75 CONTINUE
      ICFB=3
      LAYS=1
      LSTRS=0
      IPRM=0
      IF((X.GT.0.0).OR.(Y.GT.0.0)) GO TO 5
      WRITE(6,51) COL
   51 FORMAT(' COL',17F7.1)
      WRITE(6,52) ROW
   52 FORMAT(' ROW',16F7.4)
      WRITE(6,53)((THICK(J,I),J=1,16),I=1,14)
   53 FORMAT(' THICK',16F7.4)
    5 CONTINUE
      NROW=14
      NCOL=17
      DO 1 I=1,NCOL
      ICOL=I
      IF( (Y.GE.COL(I)).AND.(Y.LT.COL(I+1)) ) GO TO 3
    1 CONTINUE
    3 CONTINUE
C     ICOL IS THE COLUMN NO. OF Y
      DO 2 I=1,NROW
      IROW=I
    2 IF((X.GE.ROW(I)).AND.(X.LT.ROW(I+1)))GO TO 4
    4 CONTINUE
C     IROW IS THE ROW SECTION NO. OF X (NOT NECESSARILY THE ROW NUMBER)
      EX1=10.5E6
      EY1=10.5E6
      XN1=0.3
      E1=EX1
      U1=XN1
      G=EX1/(2.*(1.+XN1))
      ZET2=0.0
      IC1=ICOL
      IC2=ICOL-1
      IF(IC1.EQ.1)IC2=1
      IF(IC1.EQ.17)IC1=16
C     AT=0.5*(THICK(IC1,IROW)+THICK(IC2,IROW))
      A=(COL(ICOL+1)-COL(ICOL))/(COL(ICOL+1)-COL(ICOL-1))
      B=(COL(ICOL)-COL(ICOL-1))/(COL(ICOL+1)-COL(ICOL-1))
      AT=1.0*(A*THICK(IC1,IROW)+B*THICK(IC2,IROW))
      Z=-AT/2.
C     THIS COMPLETES CALC. FOR MONOCOQUE SHELL
C     NOW ADD IN SMEARED STIFFENERS
C     MOVE THIS CARD UP
C
```

Table 3-1 (Concluded)

```
C
C
      III=1
      JK1=0
      A1=1.193
      SII=0.52424
      S1=2.6903E6
      EZ1=-1.780
      EZ21=-2.453
C
C
      D1=0.0
      TL(1)=AT
      EK3(1)=EK1
      EY3(1)=EY1
      U21(1)=XNI
      G3(1)=G
      ZET3(1)=0.0
      RHO3(1)=0.0
      IF((X.GE.XSTF(1)).AND.(X.LE.XSTF(2)))GO TO 10
      IF((X.GE.XSTF(3)).AND.(X.LE.XSTF(4)))GO TO 10
      IF((X.GE.XSTF(5)).AND.(X.LE.XSTF(6)))GO TO 10
      ISTFF=0
      GO TO 50
   10 IC=ICOL
      ISTFF=1
      IF(ICOL.GT.9)IC=17-ICOL
C---- IC LOCATES COLUMN-SECTION NUMBER
      ID=ICOL-1
      IF(ID.GT.8)ID=17-ID
      IF(( ICOL.EQ.1).OR.(ICOL.EQ.17)) GO TO 20
      IF(  (ISTF(IC)+ISTF(ID)).EQ.0) GO TO 21
      D1=1.0*(COL(ICOL+1)-COL(ICOL-1)) /(ISTF(IC)+ISTF(ID))
      GO TO 21
   20 D1= (COL(2)-COL(1))/1.0 *ISTF(1)
   21 CONTINUE
      NSTI=1
      ISMN(1)=24
      ISMD(1)=1
      SMSP(1)=D1
      SMAVG(1)=0.0
      IF( ABS(Y- 78.00).LT.0.05) D1= 0.5*( 84.00- 66.00)/1.50
      IF( ABS(Y- 84.00).LT.0.05) D1= 0.5*( 90.00- 78.00)/1.00
      IF( ABS(Y- 90.00).LT.0.05) D1= 0.5*( 96.00- 84.00)/1.00
      IF( ABS(Y- 96.00).LT.0.05) D1= 0.5*(102.00- 90.00)/1.00
      IF( ABS(Y-102.00).LT.0.05) D1= 0.5*(114.00- 96.00)/1.50
      IF( ABS(Y-138.00).LT.0.05) D1= 0.5*(147.75-126.00)/1.75
      IF( ABS(Y-147.75).LT.0.05) D1= 0.5*(157.75-138.00)/1.50
      IF( ABS(Y-157.50).LT.0.05) D1= 0.5*(165.00-147.75)/1.25
      IF( ABS(Y-165.00).LT.0.05) D1= 0.5*(172.50-157.50)/1.00
      IF( ABS(Y-172.50).LT.0.05) D1= 0.5*(180.00-165.00)/1.00
   50 CONTINUE
C  50 WRITE(6,53) X,Y,IC1,IC2,AT,IC,ID,D1
      IF(D1.LT.0.01)ISTFF=0
   53 FORMAT(' ',2(E14.6,2X),2I6,2X,E14.6,2I6,2X,F14.6)
      RETURN
```

Table 3-2

WALL SUBROUTINE LISTING, ROTATED MODEL ($\pm Z_B$)

```
WFOR,GWS WALL,WALL
HSA  C3 -10/16/76-03:39:21  (0,1)
-47
C     SET UP SECTIONAL PROPERTIES IN DATA STATEMENTS
C     COL = COLUMN LOCATIONS ALONG CIRCUMFERENCE
C     ROW = ROW SECTION LOCATIONS ALONG LENGTH (NOT NECESSARILY ROW NO.)
C     THICK = THICKNESS FOR SECTIONS ACCORDING TO (ROW,COL)
C     ISTF = NO. OF STIFFENERS IN COLUMN SECTION
C     XSTF = BEGINNING AND ENDING ROWS FOR SMEARED STIFFENERS
C
C
C
      DIMENSION ISTF(20),XSTF(6)
      DIMENSION COL(21),ROW(14)
      DIMENSION THICK(20,14)
      DATA COL/0.0,12.0,24.0,30.0,36.0,48.0,67.50,82.5,90.0,97.5,105.0,
     1114.5,132.0,138.0,144.0,150.0,156.0,162.0,168.0,174.0,180.0/
      DATA ROW/0.0,7.723,8.25,18.006,18.5,24.006,24.5,51.481,52.0,57.481
     1        ,58.0,83.39,83.9,90.956/
      DATA THICK/ 20*1.375,
     22*.9875,2*1.375,2*.9875,5*.9,3*.9875,2*1.375,4*.9875,
     32*.6,2*1.375,2*.6,5*.425,3*.6,2*1.375,4*.6,
     42*.55,2*1.375,2*.55,5*.4625,3*.55,2*1.375,4*.55,
     52*.5,2*1.375,10*.5,2*1.375,4*.5,
     6.4625,.5,2*1.375,.5,7*.4625,2*.5,2*1.375,2*.5,2*.4625,
     7.425,.5,2*1.375,.5,.437,5*.425,.437,2*.5,2*1.375,2*.5,2*.425,
     8.4625,.5,2*1.375,.5,.4685,5*.4625,.4685,2*.5,2*1.375,2*.5,2*.4625,
     92*.5,2*1.375,10*.5,2*1.375,4*.5,
     1.4625,.5,2*1.375,.5,7*.4625,2*.5,2*1.375,2*.5,2*.4625,
     1.425,.5,2*1.375,.5,7*.425,2*.5,2*1.375,2*.5,2*.425,
     2.4625,.5,2*1.375,.5,7*.4625,2*.5,2*1.375,2*.5,2*.4625,
     32*.5,2*1.375,10*.5,2*1.375,4*.5,
     42*.5,2*1.375,10*.5,2*1.375,4*.5 /
      DATA ISTF/2*2,2*0,2,3,2,4*1,3,2*1,2*0,4*1 /
      DATA XSTF/7.723,18.006,24.006,51.481,57.481,83.390 /
      DIMENSION DROW(11),DTHICK(11)
      DATA DROW/90.0,91.066,92.174,101.872,113.478,125.185,
     1128.0,130.0,131.0,132.0,133,171/
      DATA DTHICK/6*0.362,0.42,0.6,0.9,1.75,3.0/
C
C       CHANGE THIS CARD FOR EXECUTION OF STAGS  FOR 4 BRANCHES
C
      IF(IBRNCH.EQ.4) GO TO 75
      IF(IBRNCH.EQ.2) GO TO 76
      RETURN
   76 CONTINUE
      ICFB=3
      DO 71 I=1,11
      TL(I)=DTHICK(I)
      IF((X-DROW(I)).LT.0.001) GO TO 72
   71 CONTINUE
   72 Z=TL(I)/2.0
      EX3(I)=0.3E8
      EY3(I)=0.3E8
      U21(I)=0.33
      G3(I)=0.11E8
```

ORIGINAL PAGE IS
OF POOR QUALITY

Table 3-2 (Continued)

```
      ZET3(1)=0.0
      RHO3(1)=0.0
      LAYS=1
      LSTRS=0
      ISTFF=0
      IPRW=0
      RHOA=0.0
      RETURN
   75 CONTINUE
      ICFB=3
      LAYS=1
      LSTRS=0
      IPRW=0
      IF((X.GT.0.0).OR.(Y.GT.0.0)) GO TO 5
      WRITE(6,61) COL
   61 FORMAT(' COL',11F7.1)
      WRITE(6,62) ROW
   62 FORMAT(' ROW',16F7.4)
      WRITE(6,60)((THICK(J,I),J=1,20),I=1,14)
   60 FORMAT(' THICK',20F6.3)
    5 CONTINUE
      NROW=14
      NCOL=21
      DO 1 I=1,NCOL
      ICOL=1
      IF( (Y.GE.COL(I)).AND.(Y.LT.COL(I+1)) ) GO TO 3
    1 CONTINUE
    3 CONTINUE
C     ICOL IS THE COLUMN NO. OF Y
      DO 2 I=1,NROW
      IROW=1
      IF((X.GE.ROW(I)).AND.(X.LT.ROW(I+1)))GO TO 4
    2 CONTINUE
    4 CONTINUE
C     IROW IS THE ROW SECTION NO. OF X (NOT NECESSARILY THE ROW NUMBER)
      EX1=10.5E6
      EY1=10.5E6
      XN1=0.3
      E1=EX1
      U1=XN1
      G= EX1/(2.*(1.+XN1))
      ZET2=0.0
      IC1=ICOL
      IC2=ICOL-1
      IF(IC1.EQ.1)IC2=1
      IF(IC1.EQ.21) IC1=20
C     AT=0.5*(THICK(IC1,IROW)+THICK(IC1,IROW))
      A=(COL(ICOL+1)-COL(ICOL))/(COL(ICOL+1)-COL(ICOL-1))
      B=(COL(ICOL)-COL(ICOL-1))/(COL(ICOL+1)-COL(ICOL-1))
      AT=1.0*(A*THICK(IC1,IROW)+B*THICK(IC2,IROW))
      Z=-AT/2.
C     THIS COMPLETES CALC. FOR MONOCOQUE SHELL
C     NOW GO IN SMEARED STIFFENERS
C     MOVE THIS CARD UP
C
C
```

Table 3-2 (Concluded)

```
      III=1
      JK1=0
      A1=1.140
      SII=0.52424
      S1=2.6903E6
      EZ1=-1.780
      EZZ1=-2.450

      D1=0.0
      TL(1)=AT
      EX3(1)=EX1
      EY3(1)=EY1
      U21(1)=XN1
      G3(1)=G
      ZET3(1)=0.0
      RHO3(1)=0.0
      IF((X.GE.XSTF(1)).AND.(X.LE.XSTF(2)))GO TO 10
      IF((X.GE.XSTF(3)).AND.(X.LE.XSTF(4)))GO TO 10
      IF((X.GE.XSTF(5)).AND.(X.LE.XSTF(6)))GO TO 10
      ISTFF=0
      GO TO 50
   10 IC=ICOL
      ISTFF=1
      IC LOCATES COLUMN SECTION NUMBER
      ID=ICOL-1
      IF((ICOL.EQ.1).OR.(ICOL.EQ.21)) GO TO 20
      IF(  (ISTF(IC)+ISTF(ID)).EQ.0)  GO TO 21
      D1=1.0*(COL(ICOL+1)-COL(ICOL-1)) /(ISTF(IC)+ISTF(ID))
      GO TO 21
   20 IF(ICOL.EQ.1) D1=(COL(2)-COL(1))/ISTF(1)
      IF(ICOL.EQ.21)D1=(COL(21)-COL(20))/ ISTF(20)
   21 CONTINUE
      NSTI=1
      ISMN(1)=24
      ISMD(1)=1
      SMSP(1)=D1
      SMANG(1)=0.0
   50 CONTINUE
      WRITE(6,63) X,Y,IC1,IC2,AT,IC,ID,D1
      IF(D1.LT.0.01) ISTFF=0
   63 FORMAT(' ',2(E14.6,2X),2I6,2X,E14.6,2I6,2X,E14.6)
      RETURN
```

Table 3-3

STAGS C INPUT DATA LISTING, ORIGINAL MODEL ($\pm Y_B$)

```
STAGS INPUT DATA.

STAGS C DETAIL SRB MODEL
    0    4    4    3    0    0
   42   21   11   21    7   21   38   21
    1    6    3    3    3    0    4
    2    1    0    0    1    0    4
    3    1    0    0    1    0    4
    4    6   37   72   24    0    4
    1    3    2    1
    1    3    3    1
    3    3    4    1
         1.        0.         1.
    5    1    0    0
        .3   215.35        .0       180.        73.
   -1   -1
        0.0        2.5       5.0       16.      28.22     39.22     41.72     44.22
   46.72     49.22     54.22     64.23     74.23     84.24     93.24    102.25
  111.25    115.75    118.00    120.26    123.01    125.76    131.27    142.27
  153.27    158.77    161.52    164.28    166.78    169.28    174.29    184.29
  194.29    199.30    201.80    204.30    205.68    207.06    209.82    212.58
  213.96    215.35
        0.0       7.5      22.5      42.0        54.        60.        66.        78.
   84.        90.        96.       102.       114.       120.       126.       138.
  147.75    157.5     165.      172.5      180.
    2    4    6    4
    0    1
    1    3    4    0       30.E6      11.E6       .28
    .546      2.105     -1.045      2.105     -1.046     -2.135      .546     -2.105
   -6.7      1.415      9.899        .0       6.649
    1    0    4    0       30.E6      11.E6       .28
   3.85      1.925        .1       1.825        .1      -1.825     3.85      -1.825
   1.993     5.592      1.621        .0        .0137       .0       1.975
    1    0    1    0       30.E6      11.E6       .28
   1.484      .3
   -.971     -.1646      .5737       -.0        .015       .0        .345
    3    1    1   21
    3    8    1   21
    1   14    1   21
    2   20    1   21
    2   28    1   21
    1   36    1   21
    0    1    1    1
    3    3
    1    1       -.25
    .52       30.E6        .33       30.E6      11.E6        .0        .28
    7    1
  90.0      133.171     0.0       180.0      73.0
   -1   -1
   90.       91.095     92.174    101.872    113.478     126.      128.      130.
  131.      132.      133.171
```

Table 3-3 (Continued)

```
          STAGS INPUT DATA.   PAGE   2

*         *         *         *         *         *         *         *
 84.0      93.0      96.0     102.0     114.0     120.0     126.0     138.0
147.75    157.5     165.0     172.5     180.0
     6     4         3         4
     0     1
     1     3         4         3        30.E6     11.E6      .28
 2.523     -3.139    3.2996   -2.5392   -2.523    0.139     -0.2996   2.5092
12.577    13.5321   13.237    2.3088    21.025
     1    11         1        21
     0     1         1         1
     1     3
     5     1         0         3
          .0        10.49      .0       180.      73.
     1     1
          0.0       1.311     2.622     5.245     7.867     9.178     10.49
          0.0       7.5       22.5      42.0      54.       60.       66.       78.
          84.       90.       96.       102.      114.      120.      126.      138.
        147.75    157.5     165.      172.5     180.
     6     4         6         4
     0     1
     1     3         4         3        30.E6     11.E6      .28
    -5.625    1.425    -5.625    1.425    5.625     .0        .0        .0
     8.571    57.56     3.833     .0       1.94      .0       2.095
     1     7         1        21
     0     1         1         1
*         *         *         *         *         *         *         *
     3     0
     1     1        -.25
          .52       30.E6      .33      30.E6     11.E6
     6     1         0         3         0         3
          .0        90.956     .0       180.      73.       104.1
     1     1
          .0        1.5       3.9       7.25      7.723     8.25      12.96     17.5
    18.006    18.5      20.5      21.006    21.5      23.5      24.006    24.5
    30.87     37.74     44.61     50.9      51.481    52.       54.       54.481
    55.       57.       57.481    58.       63.95     70.43     75.91     82.9
    83.39     83.9      86.       86.536    87.0      90.956
          .0        7.5       22.5      42.       54.       60.       66.       78.
          84.       90.       96.       102.      114.      120.      126.      138.
        147.75    157.5     165.      172.5     180.
     6     4         3         4
     1     1
    -6874.     1         1        12        16
     1     3         4         3        10.E6     4.E6
    -7.089     5.297    -8.849     .087     -7.969    2.692    -.639     .216
     6.924    68.722    17.3      19.61     .326     -1.37     -4.357
     1     3         4         3        10.E6     4.E6
    -7.586     5.465    -9.346     .255     -8.466    2.860    -.639     .216
     6.726    84.243    18.469    25.082     .275     -1.37     -4.362
     1     3         4         3        10.E6     4.E6
    -8.662     6.392   -10.382     .408     -9.522    3.253    -.539     .216
    11.276   142.895    33.596    41.681     1.477    -2.093    -6.197
```

Table 3-3 (Continued)

STAGS INPUT DATA. PAGE 3

```
*       *       *       *       *       *       *       *
  1   3   0   0   10.E6    4.E6
 13.963   285.993   74.500   59.830   226.   -1.474   4.363
  1   3   4   0   10.E6    4.E6
 -2.70    1.25    -2.70    -1.25    -2.70    0.0     -.5      0.0
 1.858    .833     .656     .0       .124     .0     -2.299
  1   3   4   3   10.E6    4.E6
 -2.70    1.25    -2.70    -1.25    -2.70    .0      -1.      0.0
 2.713    1.172    .994     .0       .421     .0     -2.174
  1   3   4   0   10.E6    4.E6
 2.625    4.3      2.625    -4.3     -7.18    4.347   -7.18    -4.347
 24.562   183.801  167.060   .0      3.875    .0     -1.584
  1   3   3   3   10.E6    4.E6
 -9.772   1.0     -9.772    -1.     -1.372    .0
 8.4      49.39    4.895     .0       .7       .0     -5.572
  1   3   0   3   10.E6    4.E6
 10.18    5.495    13.573    .0      21.98     .0      1.272
  1   3   0   3   10.E6    4.E6
 14.12    14.662   18.827    .0      59.65     .0      1.765
  1   3   4   3   10.E6    4.E6
 1.895    -.643    1.394    -2.123   -2.366    .799   -1.996   -.684
 4.886    9.921    2.015    3.015    3.988     .0      .0
  1   3   0   0   10.E6    4.E6
 21.47    51.503   28.618    .0      114.47    .0     -2.683
  1   3   0   3   10.E6    4.E6
*       *       *       *       *       *       *       *
 25.42    85.511   33.888    .0      135.55    .0      3.177
  1   3   0   0   10.E6    4.E6
 16.715   62.267   8.705     .0      34.8      .0      3.343
  1   3   0   3   10.E6    4.E6
 17.717   74.155   9.228     .0      36.9      .0      3.543
  1   3   0   0   10.E6    4.E6
 4.973    26.185   2.588     .0      10.3      .0      3.976
  1   3   0   3   10.E6    4.E6
 14.909   78.555   7.765     .0      30.9      .0      3.976
  1   3   0   3   10.E6    4.E6
 11.022   71.413   5.741     .0      22.9      .0      4.406
  1   3   0   3   10.E6    4.E6
 19.274   169.753  10.039    .0      40.2      .0      5.143
  1   3   0   3   10.E6    4.E6
 6.425    56.583   3.345     .0      13.4      .0      5.143
  1   3   0   3   10.E6    4.E6
 27.865   288.483  14.513    .0      58.       .0      5.573
  1   3   0   3   10.E6    4.E6
 29.071   327.553  15.141    .0      60.6      .0      5.814
  1   3   0   3   10.E6    4.E6
 38.392   374.193  15.639    .0      63.3      .0      6.378
  1   3   4   3   10.E6    4.E6
 -2.7     3.7
 1.14     .524     .142      .0      .0477     .0     -2.281
 11   1   1  21
  1  12   1  21
```

Table 3-3 (Continued)

STAGS INPUT DATA. PAGE 4

2	24	1	21		
3	36	1	21		
4	38	5	7		
4	38	13	15		
5	2	5	12		
5	3	5	12		
5	4	5	12		
5	8	5	12		
5	13	5	12		
5	12	5	12		
7	16	5	12		
6	18	5	12		
6	20	5	12		
5	2	15	24		
5	3	15	24		
5	4	15	24		
8	6	12	36		
9	6	12	16		
10	6	16	18		
12	6	18	20		
13	6	20	24		
5	8	15	24		
5	13	15	24		
5	12	15	24		
8	14	12	36		
9	14	12	16		
10	14	16	18		
12	14	18	20		
13	14	20	24		
5	16	15	24		
5	18	15	24		
5	20	15	24		
5	2	27	36		
5	3	27	36		
5	4	27	36		
5	8	27	36		
5	10	27	36		
5	12	27	36		
5	16	27	36		
5	18	27	36		
5	20	27	36		
0	14	24	6	.277	-10.
0	14	25	6	1.349	-10.
0	15	26	6	1.330	-10.
0	15	27	6	.539	-10.
0	15	28	6	3.466	-10.
0	16	29	6	6.661	-10.
0	17	29	6	6.661	-10.
0	18	30	6	6.945	-10.
0	18	30	6	6.945	-10.

Table 3-3 (Continued)

STAGS INPUT DATA. PAGE 5

0	19	31	5	6.683	-10.		
0	20	31	6	6.683	-10.		
0	21	32	5	3.473	-10.		
0	21	33	5	.535	-10.		
0	21	34	5	1.393	-10.		
0	22	35	5	1.407	-10.		
0	22	36	5	.779	-10.		
0	22	37	5	2.369	-10.		
0	23	38	5	2.120	-10.		
0	14	24	5	.277	10.		
0	14	25	6	1.349	10.		
0	15	26	6	1.339	10.		
0	15	27	6	.539	10.		
0	15	28	6	3.466	10.		
0	16	29	7	6.661	10.		
0	17	29	6	6.661	10.		
0	18	30	7	6.945	10.		
0	18	30	6	6.945	10.		
0	19	31	7	6.683	10.		
0	20	31	6	6.683	10.		
0	21	32	7	3.473	10.		
0	21	33	7	.535	10.		
0	21	34	7	1.393	10.		
0	22	35	7	1.407	10.		
0	22	36	7	.779	10.		
0	22	37	7	2.369	10.		
0	23	38	7	2.120	10.		
0	14	25	14	1.349	-10.		
0	15	26	14	1.330	-10.		
0	14	24	14	.277	-10.		
0	15	27	14	.539	-10.		
0	15	28	14	3.466	-10.		
0	16	29	13	6.661	-10.		
0	17	29	14	6.661	-10.		
0	18	30	13	6.945	-10.		
0	18	30	14	6.945	-10.		
0	19	31	13	6.683	-10.		
0	20	31	14	6.683	-10.		
0	21	32	13	3.473	-10.		
0	21	33	13	.536	-10.		
0	21	34	13	1.393	-10.		
0	22	35	13	1.407	-10.		
0	22	36	13	.779	-10.		
0	22	37	13	2.369	-10.		
0	23	38	13	2.120	-10.		
0	14	24	14	.277	10.		
0	14	25	14	1.349	10.		
0	15	26	14	1.330	10.		
0	15	27	14	.539	10.		
0	15	28	14	3.466	10.		

Table 3-3 (Concluded)

STAGS INPUT DATA. PAGE 6

*	*	*	*	*	*	*	*
0	16	29	15	6.661	10.		
0	17	29	14	5.661	10.		
0	18	30	15	6.945	10.		
0	18	30	14	6.945	10.		
0	19	31	15	6.683	10.		
0	20	31	14	6.683	10.		
0	21	32	15	3.473	10.		
0	21	33	15	.536	10.		
0	21	34	15	1.393	10.		
0	22	35	15	1.407	10.		
0	22	36	15	.779	10.		
0	22	37	15	2.369	10.		
0	23	38	15	2.128	10.		
0	1	1	1				
1	0						

Table 3-4

STAGS C INPUT DATA LISTING, ROTATED MODEL ($\pm Z_B$)

```
BELT,OIL TPFS,ARTSKT
ELT007-RL:1870-10/16-03:42:15-1.0)
      STAGS C SRB ROTATED 90 DEG
  0    4    4    3    0    0
 42   21   11   21    7   21   38   21
  1    6    0    0    3    0    4
  2    1    0    0    1    0    4
  3    1    0    0    1    0    4
  4    6   40   72   25    0    4
  1    3    2    1
  1    3    3    1
  3    3    4    1
       1.        0.        1.
  5    1    0    0
       .0      215.35      .0      180.      73.
 -1   -1
       0.0       2.5       5.0      16.     28.22    39.22    41.72    44.22
     46.72     49.22     54.22     64.23     74.23    84.24    93.24   102.25
    111.25    115.75    118.00    120.26    123.01   125.76   131.27   142.27
    153.27    158.77    161.52    164.28    166.78   169.28   174.29   184.29
    194.29    199.30    201.80    204.30    205.68   207.06   209.82   212.58
    213.96    215.35
       .0        12.       24.       30.       36.      48.      67.5     82.5
      90.        97.5     105.      112.5     132.     138.     144.     150.
     156.       162.      168.      174.      180.
  2    4    6    4
  0    1
  1    0    4    0     30.E6     11.E6      .28
      .546      2.105    -1.046     2.105    -1.046   -2.105     .546    -2.105
      6.7       1.915     9.899      .0       5.649
  1    0    4    0     30.E6     11.E6      .28
     3.85       1.825      .1       1.825     .1      -1.825     3.85    -1.825
     8.993      5.692     1.621      .0       .0137     .0      1.975
  1    0    1    0     30.E6     11.E6      .28
     1.484      .0
      .971     -.1648     .5737      .0       .015      .0       .345
  3    1    1   21
  3    8    1   21
  1   14    1   21
  2   20    1   21
  2   28    1   21
  1   36    1   21
  0    1    1    1
  3    0
  1    1       -.26
      .52     30.E6      .33      30.E6     11.E6     .0       .28
  7    1    0    0
     90.0    133.171     0.0      180.0     73.0
 -1   -1
     90.0     91.086    92.174   101.872   113.478   126.     128.     130.
    131.      132.     133.171
      .0        12.       24.       30.       36.      48.      67.5     82.5
     90.        97.5     105.      112.5     132.     138.     144.     150.
    156.       162.      168.      174.      180.
  6    4    3    4
  0    1
```

ORIGINAL PAGE IS
OF POOR QUALITY

Table 3-4 (Continued)

1	0	4	0	30.E6	11.E6	.28			
2.523		-.139		.2996	-2.5092	-2.523	.139	-.2996	2.5092
12.577		13.5321		13.237	2.3088	21.825			
1	11	1	21						
0	1	1	1						
1	0								
5	1	0	0						
.0		10.49		.0	180.	73.			
-1	-1								
0.0		1.311		2.622	5.245	7.867	9.178	10.49	
.0		12.		24.	30.	36.	48.	67.5	82.5
90.		97.5		105.	112.5	132.	138.	144.	150.
156.		162.		168.	174.	180.			
6	4	6	4						
0	1								
1	0	4	0	30.E6	11.E6	.28			
5.625		1.425		5.625	-1.425	5.625	.0	.0	.0
8.571		57.56		3.833	.0	1.94	.0	2.095	
1	7	1	21						
0	1	1	1						
3	0								
1	1	-.26							
.52		30.E6		.33	30.E6	11.E6			
6	1	0	0	0	0				
.0		90.956		.0	180.	73.	104.1		
-1	-1								
.0		1.5		3.9	7.25	7.723	8.25	12.86	17.5
18.006		18.5		20.5	21.006	21.5	23.5	24.006	24.5
30.87		37.74		44.61	50.9	51.481	52.	54.	54.481
55.		57.		57.481	58.	63.95	70.43	76.91	82.9
83.39		83.9		86.	86.536	87.0	90.956		
.0		12.		24.	30.	36.	48.	67.5	82.5
90.		97.5		105.	112.5	132.	138.	144.	150.
156.		162.		168.	174.	180.			
6	4	3	4						
0	1								
1	0	4	0	10.E6	4.E6				
-7.089		5.297		-8.849	.087	-7.969	2.692	-.639	.216
6.924		68.722		17.3	19.61	.326	-1.37	-8.057	
1	0	4	0	10.E6	4.E6				
-7.586		5.465		-9.346	.255	-8.466	2.860	-.639	.216
6.726		84.243		18.469	25.082	.275	-1.37	-4.082	
1	0	4	0	10.E6	4.E6				
-8.662		6.092		-10.582	.408	-9.622	3.250	-.639	.216
11.276		142.896		33.596	41.681	1.477	-2.093	-6.197	
1	0	0	0	10.E6	4.E6				
13.960		285.990		74.500	68.830	226.	-1.474	4.363	
1	0	4	0	10.E6	4.E6				
-2.70		1.25		-2.70	-1.25	-2.70	0.0	-.5	0.0
1.858		.833		.656	.0	.124	.0	-2.299	
1	0	4	0	10.E6	4.E6				
-2.70		1.25		-2.70	-1.25	-2.70	.0	-1.	0.0
2.713		1.172		.994	.0	.421	.0	-2.174	
1	0	4	0	10.E6	4.E6				
2.625		4.3		2.625	-4.3	-7.18	4.347	-7.18	-4.347
24.562		183.801		167.050	.0	3.675	.0	-1.684	

Table 3-4 (Continued)

1	0	3	0	10.E6	4.E6				
-9.772		1.0		-9.772	-1.	-1.372	.0		
8.4		49.39		4.895	.0	.7	.0	-5.572	
1	0	0	0	10.E6	4.E6				
10.18		5.495		13.573	.0	21.98	.0	1.272	
1	0	0	0	10.E6	4.E6				
14.12		14.662		18.827	.0	58.65	.0	1.765	
1	0	4	0	10.E6	4.E6				
1.895		-.640		1.394	-2.123	-2.366	.799	-1.996	-.684
4.886		9.921		2.015	3.015	3.988	.0	.0	
1	0	0	0	10.E6	4.E6				
21.47		51.503		28.618	.0	114.47	.0	2.683	
1	0	0	0	10.E6	4.E6				
25.42		85.511		33.888	.0	135.55	.0	3.177	
1	0	0	0	10.E6	4.E6				
16.715		62.267		8.706	.0	34.8	.0	3.343	
1	0	0	0	10.E6	4.E6				
17.717		74.155		9.228	.0	36.9	.0	3.543	
1	0	0	0	10.E6	4.E6				
4.970		26.185		2.588	.0	10.3	.0	3.976	
1	0	0	0	10.E6	4.E6				
14.909		78.555		7.765	.0	30.9	.0	3.976	
1	0	0	0	10.E6	4.E6				
11.022		71.410		5.741	.0	22.9	.0	4.406	
1	0	0	0	10.E6	4.E6				
19.274		169.750		10.039	.0	40.2	.0	5.140	
1	0	0	0	10.E6	4.E6				
6.425		56.580		3.346	.0	13.4	.0	5.140	
1	0	0	0	10.E6	4.E6				
27.865		288.480		14.513	.0	58.	.0	5.573	
1	0	0	0	10.E6	4.E6				
29.071		327.550		15.141	.0	60.6	.0	5.814	
1	0	0	0	10.E6	4.E6				
30.392		374.320		15.830	.0	63.3	.0	6.078	
1	0	1	0	10.E6	4.E6				
-2.70		0.0							
1.14		.524		.142	.0	.0677	.0	-8.281	
1	0	2	0	10.E6	4.E6				
-2.70		1.25		-2.70	0.0				
.979		.416		.328	.0	.067	.0	-2.299	
11	1	1	21						
1	12	1	21						
2	24	1	21						
3	36	1	21						
4	38	3	5						
4	38	15	17						
25	1	5	12						
5	2	5	12						
5	6	5	12						
5	7	5	12						
5	8	5	12						
5	10	5	12						
5	12	5	12						
5	13	5	12						
5	19	5	12						
25	21	5	12						

Table 3-4 (Continued)

000167	000	25	1	15	24		
000168	000	5	2	15	24		
000169	000	8	4	12	36		
000170	000	9	4	12	16		
000171	000	10	4	16	18		
000172	000	12	4	18	20		
000173	000	13	4	20	24		
000174	000	5	6	15	24		
000175	000	5	7	15	24		
000176	000	5	8	15	24		
000177	000	5	10	15	24		
000178	000	5	12	15	24		
000179	000	5	13	15	24		
000180	000	8	16	12	36		
000181	000	9	16	12	16		
000182	000	10	16	16	18		
000183	000	12	16	18	20		
000184	000	13	16	20	24		
000185	000	5	19	15	24		
000186	000	25	21	15	24		
000187	000	25	1	27	36		
000188	000	5	2	27	36		
000189	000	5	6	27	36		
000190	000	5	7	27	36		
000191	000	5	8	27	36		
000192	000	5	10	27	36		
000193	000	5	12	27	36		
000194	000	5	13	27	36		
000195	000	5	19	27	36		
000196	000	25	21	27	36		
000197	000	0	14	24	4	.277	-10.
000198	000	0	14	25	4	1.349	-10.
000199	000	0	15	26	4	1.330	-10.
000200	000	0	15	27	4	.539	-10.
000201	000	0	15	28	4	3.466	-10.
000202	000	0	16	29	3	6.661	-10.
000203	000	0	17	29	4	6.661	-10.
000204	000	0	18	30	3	6.945	-10.
000205	000	0	18	30	4	6.945	-10.
000206	000	0	19	31	3	6.683	-10.
000207	000	0	20	31	4	6.683	-10.
000208	000	0	21	32	3	3.473	-10.
000209	000	0	21	33	3	.536	-10.
000210	000	0	21	34	3	1.393	-10.
000211	000	0	22	35	3	1.407	-10.
000212	000	0	22	36	3	.779	-10.
000213	000	0	22	37	3	2.369	-10.
000214	000	0	23	38	3	2.120	-10.
000215	000	0	14	24	4	.277	10.
000216	000	0	14	25	4	1.349	10.
000217	000	0	15	26	4	1.330	10.
000218	000	0	15	27	4	.539	10.
000219	000	0	15	28	4	3.466	10.
000220	000	0	16	29	5	6.661	10.
000221	000	0	17	29	4	6.661	10.
000222	000	0	18	30	5	6.945	10.

Table 3-4 (Concluded)

```
000223      000      0    18    30     4      6.945          10.
000224      000      0    19    31     5      6.683          10.
000225      000      0    20    31     4      6.683          10.
000226      000      0    21    32     5      3.473          10.
000227      000      0    21    33     5       .536          10.
000228      000      0    21    34     5      1.393          10.
000229      000      0    22    35     5      1.407          10.
000230      000      0    22    36     5       .779          10.
000231      000      0    22    37     5      2.369          10.
000232      000      0    23    38     5      2.120          10.
000233      000      0    14    25    16      1.349         -10.
000234      000      0    15    26    16      1.330         -10.
000235      000      0    14    24    16       .277         -10.
000236      000      0    15    27    16       .539         -10.
000237      000      0    15    28    16      3.466         -10.
000238      000      0    16    29    15      6.661         -10.
000239      000      0    17    29    16      6.661         -10.
000240      000      0    18    30    15      6.945         -10.
000241      000      0    18    30    16      6.945         -10.
000242      000      0    19    31    15      6.683         -10.
000243      000      0    20    31    16      6.683         -10.
000244      000      0    21    32    15      3.473         -10.
000245      000      0    21    33    15       .536         -10.
000246      000      0    21    34    15      1.393         -10.
000247      000      0    22    35    15      1.407         -10.
000248      000      0    22    36    15       .779         -10.
000249      000      0    22    37    15      2.369         -10.
000250      000      0    23    38    15      2.120         -10.
000251      000      0    14    24    16       .277          10.
000252      000      0    14    25    16      1.349          10.
000253      000      0    15    26    16      1.330          10.
000254      000      0    15    27    16       .539          10.
000255      000      0    15    28    16      3.466          10.
000256      000      0    16    29    17      6.661          10.
000257      000      0    17    29    16      6.661          10.
000258      000      0    18    30    17      6.945          10.
000259      000      0    18    30    16      6.945          10.
000260      000      0    19    31    17      6.683          10.
000261      000      0    20    31    16      6.683          10.
000262      000      0    21    32    17      3.473          10.
000263      000      0    21    33    17       .536          10.
000264      000      0    21    34    17      1.393          10.
000265      000      0    22    35    17      1.407          10.
000266      000      0    22    36    17       .779          10.
000267      000      0    22    37    17      2.369          10.
000268      000      0    23    38    17      2.120          10.
000269      000      0     1     1     1
000270      000      1     0

END LLT.

@XQT STAGS
```

Table 3-5
MATERIAL PROPERTIES

Property	Material	
	D6AC Steel	2219-T87 Aluminum
E (10^6), (psi)	30	10
ρ, (lb/in^3)	0.28	0.102
F_{tu}, (ksi)	195	63
F_{ty}, (ksi)	180	51

4. SRB CAVITY COLLAPSE LOAD ANALYSIS

4.1 SRB CAVITY COLLAPSE LOADS

The SRB mathematical model was analyzed for the nominal conditions of 85 ft/sec vertical velocity at water impact as specified in Revision D of the SRB loads document (Ref. 1). The distribution of the external pressure on the components of the SRB vehicle during cavity collapse are shown in Figs. 4-1a and 4-1b. These figures are reprints of data presented in Ref. 1 and show the pressure as a function of the wetted length along the keel side (ϕ = 0) and lee side (ϕ = 180) of the vehicle. The circumferential variations of these pressures on each component are described in functional form also. The keel and lee meridians may fall along any surface meridian of the SRB vehicle. For these analyses the lee and keel meridians were assumed to fall on cross sectional planes of symmetry ($\pm Y_B$ or $\pm Z_B$). Internal skirt and bulkhead pressure loads were determined from the hydrostatic pressures, P_h and P_l given in Ref. 1, and the functional circumferential distributions as specified in Fig. 4-1. The external circumferential cavity collapse distribution is shown in Fig. 4-1b. A constant internal motor case pressure of p = -1.65 psig, as determined from Ref. 1, was used in the analysis. This negative internal pressure is additive to the effects of the external pressure.

The SRB cavity collapse load for the 85/32/5 (VV/VH/θ) condition is being analyzed. This case was determined to be the maximum pressure differential for the nominal 85 ft/sec vertical impact velocity condition. This determination was made by comparing the external pressure to the internal skirt hydrostatic pressure for each condition. Since all of the load cases have the same distribution and vary in magnitude of pressure levels only, this rough test for maximum load case is valid. The pressure differential for this method is Δp = 148.5 for the 85/32/5 case. The load values

Cavity Collapse

SRM Case and SRB Aft Skirt Pressures

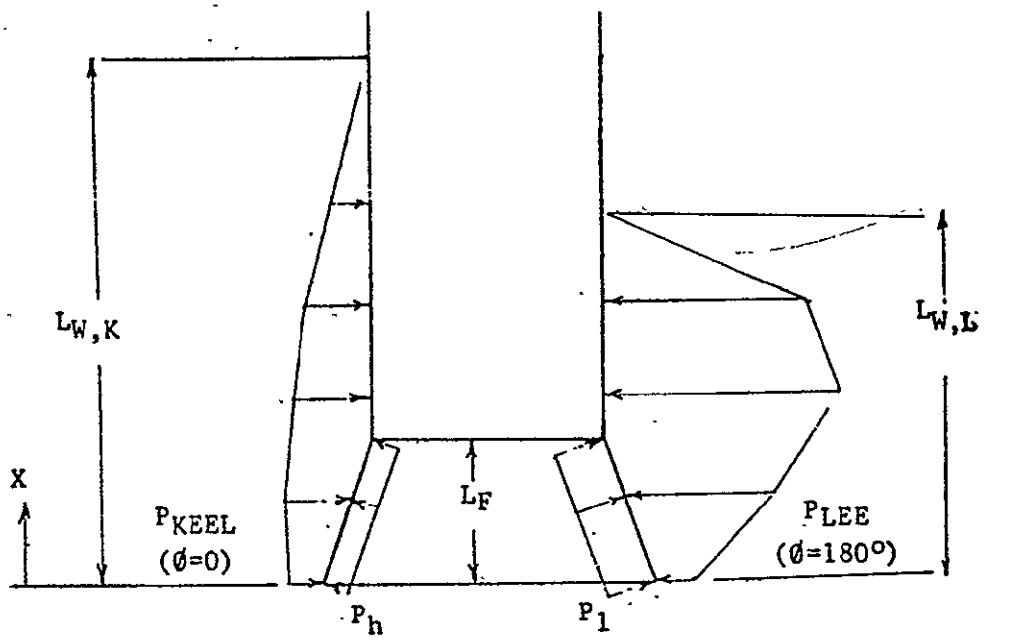

INTERNAL PRESSURES

SRM CASE

$P = P_{ULLAGE}$, UNIFORM

SRB AFT SKIRT

$P = P_h + \frac{1}{2}(1 - \cos \phi)(P_l - P_h)$

$0 \le X \le L_F$, $-180^\circ \le \phi \le 180^\circ$

EXTERNAL PRESSURES

CIRCUMFERENTIAL DISTRIBUTION

$P = P_{KEEL} + K_C (P_{LEE} - P_{KEEL})$, $0 \le X \le L_{W,L}$, $-180^\circ \le \phi \le 180^\circ$

$P = P_{KEEL}$, $L_{W,L} \le X \le L_{W,K}$, $-\phi_w \le \phi \le \phi_w$

K_C, SEE FIGURE V.C.III.2; $\phi_w = \cos^{-1}\left[\frac{2(X - L_{W,L})}{(L_{W,K} - L_{W,L})} - 1\right]$

LONGITUDINAL DISTRIBUTION

SEE FIGURES FOR P_{KEEL} & P_{LEE} VS. STATION

Fig. 4-1a - Cavity Collapse Pressure Distributions — SRM Case and Aft Skirt Pressures (Reprint from Ref. 1)

BULKHEAD PRESSURE

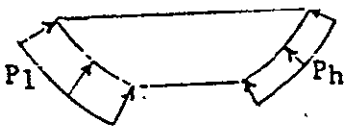

INTERNAL

$P = P_{ULLAGE}$ UNIFORM INTERNALLY

EXTERNAL

$$P = P_l + \tfrac{1}{2}(P_h - P_l)(1 - \cos \phi), \quad -180^\circ \le \phi \le 180^\circ$$

UNIFORM LONGITUDINALLY

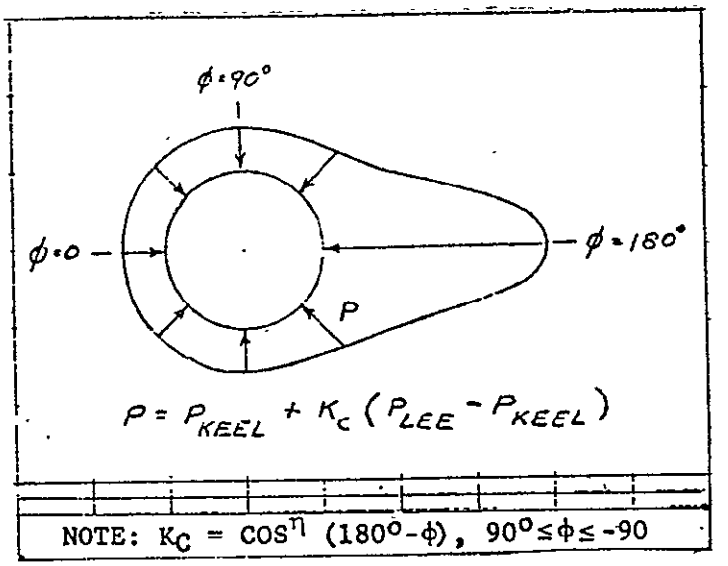

External Circumferential Distribution

Fig. 4-1b - Cavity Collapse Pressure Distributions — SRM Aft Bulkhead (Reprint from Ref. 1)

are taken from Ref. 1. The pressure factor, ratio of the maximum pressure to the maximum value given for the nominal distribution as shown in Ref. 1, is 1.176 for the 85/32/5 case. This factor is to be applied to the external pressure distribution only. Note no design factors have been applied to the loads in the analyses.

The nominal pressure distribution is to be modified by shifting the maximum pressure peak location for the lee side over a range of $\pm 1/4$ SRM diameter. This shift will account for uncertainties in the prediction of vehicle attitude and ocean conditions at water impact and cavity collapse. The fore and aft limits of the lee side distribution and the keel side distribution are unchanged for these shifts (Fig. 4-2).

The net pressure distribution for this load case is shown in Fig. 4-3 for several stations along the length of the vehicle. This distribution consists of the variable external cavity collapse pressure and constant internal SRM ullage pressure on Branches 1 and 2 of the model. The loading on Branches 3 and 4 consists of the variable internal and external cavity collapse pressure. Figures 4-3a, 4-3b and 4-3c show the net pressure distribution with the external cavity collapse pressure in the nominal position, shifted aft a distance equal to 1/8 the SRM diameter and shifted aft a distance equal to 1/4 the SRM diameter, respectively. All other values are constant for the three load distributions. The nozzle loads acting on the aft dome due to the hydrostatic pressure on the nozzle bell are small and are neglected in this final analysis.

The expressions for determining the circumferential distribution of the internal and external pressures were coded for automatic generation of the pressures in Subroutine USRLD of STAGS. Listings of the coding for the nominal, 1/8 shift and 1/4 shift distributions are given in Tables 4-1, 4-2 and 4-3, respectively.

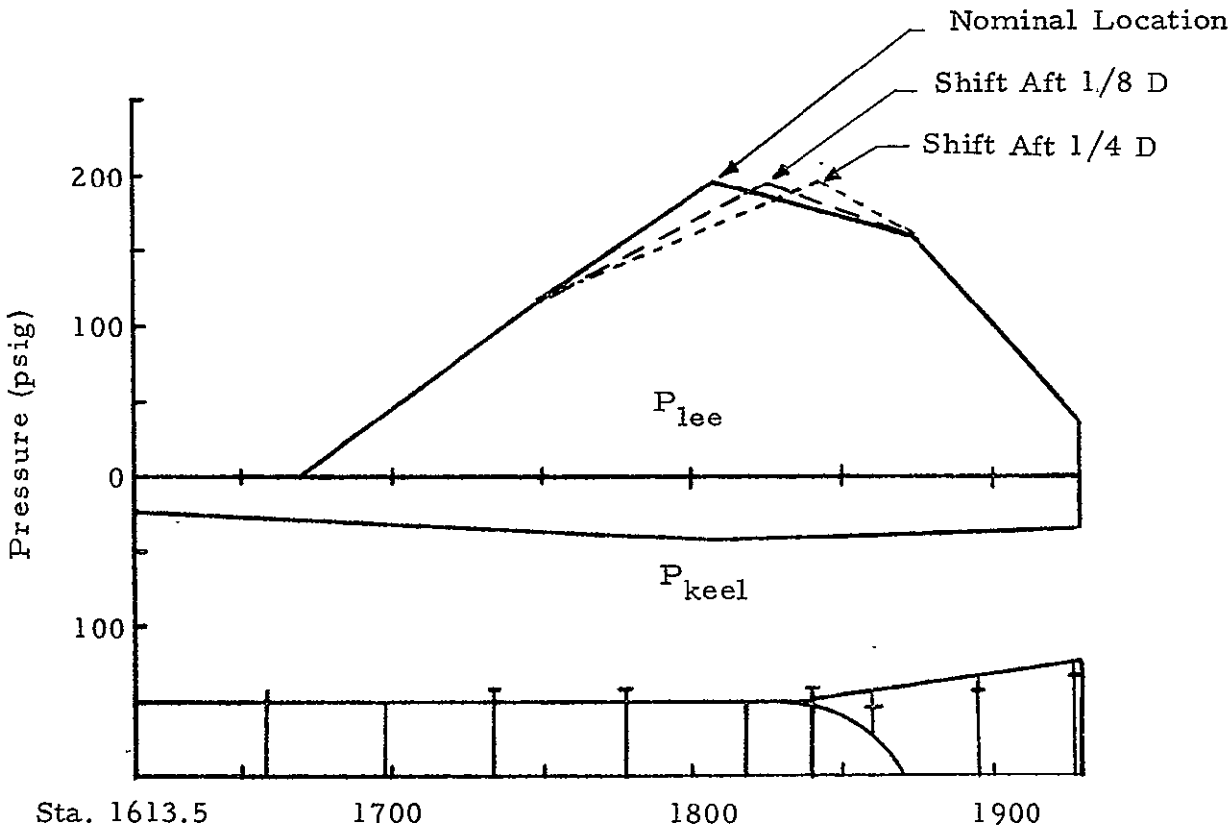

Fig. 4-2 - SRB Cavity Collapse External Pressure Distribution Keel and Lee Sides, 85/32/+5

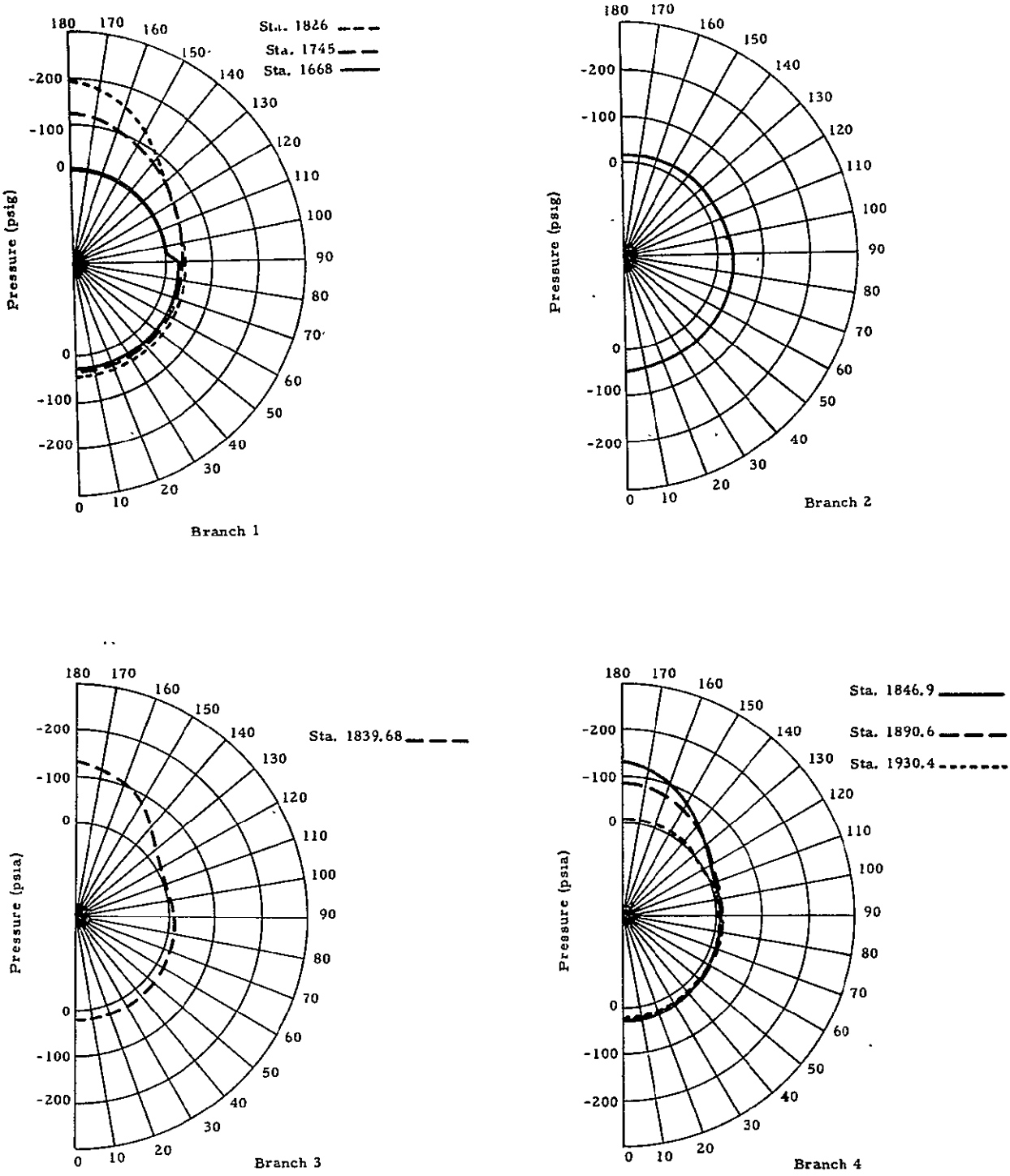

Fig.4-3a - Net Pressure Distribution 85/32/5, Nominal Position

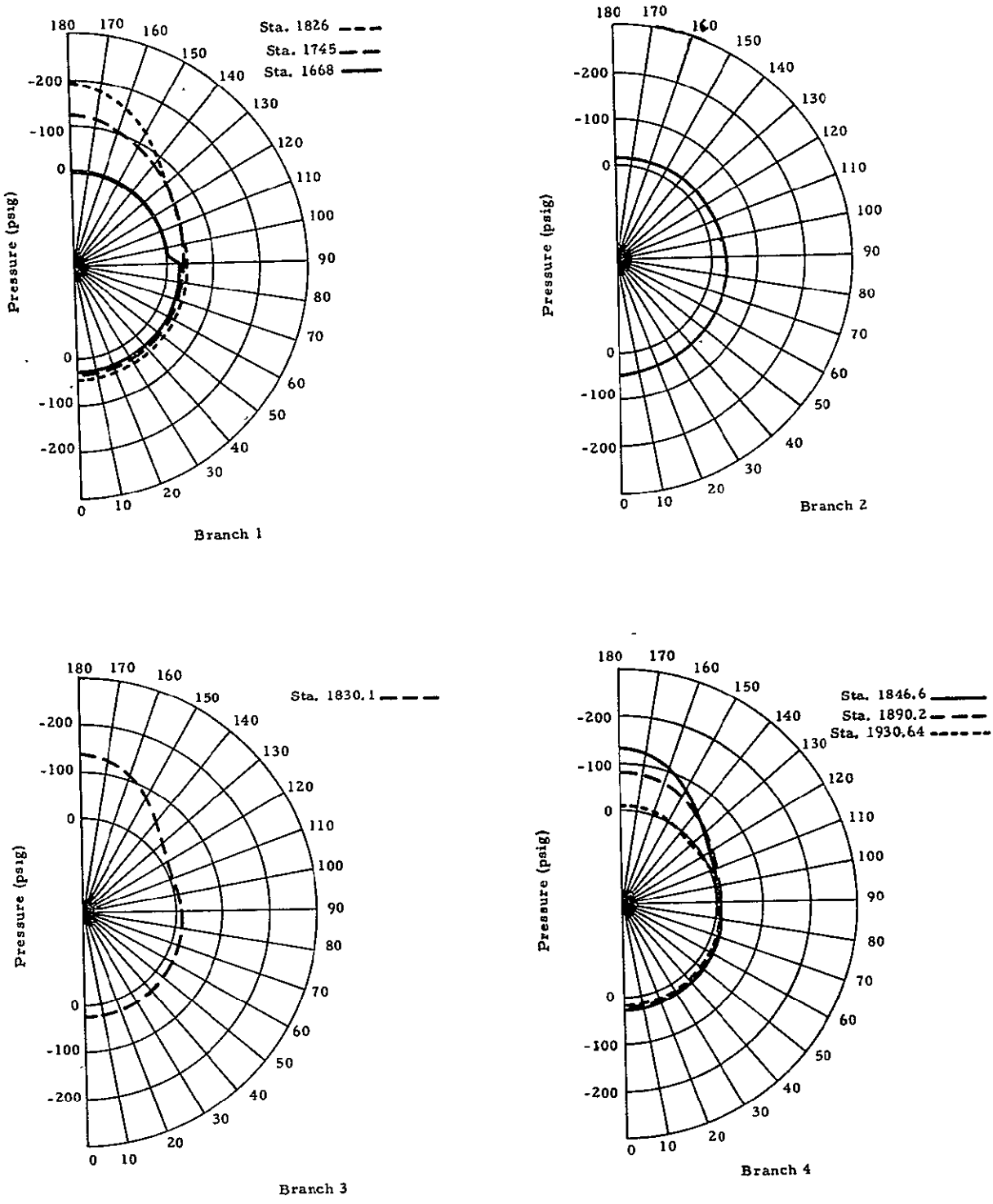

Fig.4-3b - Net Pressure Distribution 85/32/5, Shifted Aft 1/8 D

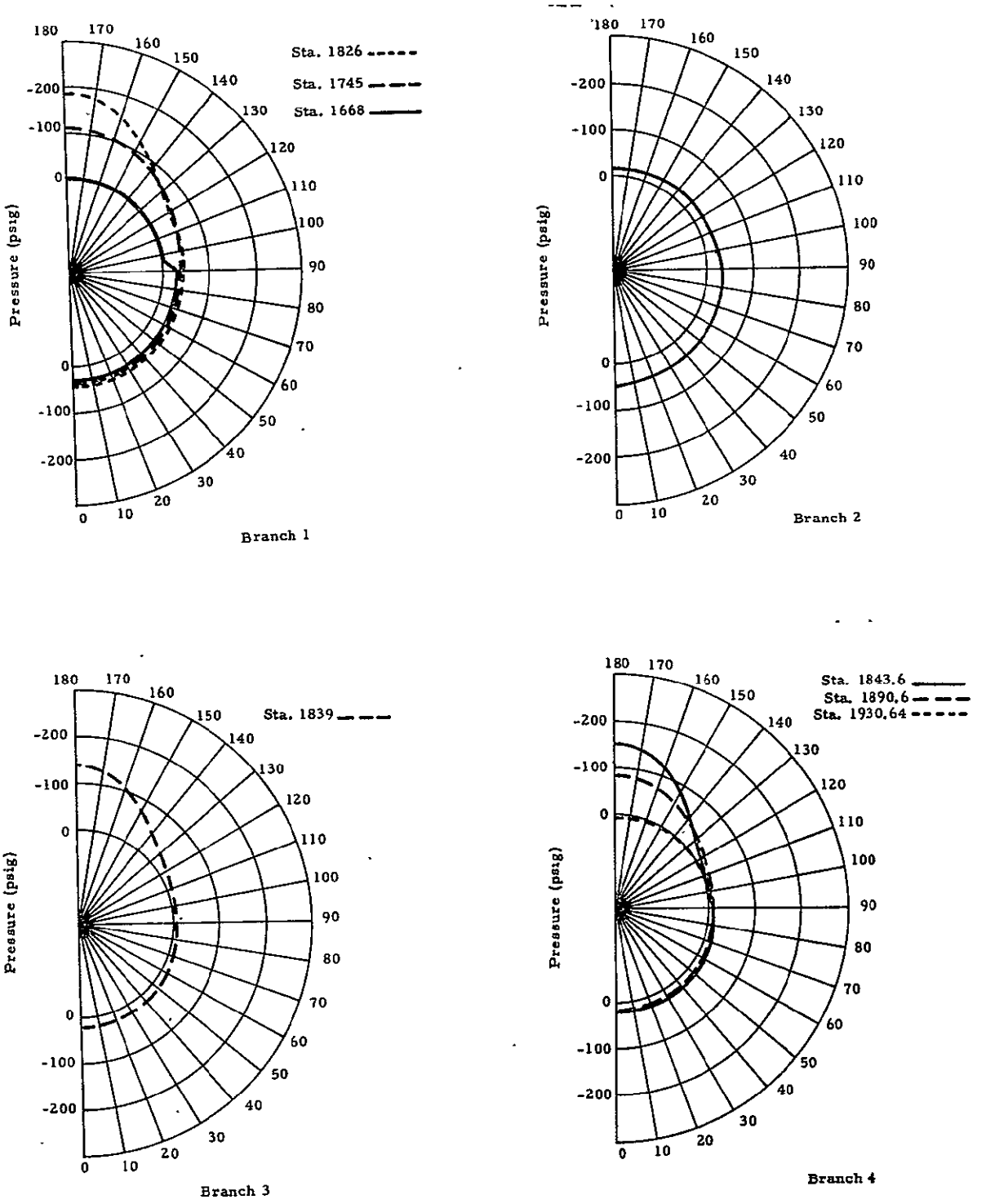

Fig.4-3c - Net Pressure Distribution 85/32/5, Shifted Aft 1/4 D

Table 4-1

USRLD LISTING FOR NOMINAL LOAD POSITION

```
WFOR,UWS USRLD,USRLD
HSA  E3 *10/16/76-03:39:33 (0,1)
*2
C ---  SUBROUTINE USRLD
C *** DATA FROM CAVITY COLLAPSE VV=85.0/VH/60.,-10/TH/10    REV.D DATA
C*** LOAD FOR 85/32/+5 CAVITY COLLAPSE LOAD CASE,MAX PRESS=194
      IF(K.EQ.2) RETURN
      REAL KC
      DO 999 L=1,NROW
      DO 999 M=1,NCOL
      FN=1.176
      PHI=(Y(M)/180.)*3.1415926
      XL=X(L)
      IF(IBRNCH.EQ.1)GO TO 100
      IF(IBRNCH.EQ.2)GO TO 200
      IF(IBRNCH.EQ.3)GO TO 300
      IF(IBRNCH.EQ.4)GO TO 400
C  *** BRANCH 1 ***
  100 PIN=-1.65
      IF(XL.GE.193.47) GO TO 110
      PKEEL=20.+.0775*XL
      IF(XL.GE.56.5) GO TO 120
      PLEE=0.0
      GO TO 190
  120 IF(XL.GE.136.5) GO TO 130
      PLEE=1.25*(XL-56.5)
      GO TO 190
  130 PLEE=-55.6+1.14*XL
      GO TO 190
  110 PKEEL=42.825-.0404*XL
      PLEE=250.36-.441*XL
  190 CONTINUE
      IF(Y(M).GT.90.) GO TO 180
      PE=PKEEL*FN
      GO TO 170
  180 ETA=1.000G578*(PLEE)**2.)+.01634*PLEE
      KC=(COS(3.1415926*PHI))**ETA
      PE=(PKEEL +KC*(PLEE-PKEEL))*FN
  170 P= PIN-PE
      GO TO 900
C  ** BRANCH 2 ***
  200 PIN=-1.65
      PL=45.5
      PH=15.5
      PE=(PL +.5*(PH-PL)*(1.-COS(PHI)))
      P=PIN -PE
      GO TO 900
C  *** BRANCH 3 ***
  300 PL=45.5
      PH=15.5
      PKEEL=34.124-.0404*XL
      PLEE=155.39-.441*XL
      IF(Y(M) .GT.90.) GO TO 310
      PE=PKEEL
      GO TO 320
  310 ETA=1.000G578*(PLEE)**2.)+.01634*PLEE
```

Table 4-1 (Concluded)

```
      KC=(COS(3.1415926*PHI))**ETA
      PE= PKEEL +KC*(PLEE-PKEEL)
  320 CONTINUE
      PIN= PH+.5*(1.-COS(PHI))*(PL-PH)
      P=PIN-(PE*FN)
      GO TO 900
C  *** BRANCH 4 ***
  400 PL=41.5
      PH=15.5
      PIN=PH +.5*(1.-COS(PHI))*(PL-PH)
      PKEEL=33.686-.0404*XL
      IF(XL.GE.35.3[6) GO TO 410
      PLEE=150.612-.441*XL
      GO TO 420
  410 PLEE=201.64-1.887*XL
  420 CONTINUE
      IF(Y(M) .GT.90.) GO TO 430
      PE= PKEEL
      GO TO 440
  430 ETA=(.0000578*(PLEE)**2.)+.01634*PLEE
      KC=(COS(3.1415926-PHI))**ETA
      PE= PKEEL + KC*(PLEE-PKEEL)
  440 P=PIN-(PE*FN)
  900 CONTINUE
      CALL FORCE(P,4,3,L,M)
  999 CONTINUE
      RETURN
```

Table 4-2

USRLD LISTING FOR 1/8 LOAD SHIFT AFT

```
@FOR,UWS USRLD,USRLD
HSA  E3 -10/16/76-00:58:04 (0,1)
-2
C      SUBROUTINE USRLD
C *** DATA FROM CAVITY COLLAPSE VV=85.0/VH/60,-13/TH/10  . REV.D DATA
C***LOAD FOR 85/32/+5 CAVITY COLLAPSE LOAD CASE,MAX PRESS=19#
       IF(K.EQ.2) RETURN
       REAL KC
       DO 999 L=1,NROW
       DO 999 M=1,NCOL
       FN=1.175
       PHI=(Y(M)-/180.)*3.1415926
       XL=X(L)
       IF(IBRNCH.EQ.1)GO TO 100
       IF(IBRNCH.EQ.2)GO TO 200
       IF(IBRNCH.EQ.3)GO TO 300
       IF(IBRNCH.EQ.4)GO TO 400
C  *** BRANCH 1 ***
  100 PIN=-1.65
       IF(XL.GE.193.5) GO TO 130
       PKEEL=20.+.3775*XL
       IF(XL.GE.56.5) GO TO 110
       PLEE=0.0
       GO TO 120
  110 IF(XL.GE.136.5) GO TO 120
       PLEE=1.25*(XL-56.5)
       GO TO 190
  120 PLEE=100.+.964*(XL-136.5)
       GO TO 190
  130 PKEEL=42.925-.0404*XL
       IF(XL.GE.211.75) GO TO 140
       PLEE=149.248+.864*(XL-193.5)
       GO TO 190
  140 PLEE=165.-.603*(XL-211.75)
  190 CONTINUE
       IF(Y(M).GT.90.) GO TO 180
       PE=PKEEL*FN
       GO TO 170
  180 ETA=(.0003578*(PLEE)**2.)+.01634*PLEE
       KC=(COS(3.1415926-PHI))**ETA
       PE=(PKEEL +(C*(PLEE-PKEEL)))*FN
  170 PE=PIN-PE
       GO TO 900
C  ** BRANCH 2 ***
  200 PIN=-1.65
       PL=45.5
       PH=15.5
       PE=(PL +.5*(PH-PL)*(1.-COS(PHI)))
       PE=PIN -PE
       GO TO 900
C  *** BRANCH 3 ***
  300 PL=45.5
       PH=15.5
       PKEEL=34.124-.9404*XL
       PLEE=152.83-.603*XL
       IF(Y(M) .GT.90.) GO TO 310
```

Table 4-2 (Concluded)

```
      PE=PKEEL
      GO TO 320
  310 ETA=(.0000578*(PLEE)**2.)+.01634*PLEE
      XC=(COS(3.1415926-PHI))**ETA
      PE= PKEEL +XC*(PLEE-PKEEL)
  320 CONTINUE
      PIN= PH+.5*(1.-COS(PHI))*(PL-PH)
      P=PIN-(PE*FN)
      GO TO 900
C     *** BRANCH 4 ***
  400 PL=91.5
      PH=15.5
      PIN=PH +.5*(1.-COS(PHI))*(PL-PH)
      PKEEL=33.686-.0404*XL
      IF(XL.GE.35.316) GO TO 410
      PLEE=155.3-.603*XL
      GO TO 420
  410 PLEE=135.-1.887*(XL-35.316)
  420 CONTINUE
      IF(Y(M) .GT.90.) GO TO 430
      PE= PKEEL
      GO TO 440
  430 ETA=(.0000578*(PLEE)**2.)+.01634*PLEE
      XC=(COS(3.1415926-PHI))**ETA
      PE= PKEEL + XC*(PLEE-PKEEL)
  440 P=PIN-(PE*FN)
  900 CONTINUE
      CALL FORCE(P,A,B,L,M)
  999 CONTINUE
      RETURN
```

Table 4-3

USRLD LISTING FOR 1/4 LOAD SHIFT AFT

```
@FOR,UNS USRLD,USRLD
HSA  1.3 *10/23/76*20:25:51-(0,1)
-2
C      SUBROUTINE USRLD
C *** DATA FROM CAVITY COLLAPSE VV=85.0/VH/60.-10/TH/10    REV.0 DATA
C*** LOAD FOR 85/32/+5 CAVITY COLLAPSE LOAD CASE-MAX PRESS=174
       IF(K.EQ.2) RETURN
       REAL KC
       DO 999 L=1,NROW
       DO 999 N=1,NCOL
       PN=1.170
       PHI=(Y(M) /180.)*3.1415926
       AL=A(L)
       IF(.GRNCH.EQ.1)GO TO 100
       IF(IBRNCH.EQ.2)GO TO 200
       IF(IBRNCH.EQ.3)GO TO 300
       IF(IBRNCH.EQ.4)GO TO 400
C  *** BRANCH 1 ***
  100  PIN=1.65
       IF(XL.GE.193.5) GO TO 110
       PKEEL=23.+.0775*XL
       IF(XL.GE.56.5) GO TO 120
       PLEEL=0.0
       GO TO 190
  120  IF(XL.GE.136.5) GO TO 130
       PLEEL=1.25*(XL-56.5)
       GO TO 190
  130  PLEEL=16.+.095*(XL-136.5)
       GO TO 190
  110  PKEEL=42.825-.0404*XL
       PLEEL=139.62+.695*(XL-193.5)
  190  CONTINUE
       IF(Y(M).GT.90.) GO TO 180
       PE=PKEEL*PN
       GO TO 170
  180  ETA=(.00005/8*(PLEEL)**2.)+.01634*PLEEL
       KC=(COS(3.1415926-PHI))**ETA
       PE=(PKEEL +KC*(PLEEL-PKEEL))*PN
  170  P= PIN-PE
       GO TO 900
C  *** BRANCH 2 ***
  200  PIN=1.65
       PL=45.5
       PH=15.0
       PE=(PL +.5*(PH-PL)*(1.-COS(PHI)))
       P=PIN -PE
       GO TO 900
C  *** BRANCH 3 ***
  300  PL=45.5
       PH=1.0
       PKEEL=34.125-.0404*XL
       PLEEL=154.0+.695*XL
       IF(Y(M) .GT.90.) GO TO 310
       PE=PKEEL
       GO TO 320
  310  ETA=(.00005/8*(PLEEL)**2.)+.01634*PLEEL
```

Table 4-3 (Concluded)

```
      KC=(COS(3.1415926-PHI))**ETA
      PE= PKEEL +KC*(PLEE-PKEEL)
  320 CONTINUE
      PIN= PH+.5*(1.-COS(PHI))*(PL-PH)
      P=PIN-(PE*FN)
      GO TO 900
C     *** BRANCH 4 ***
  400 PL=41.5
      PH=15.5
      PIN=PH +.5*(1.-COS(PHI))*(PL-PH)
      PKEEL=33.686-.0404*XL
      IF(XL.GE.35.316) GO TO 420
      IF(XL.GE.3.816) GO TO 410
      PLEE=162.33+.695*XL
      GO TO 490
  410 PLEE=105.+.952*(XL-3.816)
      GO TO 490
  420 PLEE=135.-1.837*(XL-35.316)
  490 CONTINUE
      IF(Y(N) .GT.93.) GO TO 430
      PL= PKEEL
      GO TO 440
  430 ETA=(.0000578*(PLEE)**2.)+.01634*PLEE
      KC=(COS(3.1415926-PHI))**ETA
      PL= PKEEL + KC*(PLEE-PKEEL)
  440 P=PIN-(PE*FN)
  900 CONTINUE
      CALL FORCE(P,4,3,L,M)
  995 CONTINUE
      RETURN
      END
```

4.2 SRB STAGS C LINEAR ANALYSIS

Linear analyses were performed for the 85/32/5 (VV/VH/θ) case for both the original and rotated models. Each model was analyzed for all three pressure peak locations. No design factors were applied to the loads in the computer analyses. The linear analyses showed good margins against the material yield allowables in all structural areas of the SRB. Figures 4-4 and 4-5 show the maximum stress values determined in the linear analysis for the three pressure locations. The first stress value is for the max pressure peak in the nominal position, the values denoted (1/8) and (1/4) are for the pressure peak shifted aft 1/8 D and 1/4 D, respectively.

From Figs. 4-4a and 4-5a the maximum stress values in the SRM case and dome structure are seen to be well below the material allowables for the D6AC steel. If a design factor (DF) of 1.25 is applied to the maximum stress value given for the dome skin, f = 1.25 (146,400) = 183,000 psi, the resultant stress value still falls below the ultimate material allowable (Table 3-5) giving a positive margin of safety.

The maximum stress in the steel reinforcing tee-ring at the cylinder-conical skirt interface is seen to be well below the maximum allowable stress value for both model orientations, Figs. 4-4b and 4-5b.

The computed stress values in the skirt stucture for the linear analyses are also shown in Figs. 4-4b and 4-5b. These maximum values are seen to be well below the material allowables for the 2219 aluminum. The largest stress value occurs in the skin just forward of the upper ring at ϕ = 180 deg, lee side, for original model configuration. Applying a design factor of 1.25 produces a stress value still below the ultimate material allowable. Hence, the margin of safety is

$$MS = \frac{F_{tu}}{(DF)(f)} - 1 = \frac{63,000}{(1.25)(46,200)} - 1 = +.09$$

Stress in psi

r = ring, s = skin

c = compression

t = tension

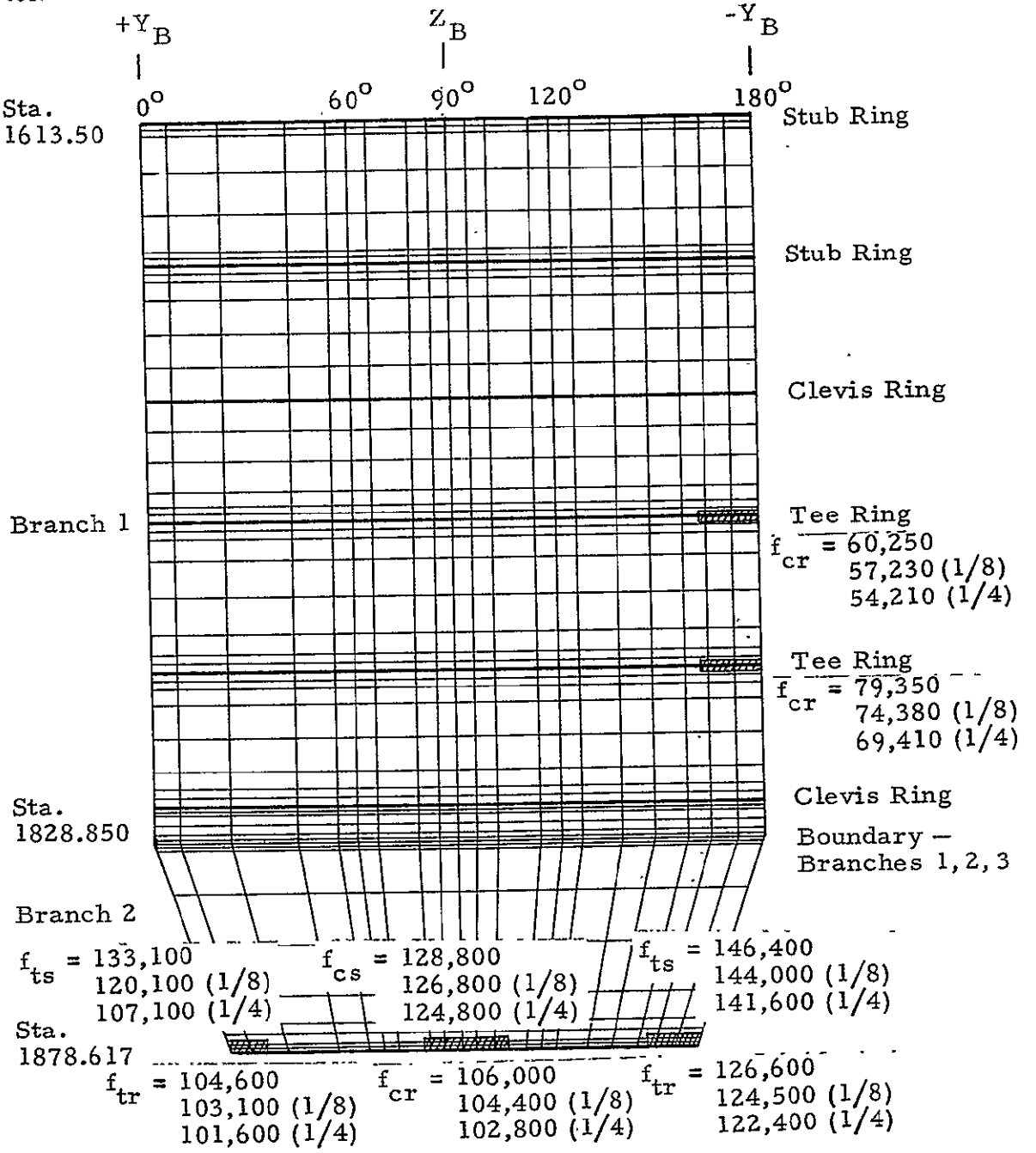

Fig. 4-4a - Maximum Stresses, Original Model, 85/32/5 Linear Analysis

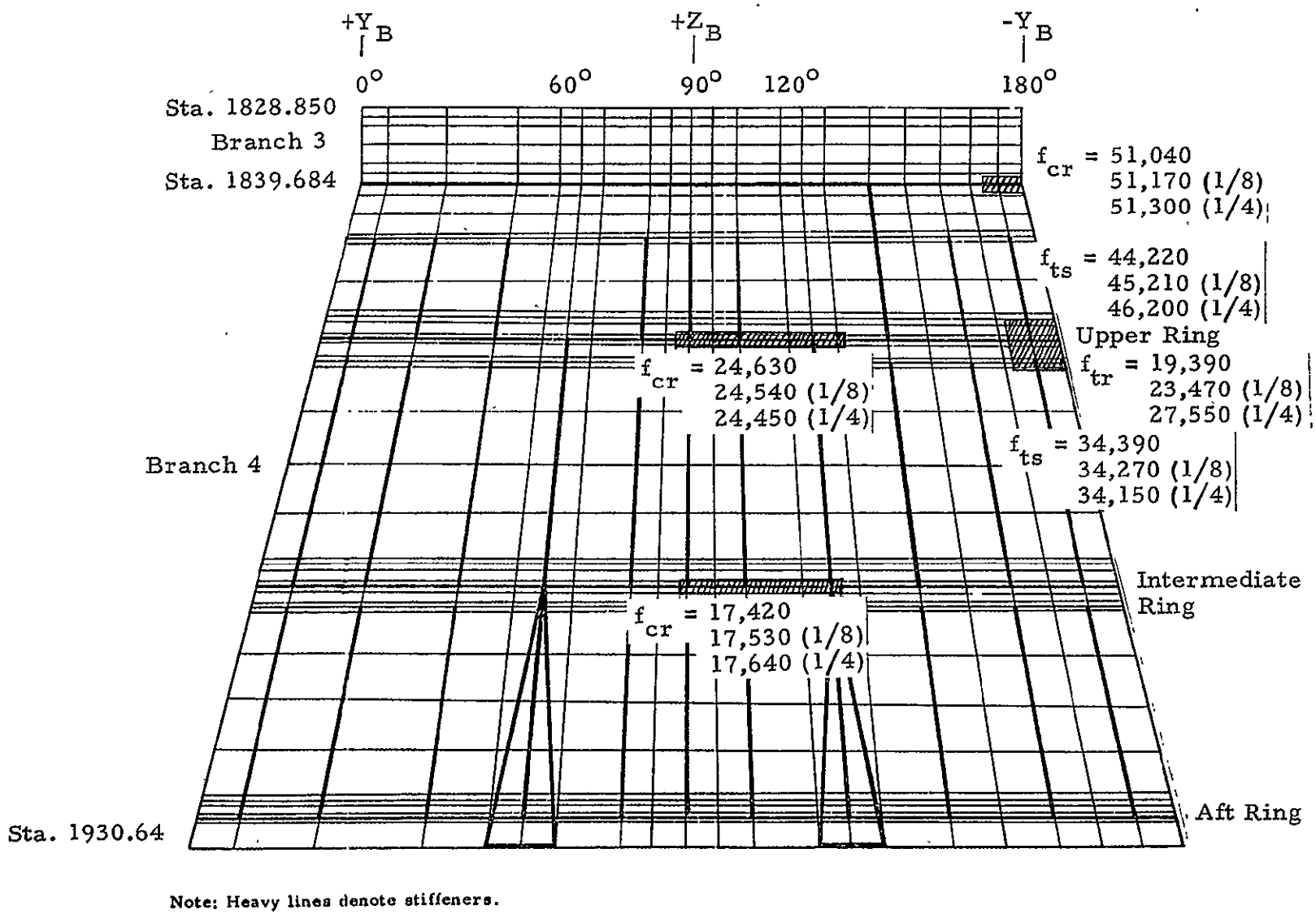

Note: Heavy lines denote stiffeners.

Fig. 4-4b - Maximum Stresses, Original Model 85/32/5 Linear Analysis

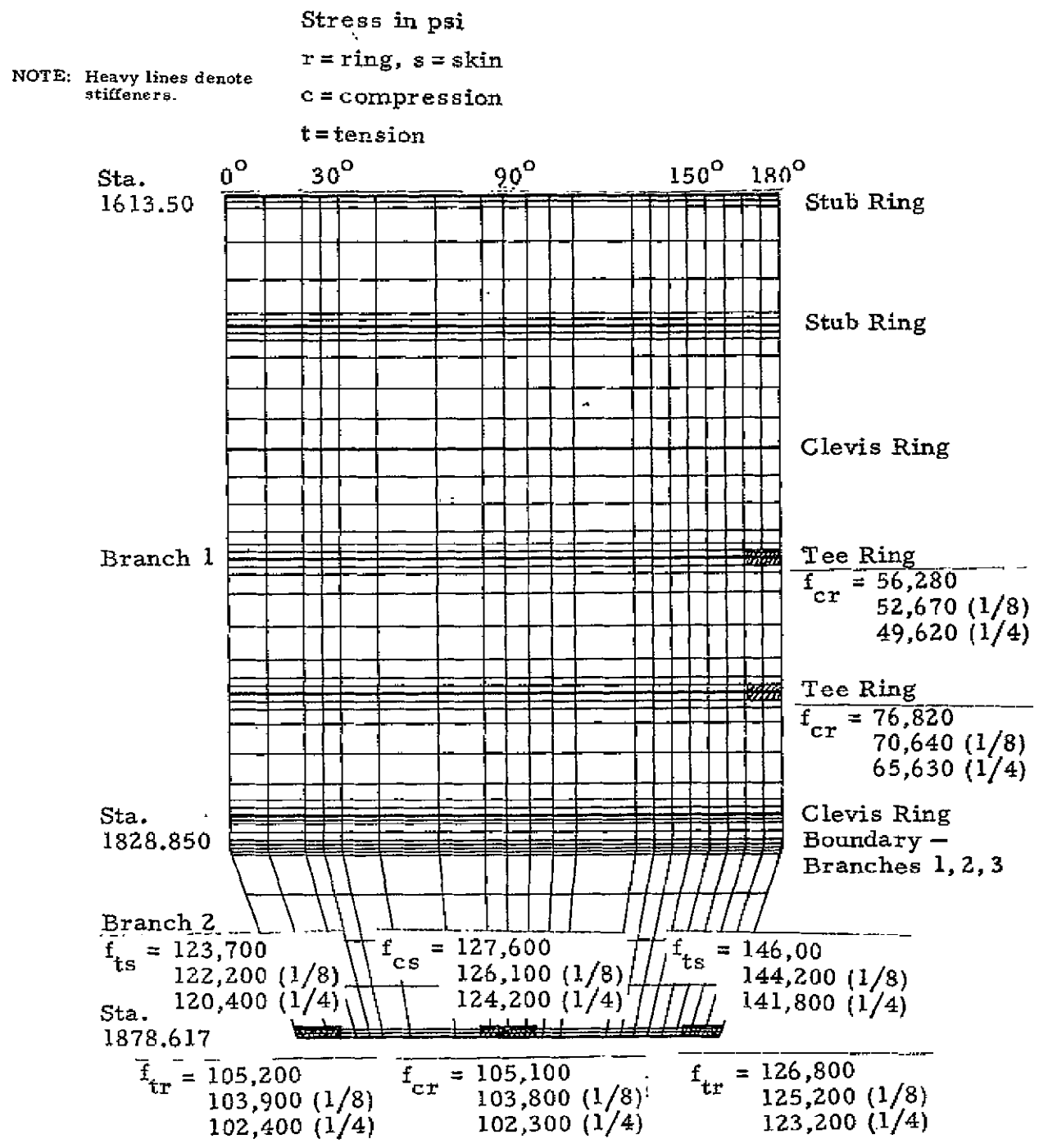

Fig. 4-5a - Maximum Stresses, Rotated Model ($\pm Z_B$) 85/32/5 Linear Analysis

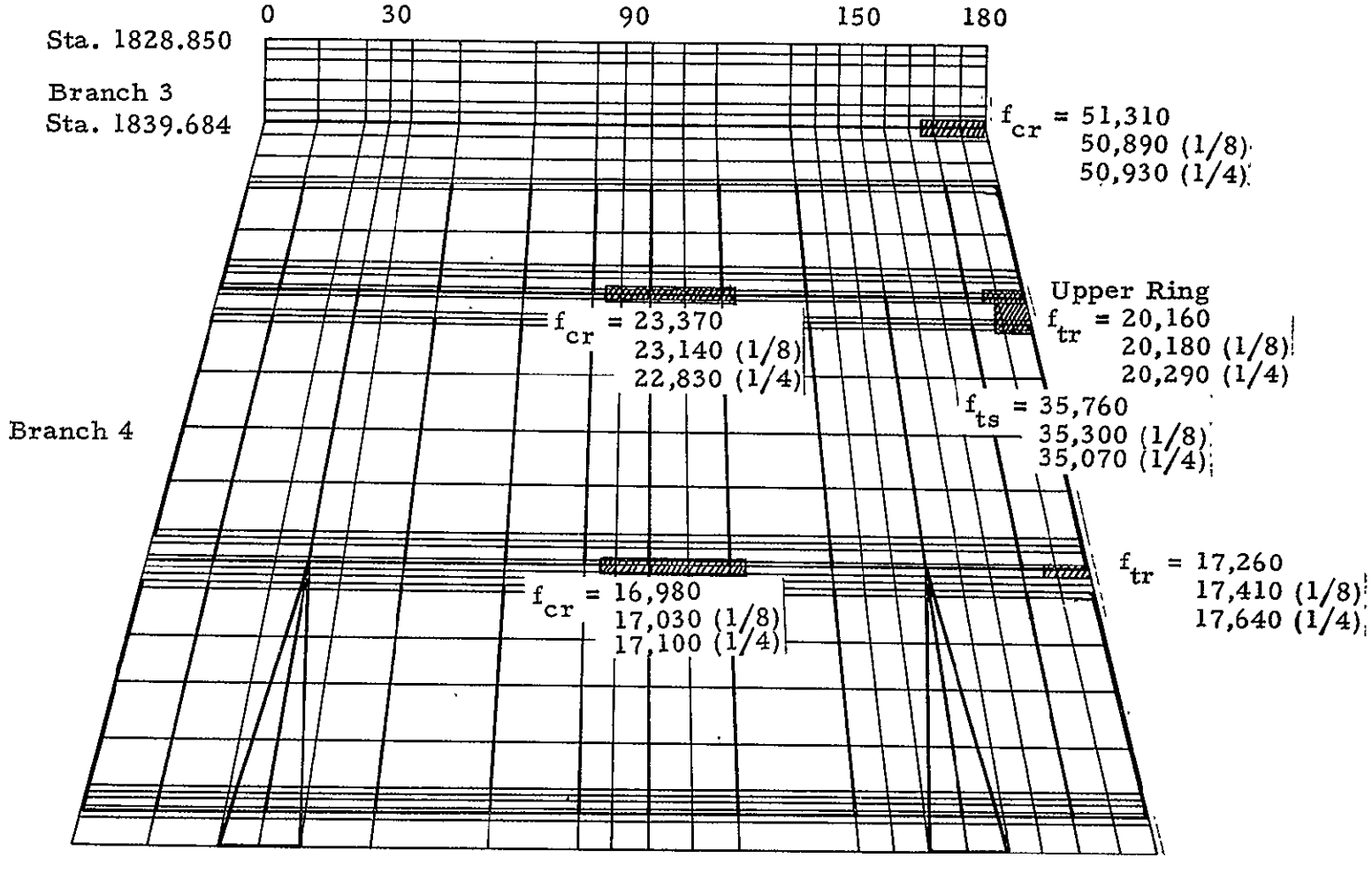

Fig. 4-5b - Maximum Stresses, Rotated Model ($\pm Z_B$) 85/32/5 Linear Analysis

The maximum stresses in the rings are also given in the figures. These values should be checked against the flange crippling stresses in a detail stress analysis to ensure structural integrity. From the size and cross-sectional dimensions of the rings, it would appear by inspection that local crippling would not be critical but this should be determined by calculation. The displacements normal to the surface for the $\phi = 0$, 90 and 180 deg meridians are shown in Figs. 4-6 and 4-8. Figure 4-7 shows the deformed shape at several cross-sectional locations for the original model, the rotated model has a similar general deformation pattern.

4.3 BIFURCATION BUCKLING ANALYSIS

Bifurcation buckling analyses were performed for the 85/32/5 load case for both the original and rotated models. The results of these studies are given in Table 4-4. The eigenvalues are seen to be at least 2.5 times the applied load with the predicted buckle occurring in the cylinder at station 1797.8 between the aft tee ring and clevis joint for both models. The buckling mode shape is shown in Fig. 4-9. Even with an appropriate knockdown factor (KDF) of 0.63 applied (Ref. 3), the resultant predicted buckling load factor (LF) is well above the design load.

$$LF = KDF \times Eigenvalue$$
$$LF = (0.63)\,(2.526) = 1.592$$

This factor results in a positive margin of safety even with the 1.25 design factor applied to the loading.

$$MS = \frac{LF}{DF} - 1 = \frac{1.592}{1.25} - 1 = +0.274$$

4.4 NONLINEAR ANALYSIS

A nonlinear analysis was performed to more accurately determine the failure load. The results of this analysis at Station 1797.8, $\phi = 180$ deg is

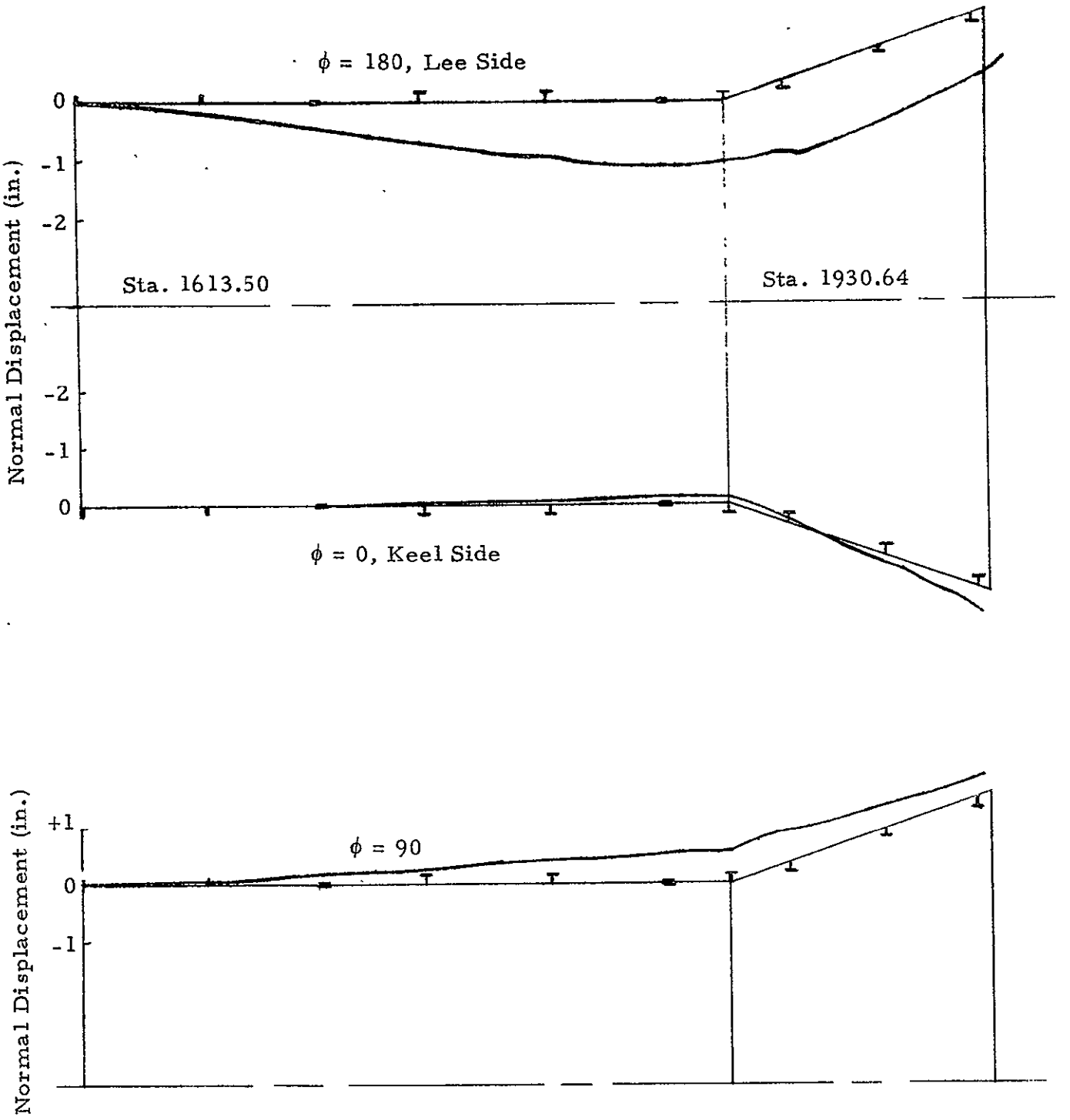

Fig. 4-6 - 85/32/5 Original Model ($\pm Y_B$) Deformed Shape, Nominal Load Position

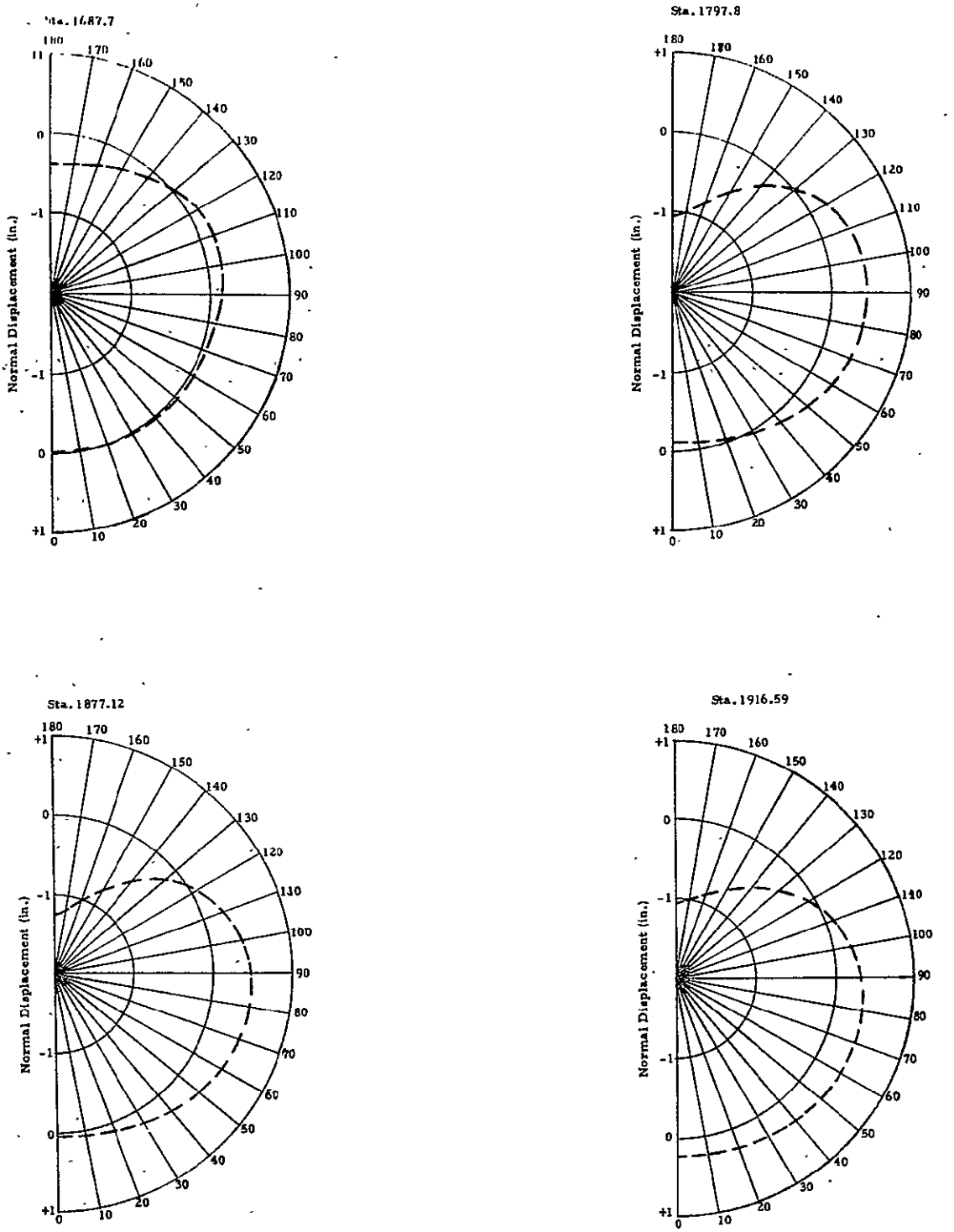

Fig. 4-7 - Normal Displacements, Original Model, 85/32/5 Nominal Position

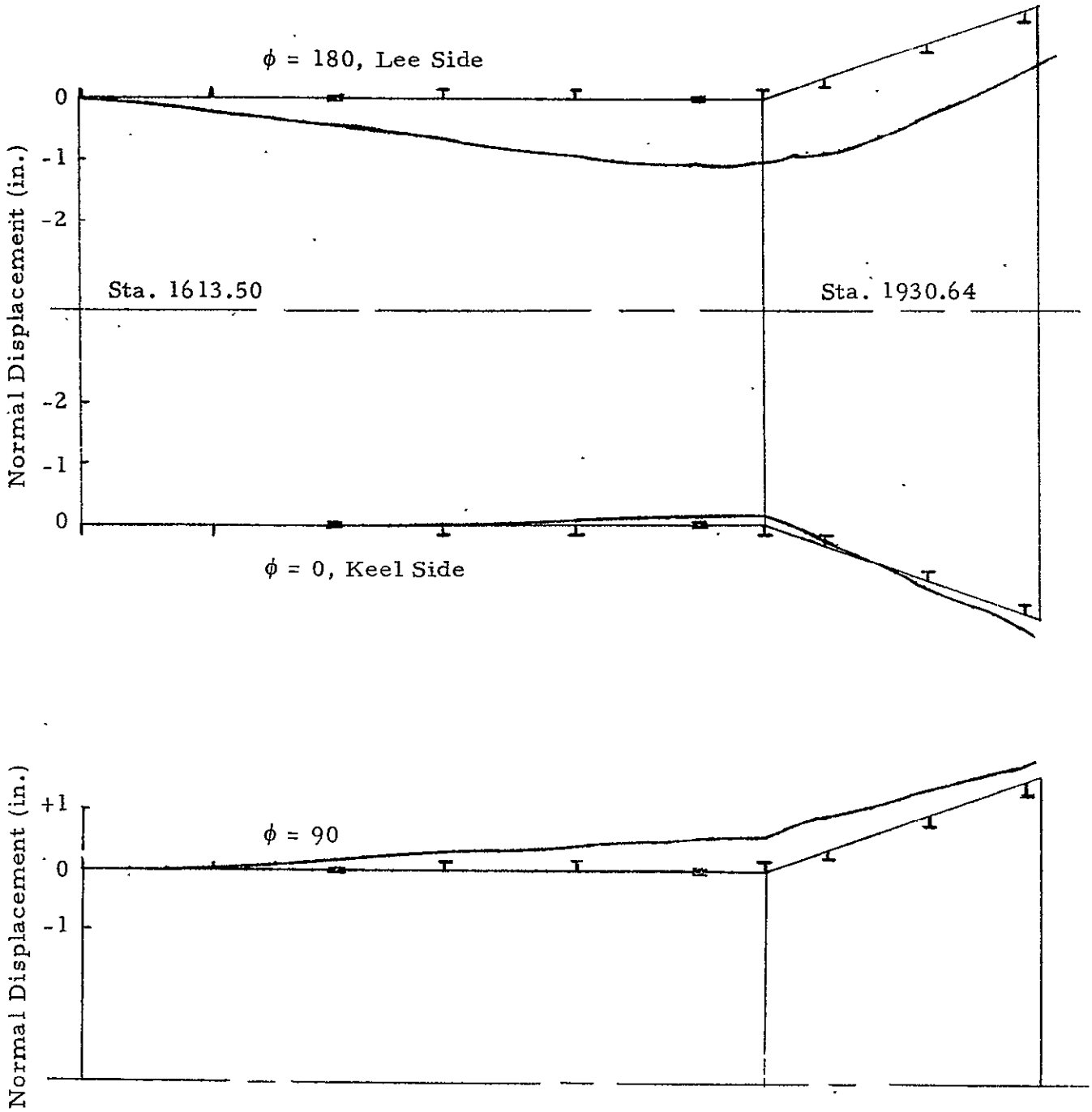

Fig. 4-8 - 85/32/5 Rotated Model ($\pm Z_B$) Deformed Shape, 1/8 Diameter Aft Load Shift

Table 4-4

BIFURCATION BUCKLING, 85/32/5 LOAD CASE

SRB Model/Load Position	Eigenvalue	Location
Original Model ($\pm Y_B$)		
Nominal	2.569	Sta. 1797.8 @ 180 deg
1/8 Aft Shift	2.785	Sta. 1797.8 @ 180 deg
1/4 Aft Shift	2.993	Sta. 1797.8 @ 180 deg
Rotated Model ($\pm Z_B$)		
Nominal	2.526	Sta. 1797.8 @ 180 deg
1/8 Aft Shift	2.750	Sta. 1797.8 @ 180 deg
1/4 Aft Shirt	2.968	Sta. 1797.8 @ 180 deg

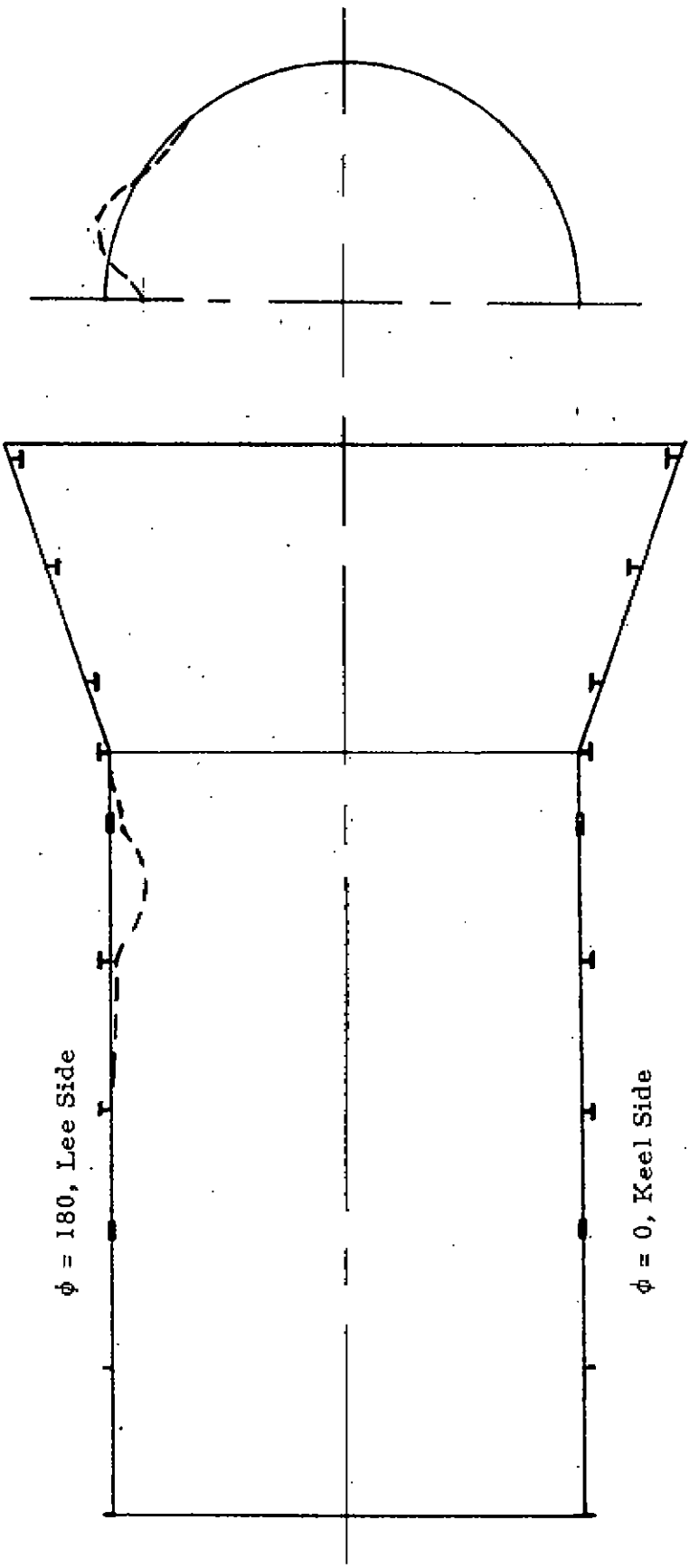

Fig. 4-9 - Bifurcation Buckling Mode Shape, Rotated Model ($\pm Z_B$) 1/8 Diameter Aft Load Shift

shown in Fig. 4-10 for the rotated model with the 85/32/5 load case in the nominal position. The linear, nonlinear and bifurcation buckling analyses are compared in this figure. The nonlinear collapse is seen to occur at a load factor of approximately 1.8. This factor is seen to be well above the applied load, LF = 1.0, indicating structural integrity will be maintained.

Stress values in the skirt structure for the applied load (load factor of 1.0) are shown in Fig. 4-11 for the nonlinear analysis of the rotated model. The major skin stress value near the Upper Ring at ϕ = 180 deg is seen to be 25% greater than the corresponding linear analysis value given in Fig. 4-5b ($\frac{44,800}{35,760} = 1.25$). The stress values in Fig. 4-11 for the rotated model skirt are seen to be below the material yield allowable. With the design factor of 1.25 applied, the maximum stress value is still below the material ultimate, $f = 44,800\,(1.25) = 56,000 < F_{tu}$. However, if this ratio of nonlinear/linear value of 1.25 is applied to the maximum stress value (f = 46,200 psi) for the original model linear analysis shown in Fig. 4-4b, the maximum skin stress value will be f = 57,750 psi. Using the design factor of 1.25 the resultant stress is greater than the material ultimate giving a negative margin of safety in the skin at this area of the skirt.

$$MS = \frac{F_{tu}}{(DF)f} - 1$$

$$= \frac{63,000}{(1.25)(57,750)} - 1$$

$$MS = -.127$$

A more detailed analysis should be performed for this area. Other areas of the structure have positive margins of safety by inspection.

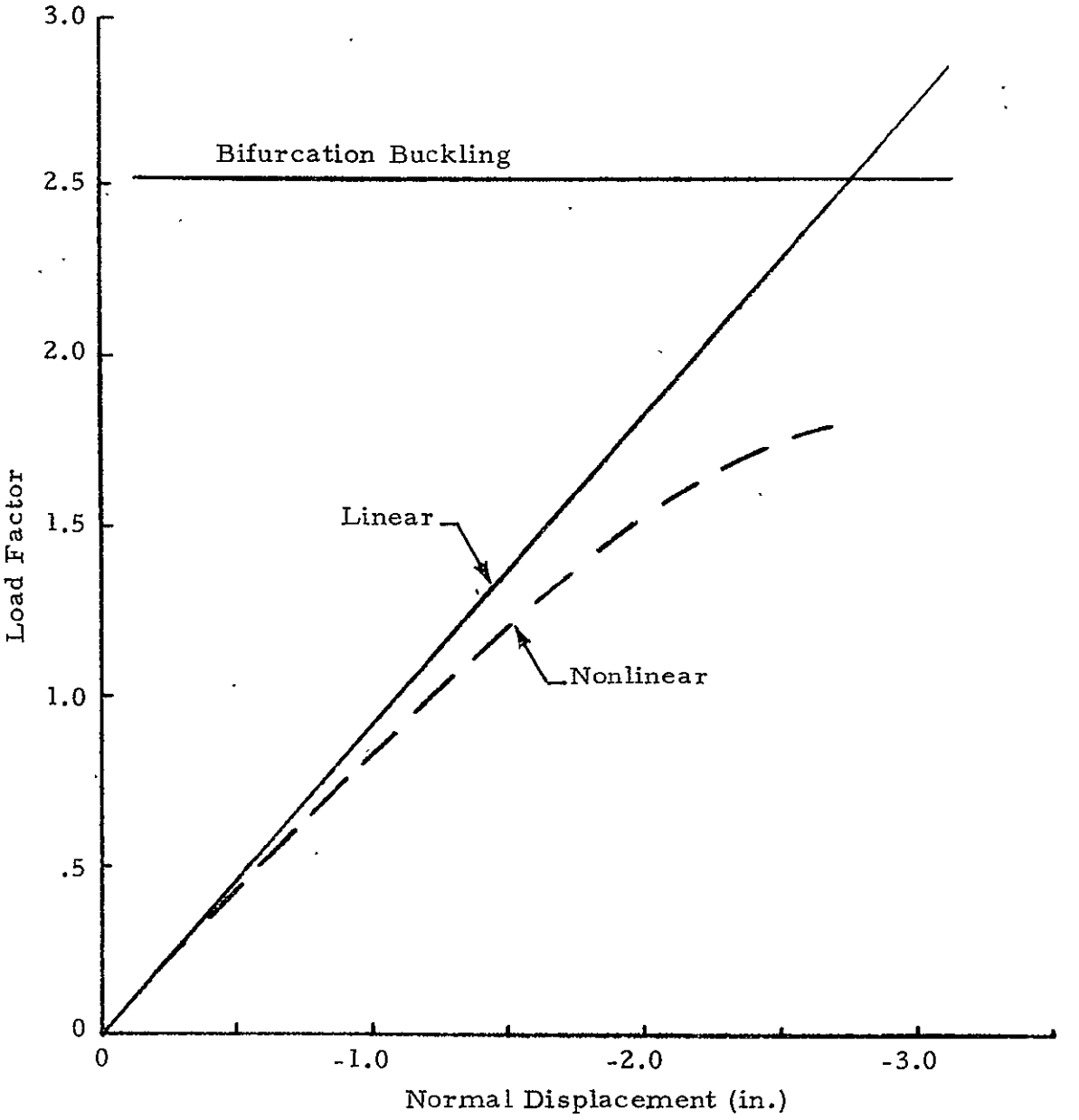

Fig. 4-10 - SRB Rotated Model, Sta. 1797.8, Lee Side, 85/32/5 Nominal Position

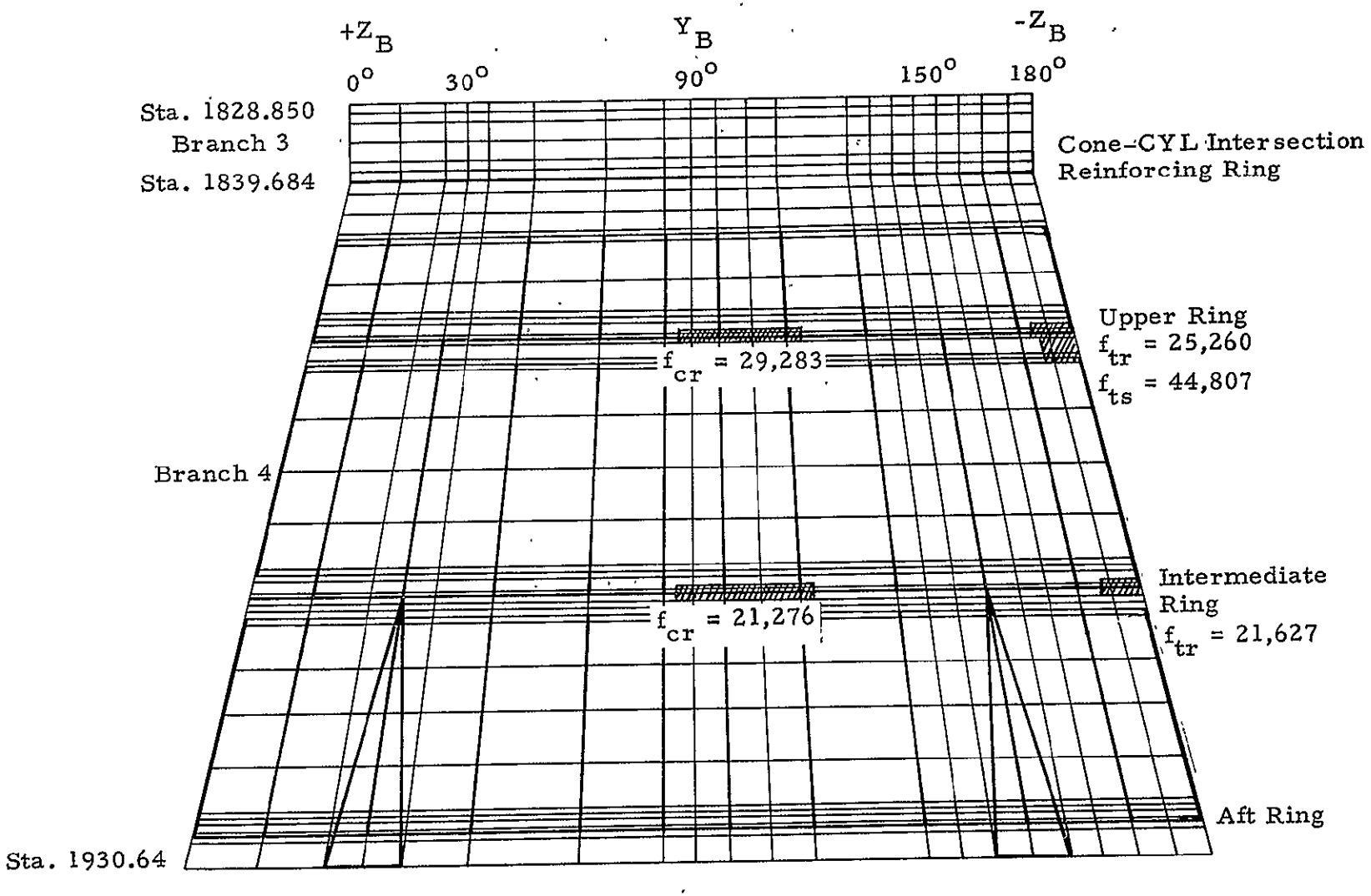

Note· Heavy lines denote stiffeners.

Fig. 4-11 - Maximum Stresses Rotated Model, 85/32/5 Nonlinear Analysis Nominal Load Position

4.5 THERMAL EFFECTS

To determine the sensitivity of the aft SRB structure to thermal loads, the rotated model described in Section 3 was used. However, the discrete stiffener used in previous models could not be used. To account for thermal gradients each stiffener cross section must be divided into sub-elements so the thermal expansion may be considered constant within each sub-element.

Stiffeners located on the exterior of the motor case were divided into 4 or 5 sub-elements so that temperatures could be allowed to vary linearly from the outer portion of the stiffener to the skin temperature at the sub-element nearest the skin. For internal stiffeners (those on the skirt or at the aft end of the dome) only one subelement was used since the stiffener and adjacent skin were of the same temperature. No variations in temperature through the skin thickness were allowed.

The skin and stiffener temperatures given in Table 4-5 were used in the analysis. A stress-free temperature of 70 F was used.

Table 4-5
TEMPERATURE DISTRIBUTIONS FOR THERMAL EFFECTS DETERMINATION

	Motor Case	Dome	Skirt
	Temperature (F)		
Skin	250	250	160
Stiffener	400	250	160

Maximum stresses resulting from the 1/4 D shift pressure distribution described previously combined with the temperatures above are shown in Fig. 4-12. The skin stresses in the skirt at $\phi = 180$ deg, adjacent to the upper ring is the only area within the skirt where problems may arise.

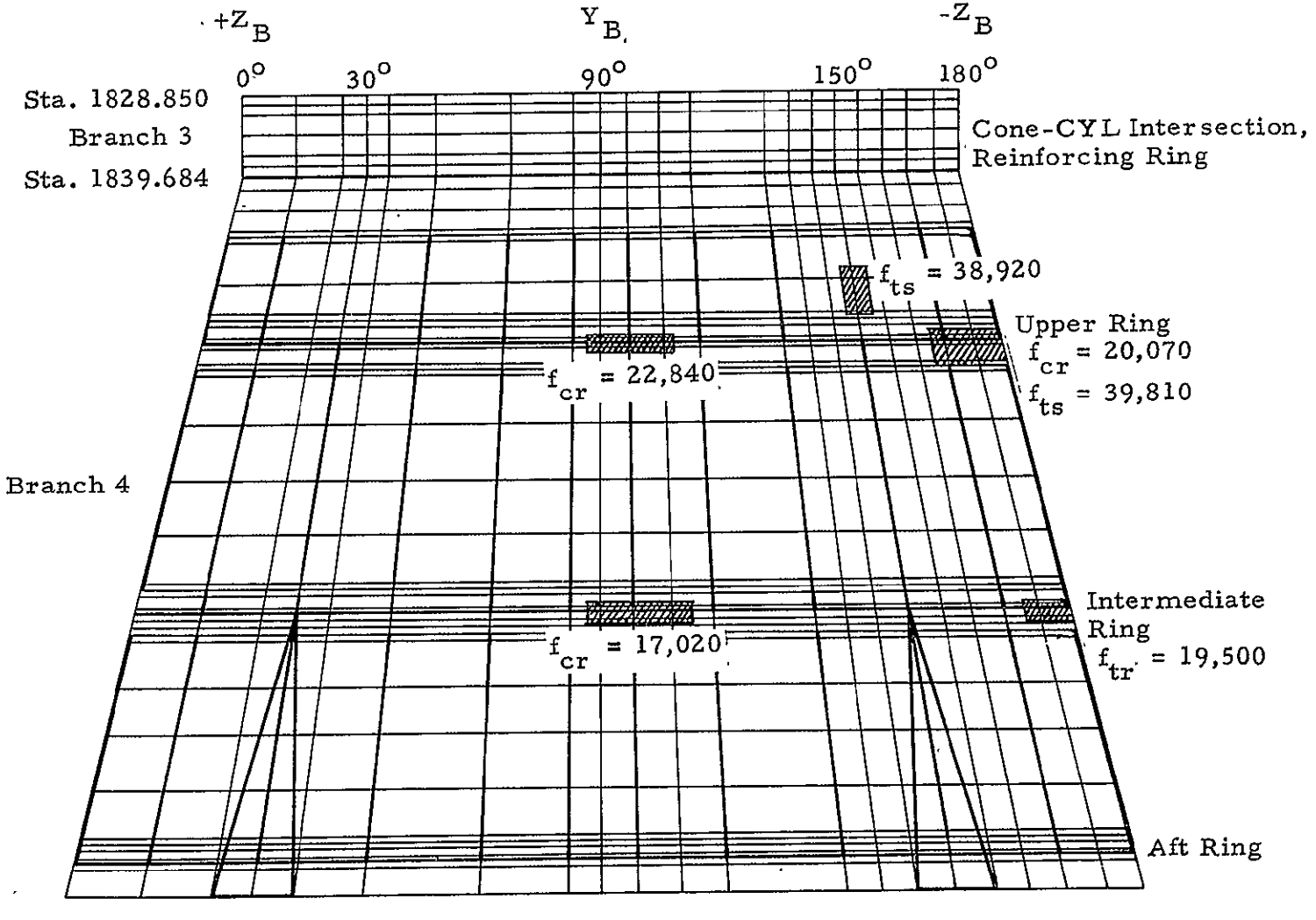

Note: Heavy lines denote stiffeners

Fig. 4-12 - Maximum Stress Rotated Model, 85/32/5 Plus Thermal Distribution 1/4 Aft Shift

The stress in the skin increased by approximately 4740 psi due to the inclusion of thermal effects. For the rotated model this increase does not indicate difficulties. However, the original model could be expected to increase by the same amount. In Fig. 4-4b it was shown that the maximum skin stress was 46,200 psi for the original model. An increase of 4,740 psi increases the maximum stress to 50,940 psi. Applying a design factor of 1.25 to this value the stress becomes 63,675 psi, approximately the ultimate stress for the 2219 aluminum used in the skirt.

5. REVIEW OF BROWN ENGINEERING SRB STAGS MODELS

Brown Engineering personnel, under support contract to NASA-MSFC, experienced several difficulties in obtaining accurate results using STAGS. These problem areas were investigated and causes were determined. Most problems were associated with the grid network chosen and the ordering of the branches of the model. The particular modeling problems were covered by the parameter studies and other grid studies in Section 2.

In the Brown SRB STAGS math models that were reviewed, the cone branch is designated as Branch 1 and the cylinder as Branch 2. The cone longitudinal grid originates at the intersection and terminates at the aft end of the skirt. The cylinder grid originates at the forward end of the cylinder segment (support plane) and terminates at the cone-cylinder intersection. This is an inefficient method for the ordering of the terms in the banded matrix solution routine used in STAGS. The most efficient method is for the cylinder to be designated Branch 1, originating at the forward end of the cylinder segment and terminating at the cone-cylinder intersection. The conical skirt would be Branch 2 with the origin at the cone cylinder intersection and terminating at the aft end of the skirt. This provides a continuous flow of node connections throughout the model, thus reducing the number of interconnected matrix terms. (This is the ordering sequence used in the model constructed in Section 3.)

A large savings in computer time is realized using this orientation. Table 5-1 shows a comparison of Univac 1108 computer run times for comparable Brown and Lockheed STAGS B SRB models with a cavity collapse load case. The ordering sequence shown in Section 3 was used for the four-branch Lockheed model. A saving of 2 hours and 6 minutes of charged time is realized by the proper ordering sequence.

Table 5-1

SRB STAGS B MODEL COMPARISON

Item	Lockheed Model	Brown Model
Number of Branches	4	2
Number of Nodes	3183	2394
Number of Equations	5187	5786
CPU Time*	0/19/21.689	0/36/46.987
I/O Time*	0/6/38.448	1/53/26.078
Total Time*	0/27/2.868	2/32/52.909

*Time is hours/minutes/seconds.

The Brown models have 21 finely spaced grid divisions in the longitudinal direction on the skirt but only eight sparsely spaced divisions on the cylinder. From Fig. 2-6 of Section 2 this is shown to inhibit the true deformations at the cone-cylinder intersection and results in higher predicted stress values in the reinforcing ring. This grid spacing would also result in higher computed values for the buckling load. The accuracy of these models could be improved by adding several closely spaced grid lines adjacent to the intersection and reinforcing ring on the cylinder branch.

The SRM aft dome cap has not been included in the Brown models. The addition of this structure would give radial stiffness to the cylinder wall in the area of the highest pressure in the cavity collapse load. Also the constant internal pressure load on the skirt, dome and cylinder was not included in the load data. These corrections should be made to obtain accurate results.

6. CONCLUSIONS AND RECOMMENDATIONS

6.1 CONCLUSIONS

The STAGS C finite difference computer program is an efficient and accurate tool for the structural analysis of general shell structures. Parameter studies should be performed and several grid patterns investigated using a simplified model of the structure and loading before the large detailed model is constructed. This method will produce a mathematical model that has the most efficient computer run time and one that will give accurate results for the linear, nonlinear and bifurcation buckling analyses.

The 85/32/5 (VV/VH/θ) cavity collapse load case was determined to be the maximum loading for the SRB skirt structure and the aft portion of the motor case. The linear analyses showed that structural integrity will be maintained for the applied load. With a design factor of 1.25 the linear analyses stresses will still give positive margins of safety using the material ultimate allowable. The bifurcation buckling analyses predicted buckling in the cylinder motor case at Station 1797.8 on the lee side of the structure. This location was typical for both the rotated ($\pm Z_B$) and original ($\pm Y_B$) models for all three load positions. The minimum eigenvalue calculated was 2.526. Even with an appropriate knockdown factor of 0.63 applied, the resultant eigenvalue of 1.592 gives a positive margin of safety for the structure.

The nonlinear analysis at the applied load (LF = 1.0) show stress values in the inelastic range in the skirt for the original model ($\pm Y_B$). This occurs in the skin just forward of the upper ring at the lee side. Applying the design factor of 1.25 results in a stress value above the material ultimate giving a negative margin of safety (-.127) at this location. Detailed analyses should be made of this area to more accurately predict the true inelastic stress distribution and the corresponding margin of safety.

6.2 AREAS FOR ADDITIONAL STUDY

Some areas for future study that need to be investigated and incorporated into the STAGS SRB mathematical model are the addition of the pressure normal to the web of the skirt rings. This will have negligible effect on the overall skirt structure but may significantly affect the stress levels in the ring elements. For the thermal analysis of the skirt, a constant temperature was used. A more accurate temperature distribution over the cylinder, dome and skirt as well as thermal gradients through the skin of the structure should be obtained and a combined pressure/thermal analysis made. Structural analyses should be performed for the cylinder for the pressure peak shifted forward 1/8 and 1/4 SRM diameters. Linear, bifurcation and nonlinear analyses with thermal effects included should be performed. A simplified 360 deg model should be coded and analyzed with the lee and keel meridians off the planes of symmetry. These results could be compared to the analysis of the same model with the loading on the symmetry planes. A comparison of these models would give a factor to be applied to the 180 deg detail model stresses to obtain relative stress magnitudes. The addition of a plot package to check data input and structure geometry would be a very beneficial addition to the STAGS C program. The deformed structure plots would add greatly to the efficient utilization of this program during structural analysis tasks.

7. REFERENCES

1. SRB Loads Data Book 2, Rev. D, SE-019-057-2H (ECR ED22-0005), George C. Marshall Space Flight Center, Marshall Space Flight Center, Ala., May 24, 1976.

2. Almroth, B.O., F.A. Brogan and G.M. Stanley, "Structural Analysis of General Shells, Vol. II, User Instructions for STAGS," LMSC D553478, Lockheed Missiles & Space Company, Palo Alto, Calif., December 1976.

3. Crockett, C.D., "SRM Attrition Rate Study of the Aft Motor Case Segments Due to Water Impact Cavity Collapse Loading," NASA TM X-73303, Marshall Space Flight Center, Ala., May 1976.

E MD